

**TNIP1 affects proliferation, apoptosis and migration of
Human Embryonic Kidney 293 cells**

Doctoral thesis
to obtain a doctorate
from the Faculty of Medicine
of the University of Bonn

Carolina Götsche Esperança Clara

from Lisbon, Portugal

2025

Written with authorization of
the Faculty of Medicine of the University of Bonn

First reviewer: Prof. Dr. Stephan Baader

Second reviewer: PD Dr. Matthias Eckhardt

Day of oral examination: 07.04.2025

From the Institute of Anatomy, Anatomy and Cell Biology

Table of contents

List of Abbreviations	6
1. Introduction	8
1.1. TNIP1 – an ambiguous signaling molecule involved in cell death	8
1.2. Structure of the TNIP protein family	10
1.3. TNIP1 – a risk locus for inflammatory and neurodegenerative diseases.....	11
1.4. Rationale and aim of the study	14
2. Materials and Methods	16
2.1. Laboratory instruments and chemicals.....	16
2.1.1. Instruments and software	16
2.1.2. Kits	17
2.1.3. Solutions and chemicals.....	18
2.2. Nucleic acid techniques	19
2.2.1. Materials for nucleic acid techniques	19
2.2.2. Amplification and characterization of pUNO-TNIP1 plasmid DNA.....	20
2.2.3. PCR amplification of the TNIP1 coding sequence.....	21
2.2.4. Subcloning of TNIP1 into the pMini vector	22
2.2.5. Cloning of TNIP1 into the eukaryotic expression vector pcDNA3.1zeo	23
2.3. Protein biochemical techniques.....	26
2.3.1. Materials for protein biochemical techniques	26
2.3.2. Preparation of cell lysates	27
2.3.3. Protein Estimation	27
2.3.4. Western Blot.....	28
2.4. Cell biological techniques.....	29
2.4.1. Materials for cell biological techniques.....	29
2.4.2. In silico analysis of TNIP1 gene expression	30

2.4.3. Culturing HEK 293 cells	31
2.4.4. Transfection of HEK 293 cells	32
2.4.5. Immunocytochemistry	33
2.4.5.1. Immunocytochemical staining procedure	33
2.4.5.2. Image acquisition	35
2.4.5.3. Evaluation of cell numbers using the Hoechst staining	36
2.4.5.4. Evaluation of TNIP1 expression levels in stained cell cultures	37
2.4.5.5. Evaluation of the Phalloidin staining	37
2.4.5.6. Evaluation of the Caspase-3 staining	38
2.4.5.7. Evaluation of the phosphorylated Histon H3 staining	40
2.4.6. Wound healing assay	42
2.4.7. Flow cytometry	44
2.5. Statistical Analysis	45
3. Results	47
3.1. Cloning of pcDNA3.1zeoTNIP1	47
3.2. Generation and characterization of transfected HEK 293 cells	49
3.3. Effect of TNIP1 on cell apoptosis	53
3.4. Effect of TNIP1 on cell proliferation	60
3.5. Effect of TNIP1 on cell migration	66
4. Discussion	69
4.1. TNIP1 expression can be altered in HEK 293 cells	69
4.2. TNIP1 promotes apoptosis	72
4.3. TNIP1 attenuates cell proliferation	74
4.4. TNIP1 deficiency decreases cell migration	76
4.5. Influence of other TNIP family members	78
4.6. Conclusion	79

5. Summary.....	80
6. List of Figures	81
7. List of Tables	82
8. References.....	83
9. Acknowledgments	101

List of Abbreviations

A20	Ubiquitin-editing NF-kappaB inhibitory protein A20; alternative names: TNFAIP3 (tumor necrosis factor alpha induced protein 3)
AHD	ABIN homologous domains
ASD	Autism spectrum disorder
AU	Arbitrary unit
BCA	Bicinchoninic acid
C3	Caspase-3
CMV	Cytomegalovirus
ct	HEK 293 mock-transfected cells (control)
CV	Coefficient of variance
DAMPs	Damage-associated molecular patterns (alarmins)
DAPI	4',6-Diamidin-2-phenylindol
dH ₂ O	Distilled water
DMEM	Dulbeccos Modified Eagle Medium
DMSO	Dimethylsulfoxide
DNA	Deoxyribonucleic acid
dNTPs	Deoxynucleotide triphosphates
ECL	Enhanced chemiluminescence
EDTA	Ethylendiamintetraacetate
EGFP	Enhanced green fluorescent protein
EGFR	Epidermal growth factor receptor
ERK	Extracellular-signal regulated kinase
FCS	Fetal calf serum
GEO	Gene Expression Omnibus
HEK 293	Human Embryonic Kidney 293 Cells
HF	High fidelity
HRP	Horseradish Peroxidase
ID	Integrated density
IKK	IkB Kinase complex; includes IKKa, IKKb and IKKy units
LB-Medium	Lysogeny broth medium

LSM	Laser scanning microscopy (used in immunocytochemistry)
MAPK	Mitogen activated protein kinase
mTOR	Mammalian Target of Rapamycin
n	Number of samples or assays performed
NBD	NEMO-binding domain
NEMO	NF-kappaB essential modulator, or IKKy (regulatory unit of the IKK)
NF-kappaB	Nuclear factor kappa light chain enhancer of B-cells
PBS	Phosphate-buffered saline
PCR	Polymerase-chain-reaction
PFA	Paraformaldehyde
PHH3	Phosphorylated Histon H3
PI	Propidiumiodide
PLL	Poly-L-Lysin
pTNIP1	TNIP1 plasmid, cells transfected with pcDNA3.1zeoTNIP1
pTNIP1(-)	Cells within the pTNIP1 group, expressing endogenous TNIP1 levels
pTNIP1(+)	Cells within the pTNIP1 group, overexpressing TNIP1
pUNO-TNIP1	pUNO-hTNIP1a obtained from InvivoGen
PVDF	Polyvinylidene fluoride
RIPK1	Receptor-interacting serine/threonine-protein kinase 1
rSAP	Recombinant shrimp alkaline phosphatase
RT	Room temperature
scr	Si-scramble RNA, used as control for si-knockdown, transfected with random sequence siRNAs
siTNIP1	Si-knockdown for TNIP1, transfected with 12 siRNAs specific to TNIP1
TBE	TRIS-Borat-EDTA
TBS	TRIS buffered saline
TLR	Toll-like receptor
TNF-alpha	Tumor necrosis factor alpha
TNIP1	TNFAIP3 interacting protein 1; alternative names include ABIN-1 (A20 binding protein 1), VAN, NAF1, nip40-1
TPL-2	Tumor progression locus protein-2
TRIS	TRIS(hydroxymethyl)aminomethane

1. Introduction

1.1. TNIP1 – an ambiguous signaling molecule involved in cell death

TNIP1 is a polyubiquitin-binding protein, first identified in 1999 because of its interaction with Nef, which was shown to downregulate CD4 in lymphocytes of patients with acquired immunodeficiency syndrome (Fukushi et al., 1999). Its initial name Naf1 (Nef associated factor 1) was soon replaced by A20 binding inhibitor of nuclear factor kappa B (ABIN-1), since Naf1 also interacted with A20, an inhibitor of NF-kappa B activation (Heyninck et al., 2004). Today, this gene is commonly named TNIP1, which is derived from its ability to inhibit tumor necrosis factor alpha (TNF-alpha) induced NF-kappaB-dependent gene expression (Verstrepen et al., 2009; Verstrepen et al., 2014).

TNIP1 is ubiquitously expressed in all organs investigated (Stelzer et al., 2016). Consistently, it is also expressed in the brain, albeit to a somewhat lower degree (Allan Brain Atlas, Moreno et al., 2022). The protein was initially localized to the cytoplasm but was also found to shuttle to the nucleus of the cell upon activation (Gurevich et al., 2011).

As previously mentioned, TNIP1 is an inhibitor of NF-kappaB activation (Mauro et al., 2006; Van Quickelberghe et al., 2018). Indeed, adenoviral gene transfer of TNIP1 in mice was shown to reduce NF-kappaB levels in murine lungs and liver (El Bakkouri et al., 2005). Vice versa, downregulation of TNIP1 via miRNA resulted in higher NF-kappaB transcriptional activity in HEK 293 cells (Dorn et al., 2018). Intriguingly, earlier studies had shown that TNIP1 knockout mice only displayed minor NF-kappaB activation, which was attributed to a possible overlap in function in the TNIP protein family (Verstrepen et al., 2009).

While these studies established a link between TNIP1 expression and NF-kappaB signaling at a molecular level, the effects in animal and cellular models appear to be ambiguous. TNIP1 seems to be involved in several death pathways including apoptosis, necroptosis and pyroptosis, which are intrinsically connected (Bertheloot et al., 2021; Li et al., 2022; Newton et al., 2024; Shamilov et al., 2020). Dziejczak et al. (2018) showed that TNIP1 deficiency sensitizes cells to both apoptosis and necroptosis through regulation of receptor-interacting serine/threonine-protein kinase 1 (RIPK1), a key

regulator of these pathways. RIPK1 modifications lead to cell survival rather than cell death. Conversely, RIPK1 activation prompts the activation of caspase-8, which initiates cell death pathways. Interestingly, Verstrepen et al. (2009) uncovered that TNIP1 also inhibits caspase-8 activation. In fact, TNIP1 depleted mice die during liver embryogenesis, due to fetal liver apoptosis, anemia and hypoplasia (Li et al., 2022; Oshima et al., 2009; Zhou et al., 2011). Moreover, TNIP1 deficiency has been associated with increased inflammasome assembly, which is part of the pyroptotic process (Shamilov et al., 2020). Consistent with the role of TNIP1 in stimulating proliferation, a recent study on glioma tissue, a tumor entity commonly presenting epidermal growth factor receptor (EGFR) mutations (Meyer-Puttlitz et al., 1997), revealed that high TNIP1 levels are associated with increased tumor proliferation rates and poorer patient outcomes (Lei et al., 2020). Furthermore, Shamilov et al. (2020) found that adequate levels of TNIP1 are necessary for proper wound healing in keratinocytes, underlining the importance of TNIP1 in cell proliferation. Additionally, TNIP1 has been implicated in the inhibition of autophagy, a crucial cell process for maintaining homeostasis (Le Guerroué et al., 2023). Through autophagy, dysfunctional cell organelles and proteins are disposed of and some of these degradation products are recycled (Mizushima and Komatsu, 2011).

In contrast, recent studies revealed a pro-apoptotic and anti-proliferative effect in TNIP1 overexpressing clear cell renal cell carcinoma (Yang et al., 2019). Similarly, TNIP1 was found to inhibit cell proliferation and growth in EGFR overexpressing tumor cell lines, which was attributed to its NF-kappaB inhibitory activity (Huang et al., 2008). Along these lines, Chen et al (2015) revealed that TNIP1 overexpression in keratinocytes decreased cell proliferation. In addition, TNIP1 has been identified as a promoter of mitophagy (Merline et al., 2023; Shinkawa et al., 2022), as well as being a substrate of autophagy itself (Mejlvang et al., 2018; Rasmussen et al., 2023).

Taken together, it becomes evident that TNIP1 is an important player in the NF-kappaB cascade and is crucial in early mouse development. Yet it remains to be elucidated, how changes in TNIP1 expression levels affect cellular functions, including cell proliferation and apoptosis, during normal development and in pathological situations. These diverse functions might be executed by interacting with various cytoplasmatic and nuclear

receptors, thereby differentially affecting NF-kappaB signaling (Flores et al., 2011; Ramirez et al., 2012).

1.2. Structure of the TNIP protein family

TNIP1 is part of the TNIP protein family and shares some common features with the other members, including the four ABIN homologous domains (AHD), as can be seen in Figure 1.

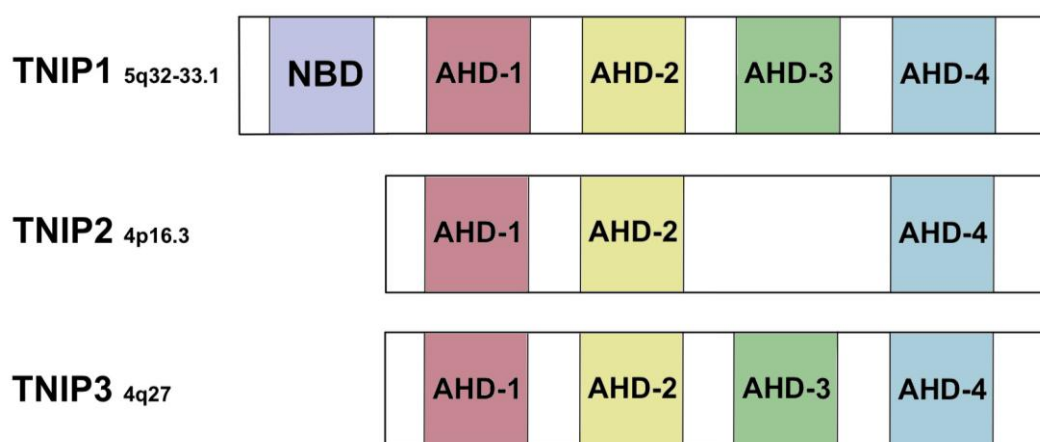


Figure 1: Schematic drawing of domain structures of the TNIP family
The ABIN (TNIP) homologous domains (AHD) are depicted above. AHD-1 allows for A20-binding, while AHD-2 is the ubiquitin-binding domain. AHD-3 has recently been connected to autophagy-related pathways and is missing in TNIP2. The function of AHD-4 is not yet known. TNIP1 contains an additional NEMO-binding domain (NBD) which enables an interaction with NEMO, a powerful regulator of NF-kappaB. In contrast to TNIP2 and TNIP3, TNIP1 is located on a different chromosome.

AHD-1 allows for A20 binding, whereas the AHD-2 domain contains a ubiquitin-binding domain, which is important for interacting with polyubiquitinated proteins (Heyninck et al., 2003). This domain is shared with NF-kappaB essential modulator (NEMO) and optineurin, a protein involved in amyotrophic lateral sclerosis pathogenesis (Verstrepen et al., 2009). AHD-3 is missing in TNIP2 and contains motifs necessary for the interaction with autophagy related proteins. Recently AHD-4 was identified, although its function is still unknown (Le Guerroué et al., 2023). Additionally, TNIP1 has a NEMO-binding domain

(NBD), as opposed to the other proteins in the TNIP family. NEMO is part of the IKK-complex, which is a core element of the NF-kappaB cascade. Before delving into TNIP1's involvement in this pathway, it should be mentioned that the IKK complex can exhibit both positive and negative regulatory effects on NF-kappaB (Israel, 2010; Lobry et al., 2007). Moreover, the NF-kappaB cascade itself can lead to either cell survival or apoptosis, depending on several cellular circumstances, ranging from differences in cell cycle to epigenetic and genetic differences (Brenner et al., 2015; Flusberg and Sorger, 2015; Van Antwerp et al., 1998). While NF-kappaB mediated pro-apoptotic signaling is usually fast and does not require protein synthesis, anti-apoptotic functions of NF-kappaB rely on gene induction and protein synthesis of several cellular inhibitors of apoptosis (Aggarwal, 2003). Thus, depending on upstream signaling and internal cell cues, NF-kappaB activation can lead to either cell survival or cell death. This dual and opposing function has been observed in many proteins, which were initially associated with merely one or the other (Flusberg and Sorger, 2015). This duality is also reflected in TNIP1, as well as in some other TNIP family members.

Since the TNIP family has several common domains, it is not astonishing that some of the known functions of these proteins are closely related. All TNIP proteins exhibit NF-kappaB inhibitory effects (Van Huffel et al., 2001; Wullaert et al., 2007). Similarly to TNIP1, TNIP2 also modulates mammalian inflammation by blocking the tumor progression locus protein-2 (TPL-2). By blocking this protein, it inhibits the MAPK/ERK pathway which otherwise stimulates inflammation (Webb et al., 2019). Further, TNIP2 was found to be crucial for cell survival and apoptosis (Liu et al., 2004). These dual functions of the TNIP proteins might be one of the reasons for their association with a plethora of diseases.

1.3. TNIP1 – a risk locus for inflammatory and neurodegenerative diseases

TNIP1's role in several autoimmune and inflammatory diseases has long been discussed. Its location on chromosome 5q33.1 was identified as a pleiotropic immune disease locus (Akbar et al., 2015; G'Sell et al., 2015; Márquez et al., 2018; Shamilov and Aneskievich, 2018), of which genomic deletions can cause hematopoietic syndromes such as myelodysplastic syndrome (Fuchs, 2012). To illustrate the importance of TNIP1 research,

I will provide some examples of clinical syndromes that are currently associated with TNIP1.

The strongest association in genome wide association studies appears to be with systemic lupus erythematosus (Adrianto et al., 2012; Alarcón-Riquelme et al., 2016; Brady et al., 2020; Khunsriraksakul et al., 2023; Morris et al., 2016), a chronic inflammatory autoimmune disorder, which affects the skin, the musculoskeletal system and many other organs. A typical and often observed complication in systemic lupus erythematosus is kidney inflammation (glomerulonephritis), which has been associated with a disruption in TNIP1 function (Korte et al., 2017). Moreover, manifestation of the disease in the brain leads to neuropsychiatric symptoms (Carrión-Barberà et al., 2021; Cox et al., 2023).

Psoriasis is another disorder of inflammatory nature linked to alterations of the TNIP1 locus (Baurecht et al., 2015; Yin et al., 2015). This was further supported by the identification of TNIP1 gene polymorphisms associated with psoriasis susceptibility (Gong et al., 2020). Previous studies had shown that the loss of TNIP1 results in a more pronounced form of psoriasis in mice (Ippagunta et al., 2016). While Chen et al. (2015) demonstrated that TNIP1 deficiency leads to increased keratinocyte proliferation, intriguingly Shamilov et al. (2020) showed that diminished TNIP1 levels affected keratinocyte vitality in culture. The involvement of TNIP1 in these inflammatory processes demonstrates its plausible role in the development of psoriasis.

Moreover, TNIPs also play an integral role in the inflammation of specialized connective tissue cells. Rheumatoid arthritis has been linked to single nucleotide polymorphisms of the TNIP1 gene and to genome alterations within the TNIP2 locus (Eyre et al., 2012; Ishigaki et al., 2022). Consistently, Igarashi et al (2012) found an upregulation of A20 and TNIP1 expression and increased pro-inflammatory cytokine expression in fibroblast-like synoviocytes derived from rheumatoid arthritis patients, proposing a pro-inflammatory role of TNIP1. Furthermore, TNIP1 has been identified as risk locus for other autoimmune disorders including Sjörgen syndrome (Lessard et al., 2013; Nordmark et al., 2013), systemic sclerosis (Allanore et al., 2011; Hinchcliff et al., 2021) and myasthenia gravis (Gregersen et al., 2012). In addition, TNIP1 has been linked to coronary artery disease (He et al., 2023; Song et al., 2017). In 2015, Akbar et al. evidenced endothelial dysfunction

in a murine model, proposing that dysfunction of TNIP1 may be involved in early stages of cardiovascular disease provoked by inflammation.

In recent years the role of TNIP1 in the pathogenesis of neurodegenerative disease has become more prominent (Enduru et al., 2024; Rajesh and Kanneganti, 2022). TNIP1 has been identified as a risk locus for Alzheimer's disease (Bellenguez et al., 2022; Dalmaso et al., 2023; Wightman et al., 2021), the leading cause of dementia (Soria Lopez et al., 2019). Typically, Alzheimer's disease is characterized by neuronal cell loss due to activated cell death pathways (Qiu et al., 2023; Rajesh and Kanneganti, 2022). Additionally, dysfunctions in glial autophagy have been postulated to play a role in Alzheimer's disease, underlining the importance of basic physiological functions to maintain cell homeostasis (Litwiniuk et al., 2023; Zhang et al., 2021). Several observations suggest that neuroinflammation, at least in part, plays a role in the development of Alzheimer's disease (Akiyama, 2000; Rajesh and Kanneganti, 2022). Typical findings in the brain of Alzheimer patients include misfolded and aggregated proteins like Amyloid-beta and tau (Thal et al., 2015). These proteins are thought to act as alarmins or DAMPs (damage-associated molecular patterns), thus leading to Toll-like receptor (TLR) activation, microglial activation (Liu et al., 2012) and NF-kappaB driven brain inflammation (Ho et al., 2024). A similar mechanism of NF-kappaB driven inflammation was proposed in amyotrophic lateral sclerosis, a disease characterized by rapid fatality due to motor neuron degeneration (Meyer, 2021). Loss of function in proteins involved in NF-kappaB inhibition like optineurin or TNIP1 has been associated with this neurodegenerative disorder (Benyamin et al., 2017; Nagabhushana et al., 2011; Restuadi et al., 2022; Van Rheenen et al., 2021). Further, both apoptotic and necroptotic mechanisms are thought to be a central part of disease development (Ito et al., 2016; Martin and Liu, 2004; Sathasivam et al., 2001).

While the link between TNIP1 dysregulation and neurodegenerative disorders like Alzheimer's disease and amyotrophic lateral sclerosis is well established, autism spectrum disorder (ASD) is only loosely linked to this signaling molecule. According to the Decipher databank (Firth et al., 2009) TNIP1 is associated with global development delay and intellectual disability. Characteristically, ASD is classified as a neurodevelopmental disorder, presenting with social deficits and repetitive, restricted patterns of behavior.

Morphological brain alterations have long been studied in ASD patients, revealing differences in brain size (Fetit et al., 2021; Rubenstein, 2011; Wolff et al., 2018) and in cellular volume (Skefos et al., 2014; Wegiel et al., 2014). These alterations may result from lack of neuronal proliferation, from premature cellular degeneration or possibly from delayed or altered neuronal differentiation (Varghese et al., 2017; Wang et al., 2023). Studies using post-mortem brain tissue revealed increased levels of apoptotic proteins (p53) and decreased levels of anti-apoptotic proteins (Bcl-2), suggesting cell death plays a role in ASD development (Fatemi et al., 2001; Fatemi and Halt, 2001; Sheikh et al., 2010a; Sheikh et al., 2010b). Moreover, increases in dendritic spine density compared to control groups were shown by Hutsler and Zhang (2010) and Tang et al. (2014), possibly indicating a deficit in dendritic pruning.

Besides many known genetic alterations, environmental factors impact on the occurrence of ASD, most notably, high levels of inflammatory proteins during pregnancy (Ashwood et al., 2004; Li et al., 2009; Majerczyk et al., 2022; Matta et al., 2019; Modabbernia et al., 2017; Shuid et al., 2021). Immune dysregulation has thus been thought to be a key pathogenic process in ASD development (Jiang et al., 2018; Meltzer and Van de Water, 2017), which is supported by the fact that several autoimmune diseases are common co-morbidities of ASD (Robinson-Agramonte et al., 2022; Theoharides et al., 2016).

Overall, there seems to be a consensus that inflammation, cell death and autophagy are at least partly at fault for the development of ASD (Deneubourg et al., 2022; Ghavami et al., 2014; Hughes et al., 2023; Ohja et al., 2018). TNIP1 has been shown to be involved in these pathways in multiple ways and is tightly associated with common ASD co-morbidities, hence appearing to be an interesting candidate gene for further research. Additionally, TNIP1 has been shown to interact with Engrailed-2 (HIPPIE Database), a homeobox transcription factor associated with ASD (Benayed et al., 2009; Gharani et al., 2004).

1.4. Rationale and aim of the study

As outlined above, TNIP1 is deeply involved in inflammatory processes. Clinical observations have shown that inflammation increases the risk for developing organ failure

due to excessive cell death. Moreover, transcriptomic analysis and histological expression data demonstrated that TNIP1 is expressed within cells of the central nervous system, as can be seen in Figure 2.

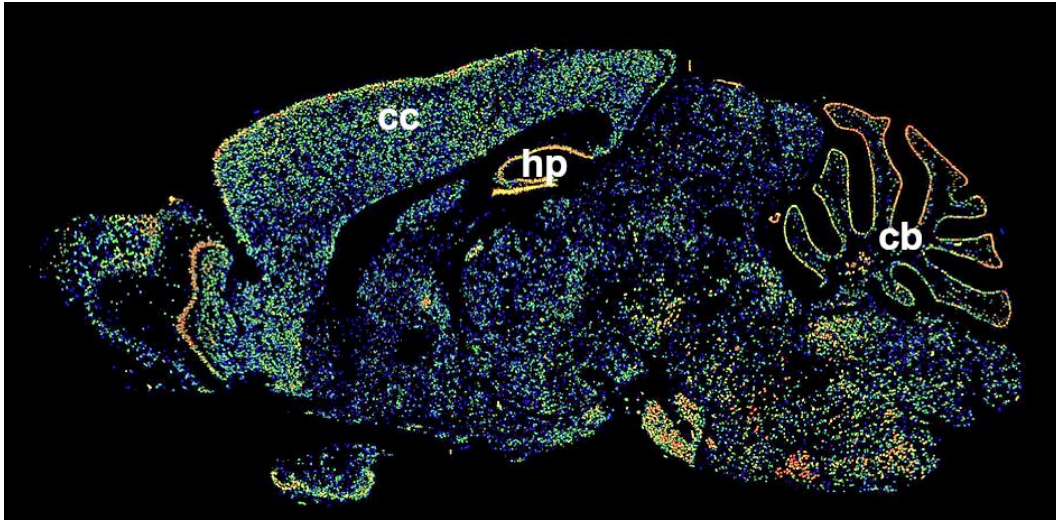


Figure 2: TNIP1 expression in the brain

In situ hybridization for TNIP1 is shown in a close to midsagittal brain section (Allan Brain Atlas). Expression levels are coded in color, from higher levels (red) to lower levels (blue). TNIP1 expression can be found ubiquitously throughout the brain (cb: cerebellum, cc: cortex cerebri, hp: hippocampus).

Despite having a solid understanding about TNIP1's signaling pathways and function in several organ systems of the body, its role in the central nervous system has not yet been addressed in any detail. Based on current TNIP1 research, I expect TNIP1 to have an impact on cell death and proliferation, but also on cellular differentiation.

In order to investigate cellular functions of a distinct gene product, molecular tools such as an expression vector, antibodies and a cellular system are needed. The cell system should allow for easy modifications on the genetic level, but also be suitable for pharmacological treatment. Hence, I chose Human Embryonic Kidney 293 cells (HEK 293 cells), a well-established cell line, that is straightforward to cultivate (Russell et al., 1977). Further, it has a high proliferation rate and even presents some characteristics of neuronal cells (Stepanenko and Dmitrenko, 2015). Thus, the aim of the current study was to establish a cell culture system, that enables the reliable overexpression and repression of TNIP1, to explore TNIP1 functions in a cellular context.

2. Materials and Methods

2.1. Laboratory instruments and chemicals

2.1.1. Instruments and software

Table 1: Instruments

Instrument	Manufacturer
Bead bath	Lab RMDR
Bio Photometer	Eppendorf
Cell culture centrifuge (Biofuge Primo)	Heraeus
Cell culture dishes (diameter: 6 cm)	Greiner Bio-one
Cell culture hood	Waldner
Cell culture incubator (37 °C, 5 % CO ₂)	ThermoFisherScientific
Cell culture microscope	Zeiss
Cell culture plates (6-well)	TPP
Centrifuge for bacterial cultures (Multifuge3 SR)	Heraeus
Centrifuge Micro 200R	Hettich
Cryogenic tubes	ThermoFisherScientific
Electrophoresis chamber	Bio-Rad
FACScan unit	BD Biosciences
Falcon tubes	Greiner Bio-one
Gel-Doc 2000 imager	Bio-Rad
Heating block (and mixer)	Star Lab
Incubator for bacterial cultures (Innova 4O incubator shaker)	New Brunswick Eppendorf
Liquid nitrogen tank	Taylor Wharton
LSM microscope Nikon A1	Nikon
Magnetic stirrer	Star Lab
Microplate Spectrophotometer (µQuant)	Biotek Instruments
Microscope Slides	Marienfeld
Neubauer counting chamber	Brand
PCR cyclor (T100-Thermal cyclor)	Bio-Rad
pH meter	Mettler Toledo
Pipette	Eppendorf
Pipette (Glas)	Hamilton
Roller mixer	STUART
Sample tubes	Eppendorf
Sonicator	Brandelin Sonopuls
Timelapse microscope (Leica DM IRE2)	Leica
Transblot Turbo	Bio-Rad
Vortex Genie 2	Scientific Industries
Western Blot chamber	Bio-Rad
Western Blot Imager (LAS 400 mini)	GE Healthcare

Table 2: Software

Software	Manufacturer
Clone manager 5	Sci-Ed Software
FIJI (Image J)	Open source (Schindelin et al, 2012)
Flowing software 2	Turko Bioscience Center
Gen 5 (BCA reading)	BioTek Instruments
GIMP (GNU Image Manipulation Program)	Open source (The GIMP Development Team, 2019)
Image Reader LAS-400	GE Healthcare
IrfanView 64	IrfanView
NEBcloner	New England Biolabs
NEBio Calculator	New England Biolabs
NIS Elements image LSM	Nikon
Quantity One	Bio rad
RStudio	Open source (RStudio Team, 2020)
SnapGene Software	SnapGene
Timelapse Leica DM SDK Software	Leica
Vivid counter (App)	Mamuro Sato (Developer)
Windows Excel	Microsoft
Windows Office	Microsoft
Windows Powerpoint	Microsoft
Zotero	Corporation for Digital Scholarship, 2024

2.1.2. Kits

Table 3: Kits

Kit	Manufacturer
NEB® PCR Cloning Kit	New England Biolabs
NucleoBond® Xtra Midi	Macherey-Nagel
NucleoSpin Mini kit for gel extraction and PCR clean-up	Macherey-Nagel
NucleoSpin® Plasmid EasyPure	Macherey-Nagel
Pierce BCA Protein Assay Kit	ThermoFisherScientific

All kits were used according to the manufacturers' protocol.

2.1.3. Solutions and chemicals

Table 4: Chemicals

Chemical	Manufacturer
2-Mercaptoethanol	ThermoFisherScientific
Agar-Agar	SERVA
Ampicillin	ThermoFisherScientific
Biozym	Biozym Bioscientific
DMSO	Sigma Aldrich
Ethanol (absolute)	AppliChem
Ethidium Bromide	ThermoFisherScientific
Glycerol (98 %)	Carl Roth
LB-Medium	Carl Roth
NaCl	AppliChem
Non-fat dried milk powder	AppliChem
Nuclease-Free Water	Invitrogen
PFA	Sigma Aldrich
Poly-L-Lysin (PLL)	Sigma Aldrich
RNase A	AppliChem
TRIS (Tris[hydroxymethyl]aminomethan)	Carl Roth
Triton X 100	Sigma Aldrich
Trypan blue stain (0.4 %)	ThermoFisherScientific
Tween	Sigma Aldrich

Table 5: Solutions

Solution	Manufacturer/ Composition
High Fidelity (HF) Buffer (5 x)	ThermoFisherScientific
PBS (phosphate buffered saline) (10 x)	13 mM NaCl, 2.7 mM KCl, 10 mM Na ₂ HPO ₄ , 2mM K ₂ HPO ₄
TBE(TRIS/borate/EDTA) Buffer (10 x)	ThermoFisherScientific
TBS (TRIS buffered saline) Buffer (10 x)	50 mM TRIS, 150 mM NaCl, dH ₂ O; pH 7.6
TBS-T Buffer (1 x)	1 x TBS, 0,1 % Tween20
TRIS/Caps Buffer for Semi-Dry Blotting (10 x)	Bio-Rad
TRIS/Glycine/SDS (TGX) Buffer (10 x)	Bio-Rad

2.2. Nucleic acid techniques

2.2.1. Materials for nucleic acid techniques

Table 6: Miscellaneous Materials for nucleic acid work

Material	Manufacturer/ Composition
Agarose Gel	1 % Biozym, Ethidium Bromide at 0.2-0.5 µg/mL, 1 x TBE
Ampicillin Agar Plates	Final concentration 100 µg Ampicillin/ mL Agar
BamHI-HF	New England Biolabs
BglII	New England Biolabs
Blasticidin	InvivoGen
Cutsmart buffer (10 x)	New England Biolabs
EcoRI	New England Biolabs
GeneRuler 1 kB	ThermoFisherScientific
GeneRuler 100 Bp	ThermoFisherScientific
Loading Dye (6 x)	ThermoFisherScientific
NEB 3.1 Buffer	New England Biolabs
NEB® PCR Cloning Kit	New England Biolabs
Phusion Polymerase	ThermoFisherScientific
rSAP (recombinant shrimp alkaline phosphatase)	New England Biolabs
T4 Ligase	ThermoFisherScientific
T4 Ligase Buffer	ThermoFisherScientific
XL1-blue competent cells	ThermoFisherScientific

Table 7: Primers

Primer	Sequence	Use	Manufacturer
BGH reverse	TAGAAGGCACAG-TCGAGG	sequencing	ThermoFisherScientific
pcDNA31_F	CTCTGGCTAACTAGA-GAAC	sequencing	ThermoFisherScientific
TNIP1 h fl_F2	AGGAGCCCTAGGAG-TGCTAC	PCR	ThermoFisherScientific
TNIP1 h fl_R2	GTGG-GAGGGTCCATCACTTG	PCR	ThermoFisherScientific
Tnip1hi3p146_1_F	GTGAGGACGGCAAC-CTGATG	sequencing	ThermoFisherScientific

2.2.2. Amplification and characterization of pUNO-TNIP1 plasmid DNA

Plasmid DNA was either prepared from glycerol stocks of bacteria containing the DNA of interest or was derived from bacteria freshly transformed with the desired plasmid DNA. Since the pUNO-hTNIP1a (pUNO-TNIP1) vector was bought from a company (InvivoGen), I had to transform the DNA into bacteria before isolating the DNA from the bacteria again. For this purpose, 50 μL of chemically competent XL1-blue bacteria were thawed on ice for about 1 hour to increase transformation efficiency. 5 ng of pUNO-TNIP1 vector were added and carefully mixed (no vortexing). The bacteria/DNA mixture was kept on ice for further 15 minutes, heat shocked at 42 $^{\circ}\text{C}$ for 45 seconds, and then quickly cooled on ice for 2 minutes. Afterwards, the transformed bacteria were added to 0.9 mL prewarmed LB-Medium without antibiotics in 14 mL round bottom Falcon tubes. They were shaken at 37 $^{\circ}\text{C}$ at 225 rpm for 1 hour. 10 μL of this bacterial mix was then added to 2 mL LB-Medium containing 1% Blasticidin (20 $\mu\text{L}/2\text{ mL}$) and incubated at 37 $^{\circ}\text{C}$ overnight. In order to characterize the bacteria, DNA was extracted from the bacteria using the NucleoSpin[®] Plasmid EasyPure Kit (Table 3). The procedure was done exactly as described by the manufacturer's protocol. A restriction analysis with EcoRI was performed using 20 enzyme units per 1 μg DNA at 37 $^{\circ}\text{C}$ for 60 minutes, followed by heat inactivation at 65 $^{\circ}\text{C}$ for 20 minutes. The NEB Buffer 3.1 was used.

As can be seen in Figure 3, the digestion resulted in three bands around 3000, 1800 and 300 bp, which corresponded to the expected fragment sizes obtained by in silico analysis (given at the right side of the figure). While this DNA was not derived from a single clone, it was still purified from

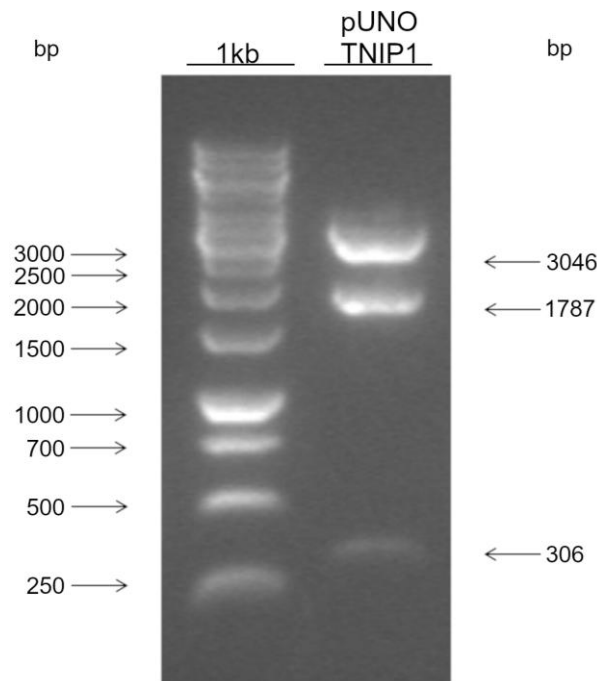


Figure 3: Characterization of pUNO-TNIP1

pUNO-TNIP1 was digested with the restriction enzyme EcoRI. The digestion yielded DNA bands at 3046, 1787 and 306 bp. This confirmed the presence of the TNIP1 gene in the pUNO plasmid. The 1kb DNA ladder (1kb) is depicted on the left-hand side of the image.

selected bacteria grown in antibiotics. Therefore, the purity of this DNA was sufficient for further cloning.

In order to obtain larger amounts of DNA, a Midi Prep was done using the NucleoBond® Xtra Midi kit. Again, restriction analysis using EcoRI was performed to verify the correctness of the prepared DNA. After having confirmed that the bacteria contained the correct plasmid, glycerol stocks of the bacteria were prepared for long term storage.

To store plasmid expressing bacteria over a long time, bacteria were grown to a linear growth phase, then 2 mL of this bacterial suspension were centrifuged at 11,000 x g for 1 minute and the supernatant was discarded. The cell pellet was resuspended in a solution containing 800 µL LB-Medium with suitable antibiotics and 200 µL of glycerol (98 %). These glycerol stocks can be stored at -80 °C for years.

2.2.3. PCR amplification of the TNIP1 coding sequence

In order to clone a full-length TNIP1 fragment into a eukaryotic expression vector, the coding sequence of TNIP1 needed to be amplified using the pUNO vector. In addition, appropriate cloning sites were added on both sites of the coding sequence. Solutions and reagents can be found in Table 6. Primers can be found in Table 7. The PCR was performed using the Master Mix shown in the table below.

PCR Master Mix

Material	Volume
Phusion Polymerase	0.5 µL
HF Buffer (5 x)	10 µL
dNTPs (10 mM)	1.25 µL
DMSO (100 %)	1.5 µL
TNIP1hF2 Forward Primer (20 pmol/µL)	1.25 µL
TNIP1hR2 Reverse Primer (20 pmol/µL)	1.25 µL
DNA (pUNO-TNIP1, 1 ng/µL)	5 µL
dH ₂ O	up to 50 µL

In order to increase the amount of DNA usable for ligation reactions the volumes listed in the table above were scaled up to 200 µL and more. This total volume was then separated into 50 µL aliquots to facilitate temperature rises and decreases in the thermocycler.

The cycler was set to the settings presented in the table below:

Cycler Settings for PCR

Steps	Temperature	Duration
1. Denaturation	98 °C	40 seconds
2. Annealing	56 °C	60 seconds
3. Extension	72 °C	90 seconds
(Steps 1 through 3 are repeated 40 times)		
4. Final Extension	72 °C	10 minutes

After PCR amplification, the DNA fragments were separated by electrophoresis on a 1 % Agarose gel. 10 µL of the PCR sample were mixed with 2 µL of loading dye and loaded onto the premade gel. The gel was prepared by dissolving 1 g Agarose in 100 mL 1 x TBE. After repeated heating in a microwave oven until complete dissolution and cooling to about 60°C, Ethidium bromide at a concentration of 1:20.000 (10 µg/mL - stock solution) was added and the gel was poured into an electrophoretic chamber. Then, the gel was kept at room temperature until it solidified. 10-15 µL of the samples were loaded per lane and the gel was run at 100 V for 60 minutes. Thereafter, the gel was either imaged using a gel documentation system (Gel-Doc 2000 imager, Bio-Rad) or the TNIP1 inserts were extracted from the gel using the „NucleoSpin Mini kit for gel extraction and PCR clean-up“. DNA concentrations were measured using the Eppendorf photometer (Table 1).

2.2.4. Subcloning of TNIP1 into the pMini vector

Since initial efforts to ligate BamHI-HF digested TNIP1 fragments into the BamHI-HF linearized expression vector failed, PCR amplified TNIP1-DNA was first cloned into a pMini vector utilizing the NEB® PCR Cloning Kit. The chosen insert to vector ratio was 3:1, the amounts of DNA were calculated using the NEBioCalculator for ligations. The NEB® PCR Cloning Kit was used exactly according to the manufacturer's protocol. After ligation and transformation of ligated products into chemically competent bacteria, bacteria were plated on Ampicillin containing Agar Plates. Single colonies were picked, and DNA was prepared with the Nucleospin Mini Prep Kit from Macherey-Nagel. Extracted DNA was digested with BamHI-HF at 37 °C for 15 minutes and products were run on a 1 % Agarose gel (Figure 4). Positive clones carrying the TNIP1 insert in the pMini vector,

yielded two bands at 2600 bp (pMini) and 1800 bp (TNIP1). It should be noted that additional bands visible in Figure 4 are likely derived from partially digested vector fragments and possibly from some contamination. Since this restriction analysis was exclusively performed to confirm the presence of the TNIP1 insert in the pMini vector to then select clones for further cultivation, achieving perfect DNA quality was not required. Thus, positive clones were selected, and larger amounts of DNA were prepared using the NucleoBond® Xtra Midi kit protocol. Afterwards, the DNA was once more characterized by restriction digestion as described above.

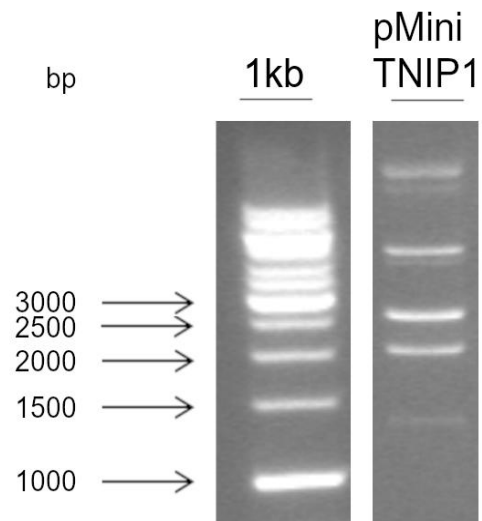


Figure 4: Characterization of pMini-TNIP1

The pMini-TNIP1 vector obtained using the MiniPrep protocol was digested with BamHI-HF. This digestion yielded bands at roughly 2600 bp and 1800 bp, hereby confirming the presence of the pMini vector and the TNIP1 insert, respectively. Additional bands likely resulted from incomplete digestion due to a rather short digestion time. The 1kb DNA ladder (1kb) is depicted on the left side of the image.

2.2.5. Cloning of TNIP1 into the eukaryotic expression vector pcDNA3.1zeo

In order to clone the full length TNIP1 sequence into an expression vector, pcDNA3.1zeo was used as a backbone. This vector was first digested and linearized using a quantitative restriction digest with BamHI-HF. The NEBcloner (New England Biolabs, Table 2) was used to determine appropriate experiment settings to obtain a close to complete digestion. Thus, digestion of 1 µg of vector-DNA was performed using 20 Units of BamHI-HF (Table 6) in CutSmart buffer and incubating the mixture at 37 °C for 15 minutes. No heat inactivation was required. To avoid self-ligations of both vector ends, the 5' ends of the cut vector-DNA were dephosphorylated, using rSAP buffered by the Cutsmart Buffer. 2 units of rSAP were used to digest 2 µg of Plasmid DNA (corresponding to 2 pmol of DNA ends) at 37 °C for 1 hour, followed by heat inactivation of the enzyme at 65 °C for 5 minutes. At the same time the TNIP1 insert was extracted from the pMini-TNIP1 vector using BamHI-HF digestion and the 1800 bp fragment was purified via gel electrophoresis.

Since both ends of the TNIP1 coding region were cut using the BamHI-HF enzyme, sticky end ligation was possible. However, this also meant that two different orientations for the TNIP1 insert were possible. Therefore, a restriction digest to determine TNIP1 insert orientation was performed after the cloning process, as will be outlined in detail below.

Both the vector and insert were run on a 1 % Agarose gel and purified using the “NucleoSpin Mini kit for gel extraction and PCR clean-up”. The purified DNA fragments were loaded onto a gel once

more, and DNA quantification was done by comparing band intensities with those of the DNA ladder (Figure 5). To ligate both DNA fragments, they were added to a reaction tube in a 3:1 insert to vector ratio using 100 ng of vector DNA. Corresponding amounts of the insert DNA were calculated using the NEBicalculator (Table 2). Ligation was performed by adding 1 unit of T4 DNA ligase in NEB ligation buffer and incubating the mixture at RT for 1 hour.

Then, 100 μ L of XL1-Blue cells were transformed with 1 μ L of ligation mixture. Bacteria were thawed and pre-treated with 1.42 M beta-Mercaptoethanol (Table 4) on ice for 10 minutes, while gently mixing every 2 minutes. 1 μ L of the ligation mix equivalent to 30 ng of DNA was added to the bacteria and incubated on ice for a further 30 minutes. The mixture was then heat pulsed at 42 $^{\circ}$ C for 45 seconds and 0.9 mL of preheated LB-Medium without antibiotics (at 42 $^{\circ}$ C) was added. The bacteria were incubated at 37 $^{\circ}$ C and 250 rpm in the shaker for 1 hour. Finally, 500 μ L of the mixture were plated on Ampicillin Agar Plates and incubated overnight.

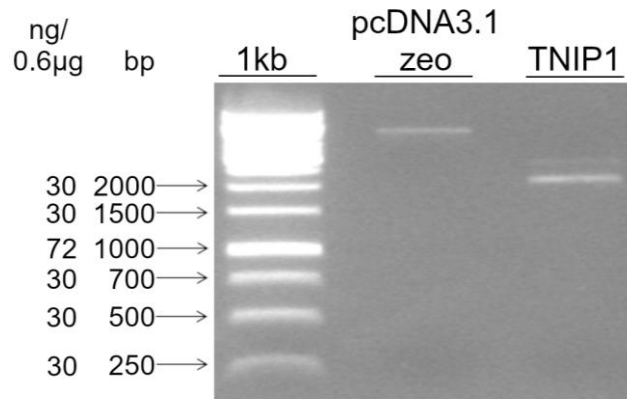


Figure 5: Estimation of DNA quantity for ligation

DNA quantity was estimated using gel electrophoresis: Generuler 1 kb was used at 0.1 μ g/ μ L and is depicted on the left-hand side of the figure (1kb). By comparison a concentration of approximately 72 ng for TNIP1 and approximately 30 ng for pcDNA3.1zeo was estimated.

Colonies were picked at random, and Colony PCR was used to identify colonies carrying the pcDNA3.1zeo vector with the inserted TNIP1 sequence. This method allows for the fast analysis of dozens of colonies at the same time with high sensitivity. A disadvantage of this method is that additional cultures and isolation techniques must be performed to determine the orientation of the insert.

Mastermixes for Colony PCR

Mastermix 1	
Material	Concentration
Bacteria suspension	5 μ L/n
BgHR	0.5 μ L/n
dH ₂ O	7.5 μ L/n
Dream Buffer 10 x	1.5 μ L/n
SeqF1	0.5 μ L/n
Mastermix 2	
Material	Concentration
dH ₂ O	3.8 μ L/n
dNTPs	0.5 μ L/n
Dream Buffer 10 x	0.5 μ L/n
DreamTaq	0.2 μ L/n

Multiple colonies were picked at random from different Ampicillin Agar Plates. Master Mixes 1 and 2 can be found in the table above. Master Mix 1 was prepared and heated to 95 °C for 5 minutes. Then, Master Mix 2 was added before running the PCR cyclers at the settings given in the table below. Afterwards, gel electrophoresis was performed on a 1 % Agarose gel at 120 V for 45 minutes.

Cycler Settings for Colony PCR

Steps	Temperature	Duration
1. Denaturation	95 °C	60 seconds
2. Annealing	55 °C	90 seconds
3. Extension	72 °C	120 seconds
(Steps 1 through 3 were repeated 40 times)		
4. Final Extension	72 °C	5 minutes

Using the colony PCR results, colonies suspected of carrying the TNIP1 insert within the pcDNA3.1zeo vector were selected for further characterization using restriction digest. As previously mentioned, due to identical restriction sites at both ends of the TNIP1 coding sequence, there were two possible orientations of the TNIP1 insert: sense or anti-sense.

Sense orientation, meaning that correct translation of the coding sequence starts at the CMV (cytomegalovirus) promoter, was desired. Restriction with EcoRI and BglII was used for this purpose. The restriction enzymes cut both within and outside of the insertion site, leading to different fragment sizes, depending on the TNIP1 insert orientation. EcoRI restriction digest was performed as described above in chapter 2.2.2. (Images are given in the results section).

Finally, three appropriate looking clones were sent to AGCT for sequencing using the primers given in Table 7. The sequences were then compared with in-silico data and larger amounts of DNA were extracted from appropriate samples using the NucleoBond® Xtra Midi kit protocol. Glycerol stocks were prepared for long-term storage.

2.3. Protein biochemical techniques

2.3.1. Materials for protein biochemical techniques

Table 8: Miscellaneous materials for protein biochemical techniques

Materials	Manufacturer/ Composition
Blotting sponges	Bio-Rad
Complete Protease Inhibitor Cocktail (0,1 mM)	Sigma Aldrich
ECL (enhanced chemoluminescence) solution (Westar Supernova)	Cyanagen
Lämmli Buffer (4 x)	Bio-Rad
Methanol	Carl Roth
Milk TBS-T (5 %)	5 % non-fat dried milk powder in 1 x TBS-T, using shaker and filter paper
Mini-Protean TGX Precast Gels (12-well 20 µL 4-15 %)	Bio-Rad
PEB (Protein extraction buffer for cells)	50 mM TRIS pH 8.0, 150 mM NaCl, 1 % Triton X-100, dH ₂ O; Pefabloc (1 x); Complete Protease Inhibitor Cocktail (1 x)
Pefabloc S-Protease Inhibitor (0,1 mM)	Carl Roth
Pierce™ Bovine Serum Albumin Standard (2 mg/mL)	ThermoFisherScientific
Polyvinylidene fluoride (PVDF) membrane	Sigma Aldrich
Precast Gel for Western Blot (Criterion TGX)	Bio-Rad
PageRuler™ Prestained Protein Ladder 10 to 180 kDa	ThermoFisherScientific

Table 9: Antibodies for Western Blot

Primary Antibodies				
Target protein	Dilution	Species	Catalog #	Manufacturer
TNIP1	1:1000	Rabbit polyclonal	15104-1-AP	Proteintech
Beta-Actin	1:5000	Mouse monoclonal	AB_2537667	Thermofisher
Secondary Antibodies				
Target protein	Dilution	Species	Catalog #	Manufacturer
Anti-Rabbit-IgG, HRP-coupled	1:30000	Goat polyclonal	AB_2313567	Jackson Immuno Research
Anti-Mouse-IgG, HRP-coupled	1:10000	Goat polyclonal	AB_10015289	Jackson Immuno Research

2.3.2. Preparation of cell lysates

HEK 293 cells were cultured at a cell seeding density of 2×10^5 cells/ well in a 6-well plate to obtain high amounts of protein. Cells were resuspended in 1 mL ice-cold 1 x PBS before confluency was reached (Table 5) and centrifuged at 500 x g and 4 °C for 8 minutes. The supernatant was discarded, and the cell pellets were lysed in 400 µL Protein Extraction Buffer. The samples were then incubated on ice for 15 minutes, and ultrasonicated (5 cycles at a power of 60 % for a total of 5 seconds). This improves cell disruption and DNA fragmentation, whilst reducing the viscosity of the extract. After that the samples were centrifuged at 13000 x g for 10 minutes and the supernatant was pipetted into final sample tubes.

2.3.3. Protein Estimation

The BCA assay was used to determine protein concentrations in the samples, using a BCA kit (Table 3) exactly as described in the manufacturer's protocol. Briefly, the BCA assay colorimetrically detects and quantifies total protein content in samples using a standard curve ranging from 25 µg/mL to 2000 µg/mL of albumin protein. Using technical triplicates, the total protein amount in the samples was determined using the Microplate Spectrophotometer µQuant (Biotek Instruments).

2.3.4. Western Blot

For Western Blotting, protein extracts were prepared as previously described. 20 µg of protein were diluted in dH₂O and Lämmli Buffer (Table 8) was added before heating the samples at 95 °C for 5 minutes.

A readymade and commercially available Western Blot Gel (Criterion TGX precast gels, Bio-Rad) was put in the Western Blot chamber, which was then filled with 1 x TGX buffer. The wells were loaded using 20 µg of protein per well. A Prestained PAGERuler was used as a weight standard. The gel was run at 100 V for 60 minutes. Separated proteins were then blotted onto a PVDF membrane. The PVDF membrane was previously incubated in Methanol for 5 minutes and then in 1 x Transfer Buffer for 5 minutes. Then, the gel was extracted from the cast and placed on the PVDF membrane between two blotting sponges on either side. The Blotting program was run at 2.5 A for 8 minutes. Afterwards, the PVDF membrane was washed three times in 1 x TBS for 10 minutes and blocked in 5 % Milk TBS-T for 1 hour. Then the membrane was incubated with antibodies from Table 9 diluted in 5 % Milk TBS-T at 4 °C overnight. The following day the primary antibody solutions were discarded and the membrane was washed in 1 x TBS-T three times for 15 minutes. Then, secondary antibodies (Table 9) diluted in 5 % Milk TBS-T were added and incubated at 4 °C for 1 hour. Beta-Actin was used as a loading control.

The secondary antibody solutions were washed off the membrane with 1 x TBS-T for 15 minutes three times and once with 1 x TBS for 15 minutes. The ECL solution needed for the HRP reaction was used at a dilution of 1:10 and the blot was imaged with precision auto settings using the LAS 4000 mini (GE Healthcare).

The captured images were opened in Image J (Schindelin et al., 2012). Using the rectangle selection tool, all the bands at the same height were selected. Using the Gel Analyzing Tool, lanes were plotted and the integrated density (ID) for each band was measured. The same procedure was applied to the control bands stained for Beta-Actin. These blots did not require background subtraction.

To calculate relative expression levels, the ID value of the TNIP1 band was divided by the ID value for its respective loading control Beta-Actin band. Subsequently, AUs (arbitrary units) for TNIP1 expression levels were calculated for each sample group: ct (mock

transfected control for pTNIP1), pTNIP1 (transfected with the pcDNA3.1zeoTNIP1 plasmid), scr (scr, control for siTNIP1) and siTNIP1 (TNIP1 knockdown with siRNA).

A statistical analysis was performed using a one-sided T-Test in R statistical software. A p-value below 0.001 was considered to be highly significant, a value between 0.05 and 0.001 was deemed significant.

2.4. Cell biological techniques

2.4.1. Materials for cell biological techniques

Table 10: Miscellaneous materials for cell biological techniques

Materials	Manufacturer/ Composition
Dharmafect Duo	Horizon Discovery
DMEM (Dulbeccos Modified Eagle Medium) 1 x + GlutaMax	Gibco
FCS (fetal calf serum)	Gibco
Fluoromount G	Southern Biotech
Hoechst 33258 (1 µg/mL)	New England Biolabs
Immunocytochemical Blocking solution	0.5 % Triton X, 10 % FCS in 1 x PBS
LSM immersion oil	Nikon
OptiMEM	Gibco
Penicillin/Streptomycin	Gibco
PFA (paraformaldehyde) solution (4 %)	40 g PFA, H ₂ O to 1000 mL, heat to dissolve, pH 7.4.
Phalloidin-TRITC (Tetramethylrhodamin B-Isothiocyanat) p1951 (50 µg/mL)	Sigma Aldrich
PI (Propidium iodide)	Sigma Aldrich
PI Staining Solution	0.1 % Triton X-100 PBS 10 µg/mL Propidium Iodide (PI) 100 µg/mL DNase free RNase A in 1 x PBS
Trypan Blue	Sigma Aldrich
Zeocin	Invitrogen

Table 11: Plasmids and siRNA

Plasmids			
Plasmid	Resistance	Fluorescence	Source
pcDNA3.1zeo	Zeocin	-	Baader lab, Bonn
pcDNA3.1zeoEGFP	Zeocin	green	Baader lab, Bonn
pcDNA3.1zeoTNIP1	Zeocin	-	Result of cloning
pUNO1-hTNIP1a	Blasticidin	-	InvivoGen
siRNA			
siRNA	Control/Target	Fluorescence	Source
scr (siscramble)	Negative control	-	Sitools Biotech
siGLO Transfection Indicator	Positive control (localizes to the nucleus)	red (Cy3)	Horizon Discovery
siTNIP1	TNIP1	-	Sitools Biotech

Table 12: Antibodies for Immunocytochemistry

Primary Antibodies				
Target protein	Dilution	Species	Catalog #	Manufacturer
Caspase-3, active (cleaved) form (p17 fragment)	1:500	Mouse monoclonal	AB3623	Millipore
Phospho-Histone H3 (Ser10)	1:500	Rabbit polyclonal	PA5-17869	Invitrogen
TNIP1	1:1000	Rabbit polyclonal	15104-1-AP	Proteintech
Secondary Antibodies				
Target protein	Dilution	Species	Catalog #	Manufacturer
Anti-Mouse-IgG, Alexa 546 coupled	1:800	Goat polyclonal	A-11003	Invitrogen
Anti-Rabbit-IgG, Alexa 488 coupled	1:800	Goat polyclonal	A-11008	Invitrogen
Anti-Rabbit-IgG, Alexa 546 coupled	1:800	Goat polyclonal	A-11035	Invitrogen

2.4.2. In silico analysis of TNIP1 gene expression

In order to obtain information about TNIP1's gene expression levels in HEK 293 cells, I used transcriptomics data published on the Gene Expression Omnibus (GEO) database (Edgar, 2002). The database is accessible through GEO Series accession number GSE267610 regarding sample GSM8270120. The database was downloaded on a local computer and evaluated using R statistical Software. The R script was a modified version of a script originally written and kindly provided by Prof. Karl Schilling (Institute of Anatomy, Bonn). The transcriptomic dataset was derived from HEK 293 cells which were either

treated with Interferon-alpha or left untreated (mock treatment). To evaluate TNIP1 expression levels, the data of mock-treated HEK 293 cells were first selected and TNIP1 expression levels were related to the average expression of all genes. Since multiple transcripts of each gene were analyzed, the results were then presented as a frequency plot, to show the number of different TNIP1 transcripts at distinct expression levels. Finally, the TNIP1 expression level was marked within the plot and compared to the expression level of all other genes analyzed by transcriptomics.

In addition, the GEO dataset GSE249290 (Lobo et al., 2024) was analyzed. This dataset was derived from HEK 293 cells growing at different densities (at confluency and subconfluency) and was used to characterize TNIP1 expression levels in these growth conditions. The R script is comparable to the one above apart from the graphical presentation, which was done as a box plot.

2.4.3. Culturing HEK 293 cells

HEK 293 cells were cultured in DMEM containing 1 % Penicillin/Streptomycin, 10 % FCS and 50 mM GlutaMax (Table 10). Cells were incubated at 37 °C in 5 % CO₂ containing air. They were passaged by discarding medium, followed by resuspension in 2 mL culture medium and centrifugation at 200 x g for 5 minutes. Afterwards the supernatant was discarded and cells were resuspended in 2 mL DMEM. Finally, cells were counted using the Neubauer cell counting chamber (Brand) and seeded in respective concentrations. For continuous growth of the cell line, cells were split 1:20 twice a week.

For long-term storage of HEK 293 cells, cells were grown up to a subconfluent state and washed once with warm 1 x PBS. Cells were then removed from the plate by gently pipetting off the cells from the bottom of the plate. This was easy to do, as HEK 293 cells do not adhere to the well strongly. The cell suspension was then centrifuged at 200 x g for 5 minutes. The cell pellet was resuspended in 10 % DMSO medium and transferred to the -80 °C freezer. The following day, cells were transferred into a liquid nitrogen tank for long term storage. To recultivate cells, they were quickly thawed at 37 °C and transferred to 5 mL of normal DMEM medium to dilute the DMSO. Cells were then centrifuged and resuspended in fresh DMEM and cultured on appropriate dishes for eukaryotic cells.

2.4.4. Transfection of HEK 293 cells

Depending on the assay cell seeding densities differed. However, within an assay, cell seeding densities were kept equal for all treatment groups. Plasmids and siRNA used for transfection can be found in Table 11.

The Transfection Mix and DNA Mix composition varied depending on the size of the cell culture well and can be found in the table below.

Transfection mixes for Plasmid/siRNA

Transfection Mix	DNA-Mix	Cell Culture Plate Size
5 μ L Dharmafect Duo 195 μ L OptiMEM	4 μ L Plasmid (c = 0.5 μ g/ μ L) 196 μ L OptiMEM	6-well
5 μ L Dharmafect Duo 195 μ L OptiMEM	100 μ L siRNA/scr 100 μ L OptiMEM	6-well
2 μ L Dharmafect Duo 48 μ L OptiMEM	1 μ L Plasmid (c = 0.5 μ g/ μ L) 49 μ L OptiMEM	24-well
2 μ L Dharmafect Duo 48 μ L OptiMEM	25 μ L siRNA/scr 25 μ L OptiMEM	24-well

Generally, the transfection process started at a cell confluency of 60-70 %. On the day of transfection, the Transfection and DNA-mixes were prepared as given and incubated at room temperature (RT) for 5 minutes. Afterwards, the Transfection mix was added to the DNA-Mix and incubated at RT for 20 minutes. The culture medium of the wells was replaced by OptiMEM. The DNA-transfection mix was added after the 20 min incubation period. Depending on the assay, after 6-24 hours the OptiMem within wells was replaced by complete DMEM.

The HEK 293 cells transfected with plasmid DNA were harvested after 48 hours, while siRNA transfected HEK 293 cells were harvested after 24 hours. The reasoning for this was that there was a difference regarding the peak expression window for plasmid versus siRNA transfection. To determine these different peak transfection windows, meaning the time frame where plasmid or siRNA expression was at the highest level, a double transfection with fluorescent substances was done, as will be outlined below.

A pcDNA3.1zeoEGFP plasmid (green fluorescent) and siGLO siRNA (red fluorescent) were used as fluorescent substances and were transfected concomitantly using the protocol described above to check transfection efficiency. The fluorescence intensity was

documented at different time points using the Leica Timelapse Microscope. Additionally, the number of transfected cells was recorded.

Appropriate controls were used for each assay. The control for the pTNIP1 group (transfected with the pcDNA3.1zeoTNIP1 vector) was a mock transfection group (ct), where cells were treated with all transfection reagents apart from a vector. The control for the siTNIP1 group (downregulated by siRNA) was provided by Sitools Biotech: a mixture of random siRNAs, called siscramble (scr).

2.4.5. Immunocytochemistry

2.4.5.1. Immunocytochemical staining procedure

For immunocytochemical assays, cells were cultured on coverslips in 6-well cell culture plates precoated with 100 µg/mL PLL (Table 4). PLL was added to the coverslips one day before cells were added. To clean coverslips, they were washed with dH₂O and incubated in the PLL-solution overnight. Then the PLL-solution was discarded, the coverslips were washed with dH₂O three times and dried before cell seeding. Cell seeding density was 1 x 10⁵ cells per well, to allow for cell-cell contacts while still enabling single cell discrimination. The transfection was performed the day after, as described above (chapter 2.4.4.).

48 hours after plasmid transfection and 24 hours after siRNA transfection, cells were fixed in 4 % PFA prepared in 1 x PBS at 37 °C for 10 minutes. After washing three times in 1 x PBS, the blocking solution (Table 10) was left on the cells at RT for 1 hour. Then, the primary antibodies (Table 12) were prepared in the blocking solution and added to the cells at 4 °C overnight. Some antibody stainings were done simultaneously, whilst others were done sequentially, as will be outlined in detail below. Afterwards, the fixed cells were washed three times with 1 x PBS. The secondary fluorescent antibody solutions (Table 12) were prepared in the blocking solution and added to the cells. Cells were incubated at RT in the dark for 1 hour. Again, the cells were washed three times with 1 x PBS to discard the secondary antibody and were finally stained in 1 µg/mL Hoechst 33258 for 10 minutes in the dark for nuclear staining. Cells were washed three more times with 1 x PBS and

coverslipped with Fluoromount G (Southern Biotech). They were left to dry in the dark for at least 24 hours before LSM imaging.

The TNIP1 staining was performed on all samples. The rabbit polyclonal primary antibody (Proteintech) was diluted 1:1000 in blocking buffer. As the secondary antibody, a 1:800 dilution of the Goat-Anti-Rabbit Alexa 488 (green fluorescent) antibody was used (Invitrogen).

Some samples were also stained with the Caspase-3 (C3) mouse monoclonal antibody obtained from MERCK/Millipore prepared as a 1:500 dilution. Secondary red fluorescent Goat-anti-Mouse Alexa 546 antibodies were used in a 1:800 dilution. Since the TNIP1 antibody was raised in rabbits and the C3 antibody was raised in mice, both primary antibodies were used at the same time. Secondary antibody staining was also performed simultaneously.

Other samples were stained with phosphorylated Histon H3 (PHH3). Since the PHH3 antibody and the TNIP1 antibody were both raised in rabbits, this staining was done in two sequential steps. First, PHH3 rabbit-polyclonal primary antibodies (Invitrogen) were prepared in a 1:500 dilution and incubated on cells at 4 °C overnight. Then, the secondary red fluorescent antibody (Goat-anti-Rabbit Alexa 456 from Invitrogen) was used in a 1:800 dilution and incubated in the dark at RT for 1 hour. Afterwards, cells were thoroughly washed with 1 x PBS (five times). The TNIP1 immunocytochemical staining followed and was performed according to the protocol described above using green fluorescent secondary antibodies (Goat-anti-Rabbit Alexa 488 from Invitrogen). This sequential staining approach resulted in some overlap in the PHH3 stained and TNIP1 stained regions. The PHH3 binding regions were stained twice, first binding to the red fluorescent secondary antibody and then binding once more to the green fluorescent antibody, resulting in a yellow tone due to overlap. Due to different cellular localizations (PHH3 is only found in the nucleus and TNIP1 in both the nucleus and the cytoplasm) the stained areas could clearly be distinguished. However, a different approach in evaluation followed as will be outlined in chapter 2.4.5.7..

Lastly, some samples were stained with Phalloidin which immunochemically detects F-Actin. This staining was done after the other immunocytochemical staining procedures

had been finished, but before cells were stained with Hoechst. Selected samples were incubated in 50 µg/mL Phalloidin-TRITC diluted in 1 x PBS for 40 minutes. Afterwards, they were washed three times with 1 x PBS.

2.4.5.2. Image acquisition

To ensure an objective evaluation of the assays, I set up rules which were strictly followed to diminish possible bias and allow for a more objective and representative analysis of the final images.

In order to compare images, image acquisition settings had to be identical for these selected samples. I.e., pTNIP1 treated and ct (mock transfected) cells were imaged in the same manner, as were siTNIP1 and scr cells. While for the first doublet, the pTNIP1 cells were used as the standard to obtain optimal image quality, for the siTNIP1 group of cells, the scr cells were used to provide the reference setting. This ensured that the staining was not overexposed and thus limited in measuring grayscale values. This procedure implied that results across different pairs (for example ct vs. siTNIP1) could not be compared, however, that was considered neither necessary, nor reasonable.

All images were taken with the Nikon LSM equipped with a 60X oil immersion objective (CFI Plan Apochromat Lambda D 60X Oil from Nikon). Pixel scan size was set at 2048 pixels. Some images were taken with a zoom factor of 1.0, while other images were taken with a zoom factor of 4.0. The following image acquisition settings remained the same for each control/sample doublet: photomultiplier tube, high voltage, offset and laser of each color channel. The color channels in question can be found in the table below.

Color channels for Immunocytochemistry

Channel	Laser	Emission	Color	Staining
Channel 1- DAPI	405.0	425 - 475	blue	Nucleus (Hoechst)
Channel 2 - Alexa 488	488.0	500 - 550	green	TNIP1
Channel 3- Alexa 555	561.0	570 - 620	red	Phalloidin (F-Actin) / Caspase-3 / phosphorylated Histon H3

As mentioned above, the settings for control cells and treated cells were always identical. To set these microscopical parameters for the green channel, I chose sections which showed the highest staining intensity, thus avoiding overexposure and improving the overall sensitivity of measurements. This channel was used for TNIP1 immunocytochemistry and was quantitatively evaluated. The blue and red channels were set up in a similar way to exclude background noise and avoid overexposure.

To compare the intensity of fluorescence across treatment groups, I always chose representatively stained areas and regions in which single cell discrimination was possible. At least three different images were taken of each coverslip (n = 9 total images of each treatment group).

2.4.5.3. Evaluation of cell numbers using the Hoechst staining

Nuclear staining with Hoechst 33258 was used to assure a reliable and comparable method of discriminating cell counts across different assays. Therefore, cell counting was chosen as a method of relating a staining intensity value to a certain number of cells. A cell counting procedure was established using the tap counter app „vivid counter“ (analogue to the mechanical cell counting device used in cell cultures). The images' blue channel (nuclear Hoechst staining) was opened in GIMP. Cells were counted by tapping the app screen, while simultaneously marking off counted cells in GIMP with a red marker tool. Then, results were cross-checked with the RGB-image, scanning for potential mismatches, like pigmentation conglomerates.

Moreover, several cell counting rules were established. In the images taken with a zoom factor of 1.0, it was decided to only count cell nuclei, that appeared in the image frame in their entirety. If multiple cell nuclei could not be differentiated from each other, they were not counted. If cells were in mitosis they were counted as two separate cells as soon as the nuclei were clearly separated. In images taken at 4.0 x zoom factor all cells which had at least 50 % of their nuclei positioned within the image were counted.

2.4.5.4. Evaluation of TNIP1 expression levels in stained cell cultures

To compare TNIP1 expression levels across treatment groups in immunocytochemically stained cell cultures, the average staining intensity of selected regions of interest was measured. Since the average staining intensity is also dependent on the number of cells present in a region, the average staining intensity was correlated to the number of cells pictured within the given region of interest.

In detail, the RGB image was split into its different color channels and the integrated density (ID) of the green channel (TNIP1 staining) was calculated using the Image J analysis and measuring tool. The ID is the product of the area and the mean gray value of a selected region, thus representing the sum of all pixel values of this region. In this case, the region corresponded to the limits of the captured image. The ID of each region was then divided by the cell number captured in this region. To compare data between groups, staining intensity AUs were created using the ct group images calculating the mean of the ID divided by cell number. This value served as a reference. An average staining intensity (in AU) was then calculated for each treatment group among all assays:

$$\text{staining intensity of sample } X \text{ [AUs]} = \frac{\text{sample } X \left(\frac{ID}{\text{cell number}} \right) \times 100}{\text{average of ct} \left(\frac{ID}{\text{cell number}} \right)}$$

“X” refers to a pTNIP1, scr or siTNIP1 sample, while ct is the HEK control group.

Statistical analysis was performed with a one-sided T-Test using R statistical software. A p-value below 0.001 was considered to be highly significant, a value between 0.05 and 0.001 was deemed significant.

2.4.5.5. Evaluation of the Phalloidin staining

Phalloidin staining was used for the immunocytochemical detection of F-Actin. This staining enables one to see the close-to full extension of a cell and measure the cell size. Images for the Phalloidin staining were taken with a 4.0 x zoom factor. Cell size analysis was done on 5 images per assay, totaling 15 images per treatment group. The cell area

was used as a surrogate parameter for cell size. Cell area was measured in the red (Phalloidin) channel using the freehand selection tool in Image J tracing the F-Actin cytoskeletal staining with Phalloidin. This was done abiding by the following rules: 1) Only one cell was to be selected including its cell processes. 2) The cell in question was to be fully displayed in the image. 3) If there was any overlap of different cells' processes, they were to be divided in half.

Considering this subjective way of discriminating cell area, an inter-rater test was performed using three different subjects rating four different images to account for inter-rater variability. The single-random-raters inter-rater correlation coefficient was then calculated with the psych package's ICC2 using R statistical software.

To compare data in between groups, AUs were calculated using the mean area values of the ct group as a reference. Since area measurements were normally distributed, the statistical analysis was performed with the Welch Two-Sided T-Test using R statistical software. A p-value below 0.001 was considered to be highly significant, a value between 0.05 and 0.001 was deemed significant.

2.4.5.6. Evaluation of the Caspase-3 staining

Caspase-3 (C3) is a well-established marker of apoptosis. C3 is a protease of the apoptotic pathway and gets activated by cleavage of the N-terminal pro-domain by caspase-8 and other enzymes (Ponder and Boise, 2019). The antibody that was used only stained cleaved C3.

Since cell staining might vary within a culture dish, for instance due to differences in antibody diffusion, I chose two different magnifications to obtain images. Both magnifications were intended for analysis of average staining intensity of the C3 staining, while the higher magnification would allow for a closer examination of the pTNIP1 group, as will be outlined below.

Thus, some of the images for the C3 staining were taken using a zoom factor of 1.0 (total of 9 images per treatment group), while others were taken using a zoom factor of 4.0 (total of 15 images per treatment group). Both groups were analyzed separately, following the

same protocol. The staining intensity of the red channel (C3) was analyzed in the same exact manner as the green channel, as described in chapter 2.4.5.4., to compare C3 expression levels among treatment groups. Once again, the average integrated density (ID) divided by cell number of all ct group images was used as an AU reference and AUs were calculated. For statistical analysis the Wilcoxon Rank Test was implemented in R statistical software.

Additionally, I decided to investigate whether there were differences in C3 expression levels within the pTNIP1 group, the group transfected with the pcDNA3.1zeoTNIP1 plasmid. This was possible, since the plasmid transfection rate was only around 40 % and cells expressing only endogenous levels of TNIP1 (called pTNIP1(-)) and cells overexpressing TNIP1 (called pTNIP1(+)) were pictured in the same image. I aimed to explore whether C3 expression levels were different in pTNIP1(+) and pTNIP1(-) cells. It should be briefly mentioned that this analytic approach could not be applied to the siTNIP1 group, since it was not possible to distinguish between si-mediated knockdown affected cells and non-affected cells in the images.

Although the difference between pTNIP1(+) cells and pTNIP1(-) cells is apparent when visually inspecting the image, a systematic approach was required to distinguish between the groups. Since TNIP1 is endogenously expressed and mostly present in the cytoplasm, to portray only pTNIP1(+) cells, the image would have to be gated in a way of only showing cells that well-exceeded the mean value of endogenous TNIP1 expression. To determine the threshold at which TNIP1 expression levels were no longer characterized as endogenous, but overexpressed, the mean value of TNIP1 expression was determined in each assay and the standard deviation of this mean value was added on top. Since microscopical settings varied between the three assays, three different threshold values were calculated. To obtain these threshold values, the mean gray value of the cytoplasm of several HEK 293 cells of the corresponding ct group was measured using Image J. Then, the standard deviation was calculated and added to the threshold value. Having gated the image with this upper threshold value, it then only showed cells expressing TNIP1 levels above the normal endogenous range. The cells pictured using this threshold were identified as pTNIP1(+) cells.

Thus, 15 high magnification (zoom factor 4.0) images derived from three different assays were used to identify equal amounts of TNIP1 overexpressing cells (pTNIP1(+)) and control cells (pTNIP1(-)). The ID was measured in each region of interest and corrected for background staining by subtracting the ID of a cell free region (background noise):

$$ID \text{ of cell selection} = ID \text{ of cell} - \left(\frac{ID \text{ of background}}{Area \text{ of background}} \times Area \text{ of cell selection} \right)$$

This formula is suitable for measuring regions of different sizes between cell regions and background regions. The AU measure represents the average staining intensity of each region of interest divided, using the mean ID value of all pTNIP1(-) cells included in the analysis as the AU reference. Using R statistical software, a Two-Sided T-Test was performed to reveal statistical significance. A p-value below 0.001 was considered to be highly significant, a value between 0.05 and 0.001 was deemed significant.

2.4.5.7. Evaluation of the phosphorylated Histon H3 staining

Histon H3 is part of the histon complex and gets heavily phosphorylated in the early prophase and all throughout the metaphase of mitosis/meiosis. Since Histon H3 gets dephosphorylated again thereafter, the phosphorylated form of Histon H3 (PHH3) is a suitable marker for proliferating cells (Elmaci et al., 2018).

Given that both the TNIP1 and the PHH3 antibody were raised in rabbits, this staining was done in two sequential steps as described above (see chapter 2.4.5.1.). As previously mentioned, this meant there was some overlap in PHH3 stained and TNIP1 stained areas. Since the PHH3 staining was performed first, the binding sites of the red fluorescent antibody are specific to PHH3 and when looking at the red channel only PHH3 bound sites can be observed. However, the TNIP1 staining was performed afterwards and the secondary green fluorescent antibodies were found to bind both to TNIP1 binding sites and PHH3 binding sites. Therefore, the green channel not only shows the TNIP1 binding sites, but also the PHH3 binding sites. Of course, this meant that staining intensity of the green channel could not be used as a parameter of analysis. Still, it was easy to distinguish both stainings in the RGB image: for one, PHH3 stained regions appeared yellow due to the overlay of both the red fluorescent PHH3 secondary antibodies and the green

fluorescent TNIP1 secondary antibodies. Moreover, the staining pattern of the antibody was different: PHH3 was strictly nucleus bound, while TNIP1 was present in both nucleus and cytoplasm.

As previously mentioned, staining intensity could not be used as a parameter, since the TNIP1 channel displayed both TNIP1 and PHH3 binding sites. Thus, I decided to use absolute cell count of positively stained cells as a method of analysis. I chose two approaches, both of which required me to count the PHH3 positively stained cells.

For this purpose, the total cell count of each image was obtained according to the rules described in chapter 2.4.5.3.. Then, to count the PHH3 positively stained cells, the red (PHH3) channel of each image of a sample was opened in Image J and a threshold was set to eliminate background noise. The upper threshold was set at 150, the lower threshold at 0. Again, cells were counted according to the rules mentioned above. Afterwards the expression level of PHH3 was calculated based on absolute cell numbers:

$$PHH3 \text{ expression level} = \frac{\text{total PHH3 positive cells}}{\text{total cells}}$$

For the ct/ pTNIP1 comparison group, the PHH3 expression level was calculated in AU. The average PHH3 expression level for all ct samples served as the AU reference for these groups. For the scr/siTNIP1 comparison group, the PHH3 expression level was also calculated using AU. However, the average PHH3 expression level from all scr samples was used as the AU reference. Statistical analysis was performed using the Wilcoxon Rank Test in R.

In addition to this approach, I opted to examine whether PHH3 expression levels differed among cells in the pTNIP1 group, the group transfected with the pcDNA3.1zeoTNIP1 plasmid. As described above, this was possible since the vector transfection rate was around 40 % and cells expressing endogenous levels of TNIP1 (pTNIP1(-)) and cells overexpressing TNIP1 (pTNIP1(+)) were captured in the same image. Once again, it should be mentioned that this approach was not suitable for the siTNIP1 group, as a clear differentiation between si-knockdown affected and non-affected cells was not possible. To identify and count both pTNIP1(+) and pTNIP1(-) cells the gating method described in chapter 2.4.5.6. was employed.

Once pTNIP1(+) and pTNIP1(-) cells were counted, images were merged with the red (PHH3) channel to check for concomitant PHH3 expression and cells were counted in the manner described above. Then, PHH3 expression levels in pTNIP1(+) and pTNIP1(-) cells were calculated. AUs were established using the mean PHH3 expression level in pTNIP1(-) cells:

$$\text{Expression level of PHH3 in pTNIP1(-) cells} = \frac{pTNIP1(-)cells \cup PHH3(+)cells}{pTNIP1(-) cells}$$

$$\text{Expression level of PHH3 in pTNIP1(+) cells} = \frac{pTNIP1(+)cells \cup PHH3(+)cells}{pTNIP1(+) cells}$$

The statistical analysis of the expression levels was performed using the Wilcoxon Rank Test implemented in R statistical software. A p-value below 0.001 was considered to be highly significant, a value between 0.05 and 0.001 was deemed significant.

2.4.6. Wound healing assay

The wound healing assay, also termed scratch assay, is often used to analyze cell mobility in a dense cell population (Jonkman et al., 2014), although, as will be discussed later, this assay does not distinguish between migration, proliferation and cell death per se. To perform a wound healing assay a scratch is made into a subconfluent grown cell turf, which can then refill over time. The area of the gap is recorded and measured at different points in time.

Since I wanted to compare the migration patterns of overexpressing (pTNIP1) and control (ct) cells, as well as TNIP1 diminished (siTNIP1) and control (scr) cells, HEK 293 cells were first transfected with pcDNA3.1zeoTNIP1, siTNIP1 or scr. The duration of the scratch assay was meant to capture the peak expression window of the reagents and not exceed 20 hours, at which point most scratches have already closed up. Therefore, different time windows were chosen depending on the transfection reagent, i.e. plasmid or siRNA. The wound healing assay captured hours 14-34 for cells treated with scr/ siTNIP1, since peak siRNA activity presents around the 24-hour mark. For cells transfected with the

pcDNA3.1zeoTNIP1 plasmid, the time window for the scratch assay ranged from 24-44 hours, since peak vector expression is observed between 24-48 hours.

Cells were seeded at a density of 1×10^5 cells in a 24-well cell culture plate, assuring a subconfluent cell turf. Cells were transfected according to the protocol described in chapter 2.4.4. and in agreement with the timeline specified above. To start the experiment the medium in the wells was exchanged with fresh DMEM and a scratch was made from top to bottom in the middle of each well using a 200 μ L pipette tip. The conditions of the timelapse microscope chamber (Leica DM IRE2, Leica) were set at 5 % CO₂ and 37 °C. The program was defined to take a „Brightfield“ image of three different positions in each well every hour for 20 hours. These images always depicted both sides of the scratch.

The goal was to analyze wound closure rate as a parameter of cell migration. Firstly, the cell free scratch area was measured by using the freehand selection tool in Image J. To define borders most accurately, the following guides were given: Single cells, not part of the cell line surrounding the scratch (already lying in the otherwise cell empty scratch) were not measured separately or subtracted, they were included in the wound area. As the assay went on, it became increasingly difficult to decide whether a cell was an outlier (as previously described) or whether it was part of the migrating and proliferating cell wall. To improve accuracy, line drawings were always compared in preceding and succeeding images. If the cells were not completely portrayed, they were counted as part of the cell wall (not included in the wound area). Considering this subjective way of measurement, an inter-rater test was later performed with three different subjects to account for inter-rater variability. The single-random-raters inter-rater correlation coefficient was calculated using the psych package's ICC2 in R statistical software.

Once wound areas were measured at different timestamps, the wound closure rate was calculated for every image for selected points in time (t (hours) = 0, 5, 10, 15, 20) for every assay in each treatment group according to the following formula:

$$\text{wound closure rate} = \frac{A(t = 0) - A(t = x)}{A(t = 0)} \times 100 \%$$

A(t = 0): Wound area at start (t = 0)

A(t = x): Wound area at times x = (0, 5, 10, 15, 20) in hours

The wound closure rate (as a parameter of cell migration rate) was calculated for each assay for every treatment group. Since the area approached zero in some samples, a non-parametric statistical test was used for analysis. The Friedman Test was performed on the whole data set, as well as individually at specific time slots, allowing one to analyze variance across multiple time stamps in the scratch assay. This was then followed up with a pairwise comparison test (Eisinga et al., 2017), discriminating between treatment groups, using the p-value adjustment method “bonferroni”. A p-value below 0.001 was considered to be highly significant, a value between 0.05 and 0.001 was deemed significant.

2.4.7. Flow cytometry

Flow cytometry is often used to analyze cell proliferation. This technique allows one to count thousands of cells in seconds and divide them by the staining profile, cell size and cell surface. DNA staining agent propidium iodide (PI) was used to identify proliferating cells. PI stains cells in G1/2 and G0 phase stronger than cells in the S phase, due to higher DNA amounts (Darzynkiewicz and Juan, 1997).

For flow cytometric analysis, cells were seeded at a density of 2×10^5 cells per well in a 6-well cell culture plate. To achieve a degree of cell cycle synchronization, cells were split at the same time. They were then transfected according to the protocol described in chapter 2.4.4.. Cell harvest occurred after 24 hours for groups scr and siTNIP1, while groups ct and pTNIP1 were harvested after 48 hours, according to the peak expression windows of the respective transfection agents. Then, cells were resuspended in 0.5 mL 1 x PBS and gently mixed by aspiration, avoiding the creation of cell clumps. Next, cells were fixed by transferring the suspension into centrifuge tubes containing 4.5 mL of 70 % ethanol on ice. Cells were kept at 4 °C for a minimum of two hours. For cell staining, the ethanol-suspended cells were centrifuged at 300 x g for 5 minutes, then the ethanol was

decanted thoroughly. The cell pellet was suspended in 5 mL of 1 x PBS, left at RT for 30 seconds and then centrifuged at 300 x g for 5 minutes. Next, the cell pellet was suspended in 1 mL of PI staining solution (Table 10) and kept in the dark at RT for 30 minutes, before transferring samples to the flow cytometer (FACScan unit, BD Biosciences). The flow cytometer was calibrated, and basic settings were established using ct (mock transfected) samples. Channel FL3 was used for PI extinction measurements (Laser set at 488nm).

Analysis followed with the Flowing software 2 (Turko Bioscience Center). All cell populations were gated in the same manner to avoid doublets and outliers: The cell count number was set to 10.000, the peak multiplier was set to 2.2 and the width multiplier was set to 1.4. These settings remained the same for every treatment group. Cell cycle gates G1, G2 and S were created and calculated for each sample. The fraction of G1 events (single DNA content) to the sum of events in G2 and S (intermediate to double DNA content during or after DNA replication) was calculated and named the “mitotic index”, to determine the mitotic activity of different treatment groups:

$$\text{mitotic index} = \frac{G1 \text{ Events}}{G2 \text{ Events} + S \text{ Events}}$$

The average coefficient of variance (CV) at G1 was calculated across treatment groups, to evaluate quality of information. According to Ormerod et al. (1998) the CV of the G1 peak should be lower than 8 % for a good quality assay. Statistical analysis was performed using the Wilcoxon Rank Test in R statistical software. A p-value below 0.001 was considered to be highly significant, a value between 0.05 and 0.001 was deemed significant.

2.5. Statistical Analysis

The statistical analysis was performed using the R Statistical Software package in RStudio version 4.3.2 (R Core Team 2023). To determine the most suitable statistical tests for each assay, the Levene Test was used to evaluate differences in variance across treatment groups. All assays were evaluated for normal Gaussian distribution using the

“DescTool” package (Signorell, 2024) by drawing histograms and quantile-quantile-plots. Additionally, it was taken into consideration that some measurements theoretically getting continuous values were considered parametric (cell size), while others (ratios) were mainly considered non-parametric. Parametric datasets were analyzed using one-sided (Western Blotting and TNIP1 staining) and two-sided T-tests (Caspase-3 and Phalloidin staining) with a significance level of $p < 0.05$. Non-parametric datasets were analyzed using a two-sided Wilcoxon Rank Test with a significance level of $p < 0.05$. In some instances, more specific tests like the two-sided Friedman Test were used for non-parametric data to allow for analysis over different time points (wound healing assay). Again, a p-value below 0.05 was considered significant. Generally, p-values below 0.001 were considered to be highly significant. The tests used are specified in the corresponding assay chapters. For inter-rater reliability testing, the package “psych” was employed (Revelle, 2024). Graphical depictions of the results were created using the “ggplot2” package (Wickham, 2016).

3. Results

3.1. Cloning of pcDNA3.1zeoTNIP1

In order to express full length TNIP1 in eukaryotic cells, TNIP1 needed to be cloned into an expression vector. I used a pcDNA3.1 zeocin vector, since it was well established in the lab. This vector drives gene expression under the CMV (cytomegalovirus) promoter. The human TNIP1 sequence was derived from a Blasticidin-resistant pUNO-TNIP1 vector obtained from InvivoGen. This vector encoded isoform 3 transcript variant 5, containing all known domains of TNIP1.

At first, I tried to clone the TNIP1 amplicon, which had BamHI sites on both ends, by sticky end ligation into a BamHI linearized pcDNA3.1zeo vector. This direct cloning of PCR amplified TNIP1 into pcDNA3.1zeo did not work. Therefore, TNIP1 was first subcloned into a pMini vector using the NEB[®] PCR Cloning Kit. The TNIP1 sequence was amplified from the pUNO-TNIP1 vector using BamHI containing primer sets. After successfully establishing the PCR protocol, high amounts of the TNIP1 insert were generated and the TNIP1 product was ligated into the pMini vector. This vector was then digested with BamHI-HF to extract the 1800 bp sized TNIP1 fragment which had BamHI restriction sites on both sides by gel electrophoresis. The expression vector pcDNA3.1zeo was cut with BamHI-HF and was then dephosphorylated using rSAP to avoid self-ligation. Using T4-Ligase, vector and insert were fused. Finally, XL-1 blue cells were transformed with the ligation mixture. Single colonies were picked and the vector

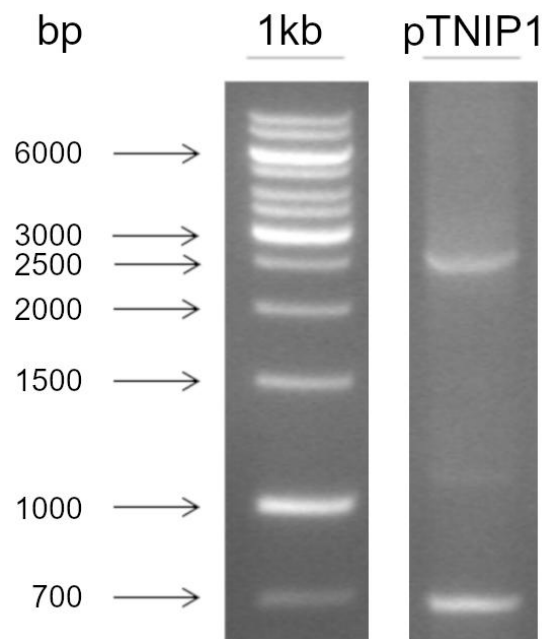


Figure 6: Colony PCR of bacteria transformed with pcDNA3.1zeoTNIP1

The colony PCR was expected to show a single band at 2600 bp. The band at 700 bp might be some bacterial DNA products amplified in parallel. The 1kb DNA ladder (1kb) is depicted on the left-hand side of the image.

products were analyzed using colony PCR (see Figure 6), restriction analysis (Figure 7) and sequencing. Since colony PCR is a quick and simple method to screen for positive clones, it was performed first. After picking several clones, the bacterial suspension was directly analyzed by PCR using primers Seq1 and BghR. Colonies revealing a fragment of 2600 bp were selected and further analyzed. Please note, that the 700 bp fragment seen in Figure 6 is most probably a bacterial DNA amplicon. To rule out that any erroneous DNA was integrated into these bacteria, a restriction digest was performed.

Restriction digestion additionally enables one to look for the orientation of the TNIP1 fragment within the vector. This is an important step, since cloning was done with BamHI restriction sites on both ends of the TNIP1 fragment, which principally enables the insertion in both orientations.

EcoRI was the restriction enzyme chosen to check for insert orientation. Digestion with this enzyme should reveal fragment sizes of 5162, 1567 and 306 bp for sense orientation and DNA fragment sizes of 6536, 306 and 193 bp for antisense insertion. As can be seen in Figure 7, both orientations can clearly be distinguished. Additionally, BglII was used to characterize the correctness of the insertion. Again, the expected DNA bands could be seen in electrophoresis, further supporting these results (data not shown).

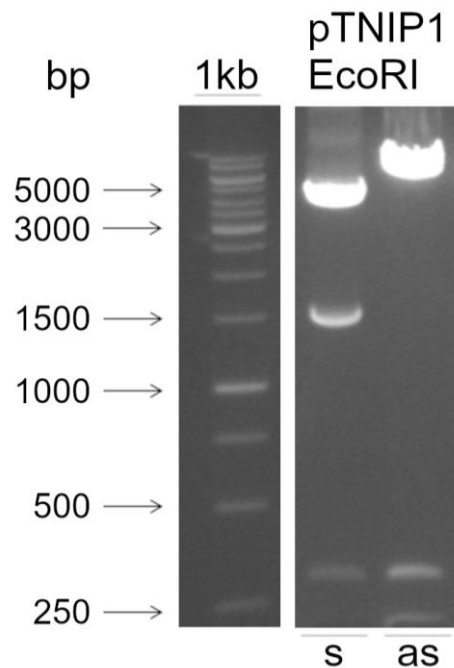


Figure 7: Characterization of pcDNA3.1zeoTNIP1 using restriction analysis

To characterize the orientation of the TNIP1 insert within the pcDNA3.1zeo vector, the plasmid was digested with EcoRI. The digestion revealed the expected sizes for a sense orientation within the vector. Expected band sizes: 5162, 1567 and 306 bp for sense (s) and 6536, 306 and 193 bp for antisense (as) orientation. The 1kb DNA ladder (1kb) is depicted on the left side of the image.

Since single nucleotide exchanges and minor sequence errors cannot be determined by the procedures described so far, the insert and surrounding DNA sequences were sequenced.

Sequencing was performed using three different primers (see chapter 2.2.5.), hereby ensuring every sequence of TNIP1 was covered twice. It was revealed that the chosen sample had no mutations and that the insert was positioned in the correct (sense) direction.

The plasmid was therefore appropriate for further use. A sequence map can be found in Figure 8, which also contains the restriction sites mentioned above. Finally, a Midi-prep was performed to generate high amounts of the plasmid using the NucleoBond® Xtra Midi kit protocol. Glycerol stocks were prepared and frozen at -80°C.

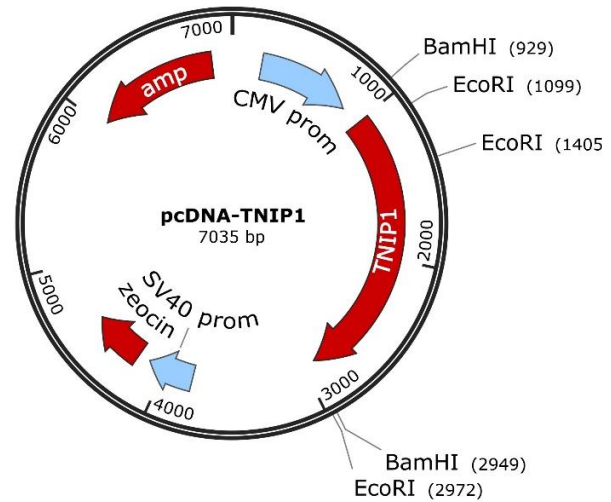


Figure 8: Plasmid map of pcDNA3.1zeoTNIP1

The plasmid map depicts the pcDNA3.1zeo vector with TNIP1 inserted in sense orientation. Major coding products are shown in red, regulatory elements in blue, and relevant restriction sites are portrayed outside the plasmid circle. The map was created using SnapGene software.

3.2. Generation and characterization of transfected HEK 293 cells

Key experiments of this thesis relied on the ability to up- and downregulate TNIP1 expression in a cell model. Therefore, the expression levels of TNIP1 expression were first investigated in different cell lines (data not shown). Based on these experiments, HEK 293 cells were deemed a promising candidate cell line for this thesis. Hence, an in-silico analysis to gather further information on TNIP1 expression levels was performed. A freely available data set from the Gene Expression Omnibus database (Edgar, 2002) was used for this purpose. TNIP1 transcripts were extracted from the Omnibus data by using a list of TNIP1 transcripts published by the ENSEMBL community (Harrison et al., 2024).

TNIP1 expression levels in HEK 293 cells were found to be moderate and thus appropriate for overexpression and repression of TNIP1 expression (Figure 9). Additionally, a dataset of transcriptomics data derived from HEK 293 cells grown to confluency and at a subconfluent level was analyzed and revealed that cell density impacts on TNIP1 expression levels. When cultured at subconfluency (low density), TNIP1 expression is significantly lower than in HEK 293 cells cultured at confluency (high density). Interestingly, analyzing this relationship between TNIP1 expression and cell seeding density in other cell lines resulted in different TNIP1 expression behaviors (data not shown).

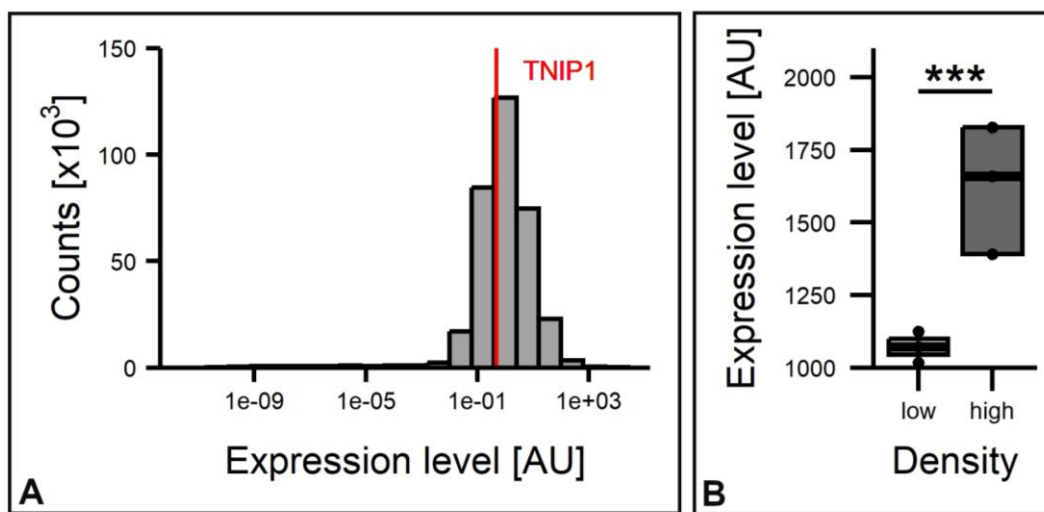


Figure 9 (A and B): Cell density influenced TNIP1 expression in HEK 293 cells

A: In silico analysis of TNIP1 expression in HEK 293 cells. The frequency plot demonstrates the number of transcripts of distinct gene expression levels found in HEK 293 cell cultures. A total of more than 350,000 transcripts were included. The TNIP1 expression level is marked by a red line, demonstrating TNIP1 expression levels to be moderate in HEK 293 cells. Please note that the x-axis is depicted in a logarithmic scale.

B: TNIP1 expression levels were measured at different cell densities, revealing that while subconfluent (low) cell densities yield low TNIP1 expression levels, confluent (high) densities lead to higher TNIP1 expression at a significance level of $p < 0.001^{***}$ (ANOVA, $n = 3$). The y-axis depicts the TNIP1 expression level in AU, while the x-axis shows the different cell densities analyzed.

To establish a functional transfection protocol which worked equally well for siRNA and plasmids, different reagents and different reagent concentrations were tested. For an easy evaluation of transfection efficiency, pcDNA3.1zeoEGFP (green fluorescent) and siGLO

siRNA (red fluorescent) were used, which both express fluorescent proteins in living cells and can be imaged without staining procedures. It was determined that a final concentration of 0.5 $\mu\text{g}/\mu\text{L}$ of plasmid using the Dharmafect Duo transfection reagent at 0.25 % was optimal for transfection. For siRNA transfection, a final concentration of 100 nM of siGLO and 0.25 % of transfection reagent Dharmafect Duo was found to yield optimal transfection rates. Counting the number of transfected cells revealed that about 40 % of cells expressed EGFP, while all cells showed red fluorescent siGLO staining (Figure 10).

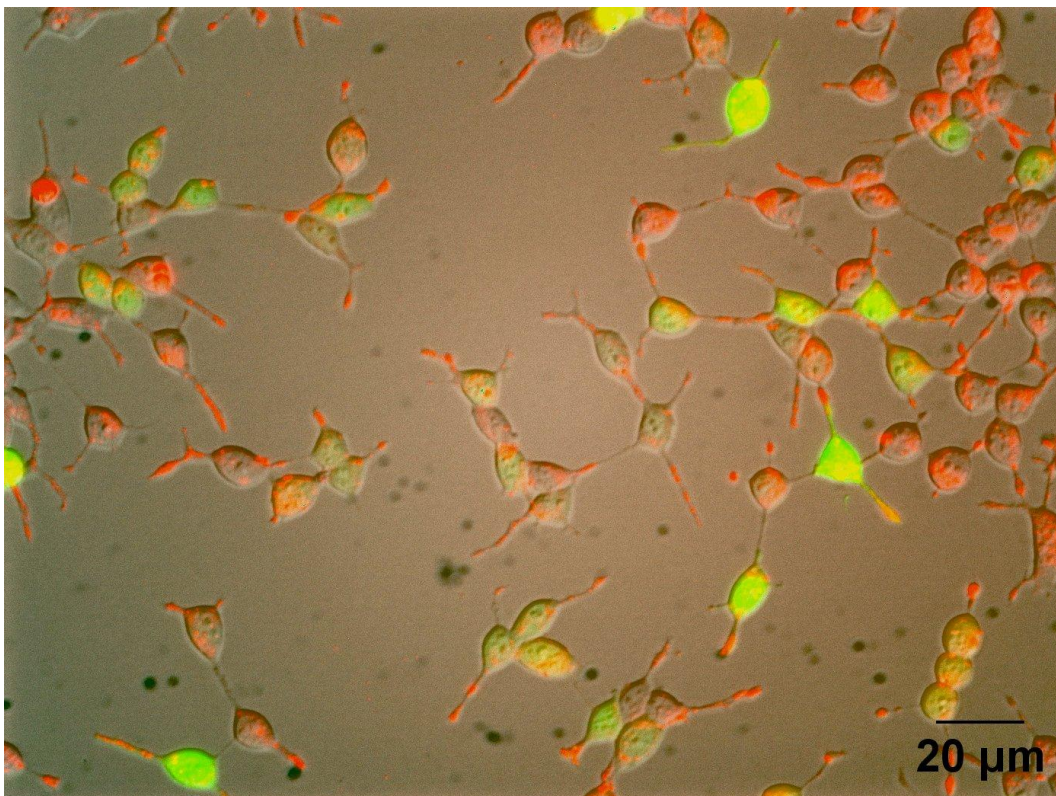


Figure 10: HEK 293 cell transfection efficiency

HEK 293 cells were transfected with an EGFP-Plasmid (green) and siGLO-siRNA (red) and imaged using the Timelapse microscope (Leica DM IRE2). While all cells appeared to be transfected with the siGLO agent, only about 40 % of the cells expressed the EGFP vector.

Next, the time windows of peak expression for both plasmid and siRNA transfection were identified: Plasmid expression appeared to be highest after 24 to 48 hours, while siRNA expression peaked around the 24-hour mark.

Western Blotting was employed to determine whether TNIP1 could be overexpressed using the pcDNA3.1zeoTNIP1 expression vector and whether endogenous expression could be diminished using siRNA. A TNIP1 specific antibody was used to detect TNIP1, Beta-Actin was used as a positive loading control.

Thus, three independent Western Blots were performed, and band intensities were analyzed densitometrically. HEK 293 cells transfected with the pTNIP1 expression vector expressed significantly more TNIP1 than the control group. On the other hand, cells transfected with siTNIP1 and scr did not reveal significant differences in TNIP1 expression levels. Using a one-sided Two-Sample T-Test at a significance level of $p < 0.05$ revealed the pTNIP1 group expressed significantly more TNIP1 in comparison to the ct group ($n = 3$, $p = 0.008^{**}$). There was no significant difference in the scr/siTNIP1 group ($n = 3$, $p = 0.825$). Below, TNIP1 expression levels of the different treatment groups can be seen, next to one of the Western Blots that was performed (Figure 11).

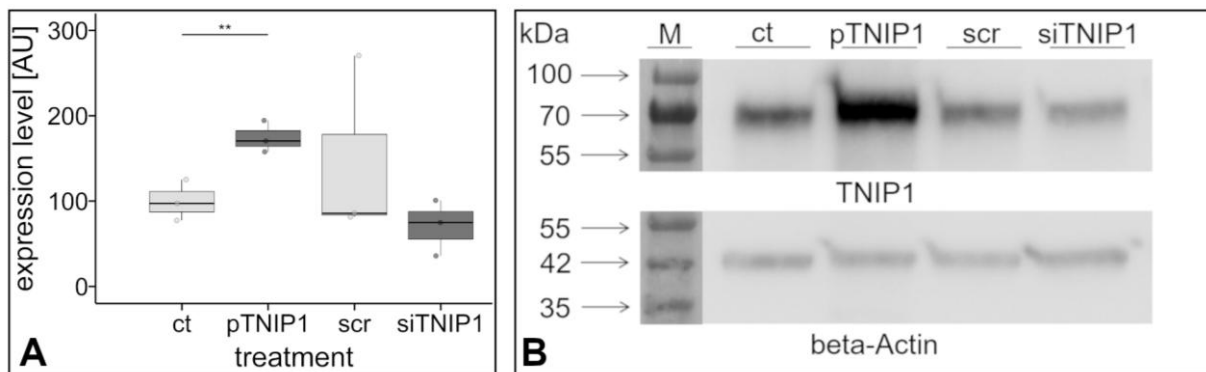


Figure 11 (A and B): Overexpression and knockdown of TNIP1 in Western Blot

HEK 293 cells were transfected according to protocol. Beta-Actin was used as a positive loading control.

A: Box plot. The y-axis shows the TNIP1 expression level in AUs. The x-axis shows the different treatment groups and their corresponding control groups: pTNIP1 (transfected with pcDNA3.1zeoTNIP1) and ct (mock transfection, control for pTNIP1), siTNIP1 (transfected with downregulating siRNA) and scr (control for siTNIP1). The one-sided Two-Sample T-Test revealed a significant difference in the ct/ pTNIP1 group ($n = 3$, $p = 0.008^{**}$). There was no significant difference found in the scr/ siTNIP1 group ($n = 3$, $p = 0.825$).

B: Western Blot. In the upper half of the image, the bands for TNIP1 can be observed at 72 kDa, while the lower half portrays the corresponding Beta-Actin bands at 42 kDa. The PageRuler™ Prestained Protein Ladder can be seen on the left-hand side of the figure.

Since transfection efficiency might obscure real overexpression rates in Western Blotting and having seen a tendency for downregulation in the Western Blot, I analyzed TNIP1 expression in immunocytochemically stained cell cultures. This assay needs careful consideration, since the immunocytochemical staining intensity might vary quite significantly between different stainings. Therefore, I took care that microscope settings for the samples pTNIP1/ siTNIP1 were always normed using the respective controls ct/ scr. Intensity measurements revealed a highly significant difference between groups (one-sided Two-Sample T-Test, $n = 6$, $p < 0.001^{***}$ for ct/ pTNIP1, $p < 0.001^{***}$ for scr/ siTNIP1), portrayed in Figure 12. It should be mentioned, that each n is composed of roughly 80-150 cells measured but was compared as a group to avoid artificially increasing sample size.

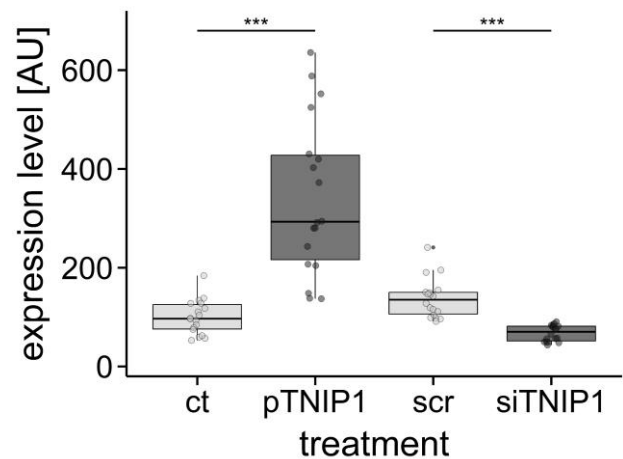


Figure 12: Modulation of TNIP1 expression in HEK 293 cells

HEK 293 cells were transfected with pcDNA3.1zeoTNIP1 (pTNIP1) or siRNA (siTNIP1, si-knockdown) and stained immunocytochemically for TNIP1, control groups (ct and scr) were prepared accordingly. Signal intensities were measured by Image J and single cell cultures were quoted as independent experiments. Highly significant differences between groups were observed ($n = 6$): ct/ pTNIP1 ($p < 0.001^{***}$) and scr/ siTNIP1 ($p < 0.001^{***}$), as revealed by testing with a one-sided Two-Sample T-Test.

3.3. Effect of TNIP1 on cell apoptosis

Since TNIP1 was known to be involved in several cell death pathways, I examined cells for apoptotic morphological characteristics. A common trait of dying cells is cell shrinkage or, in rarer cases, initial cell hypertrophy. Cell size was measured in Phalloidin stained HEK 293 cells transfected with a pcDNA3.1zeoTNIP1 plasmid or in cells with diminished TNIP1 expression by siRNA downregulation. Visual inspection of these cells did not reveal

any apparent differences. Cells had comparable sizes, no differences in cell processes or cell shrinkage could be observed between treatment groups. Even when only considering TNIP1 overexpressing cells, no changes in morphology could be seen. To verify this visual

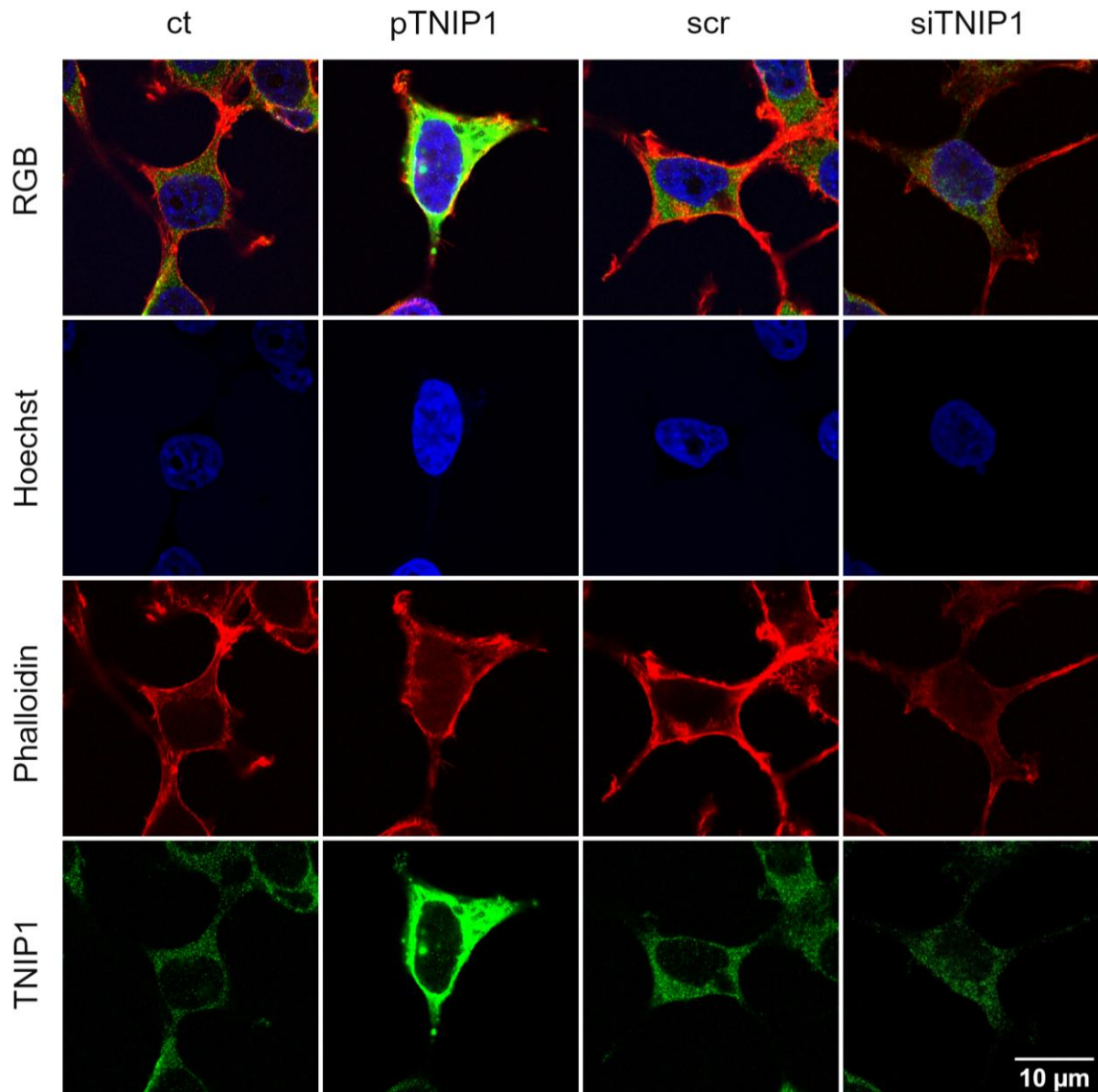


Figure 13: HEK 293 cell size was not affected by TNIP1 modulation

HEK 293 cells were transfected according to protocol. Immunocytochemical staining of F-Actin with Phalloidin-TRITC p1951 (red), TNIP1 (green) and nuclear staining with Hoechst 33258 (blue) was performed after cells were fixed. No morphological changes relating to apoptosis, nor changes in cell size were observed in the different treatment groups: ct (mock transfection, control for pTNIP1), pTNIP1 (pcDNA3.1zeoTNIP1), scr (scramble, control for siTNIP1) and siTNIP1 (downregulating siRNA).

impression, I measured the area of single cells. Staining with Phalloidin allowed for a clear outline of HEK 293 cells as can be seen in Figure 13.

Welch's two sample T-Test revealed no significant difference between groups ct/ pTNIP1 ($n = 3$, $p = 0.429$) and scr/ siTNIP1 ($n = 3$, $p = 0.077$), demonstrating that the cell area did not change considerably (Figure 14).

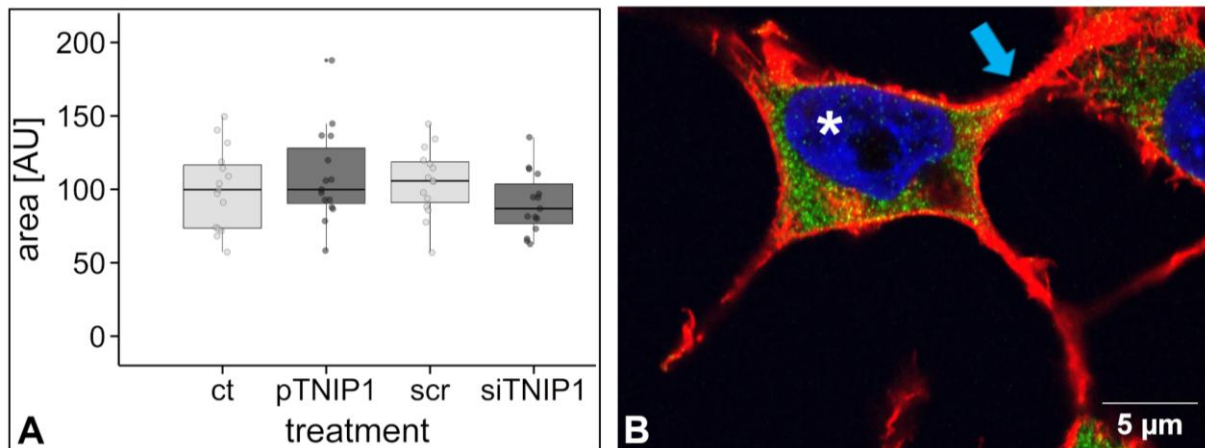


Figure 14 (A and B): TNIP1 overexpression or knockdown did not affect HEK 293 cell size

HEK 293 cells were transfected with a pcDNA3.1zeoTNIP1 expression vector and with downregulating siRNA. Cells were then stained for TNIP1 and F-Actin. Hoechst 33258 was used for nuclear correlation staining. Cell area was measured using free-hand selection tools in Image J. The inter-rater correlation coefficient was excellent (0.92). The Welch Two Sample T-Test revealed no significant differences between groups ($n = 3$, $p = 0.429$ for ct/ pTNIP1, and $p = 0.077$ for scr/ siTNIP1).

A: Box plot. Cell area is portrayed in AU on the y-axis. The x-axis shows the different treatment groups: ct (mock transfection, the control for pTNIP1), pTNIP1 (pcDNA3.1zeoTNIP1), scr (siscramble, control for siTNIP1), siTNIP1 (downregulating siRNA).

B: Immunocytochemical stained cell. The image was taken from the scr group and shows a cell immunocytochemically stained for TNIP1 (green fluorescent), Hoechst nuclear staining (blue fluorescent, white asterisk) and F-Actin with Phalloidin (red fluorescent, blue arrow).

In order to evaluate whether measurements were dependent on the investigator, an inter-rater reliability test was performed using three judges and four objects. The raters had a reliability of 92 %, which is considered excellent according to Koo and Li (2016).

Since changes in cell size are a hallmark of advanced stages of cell death, I immunocytochemically stained transfected HEK 293 cells with an activated Caspase-3

(C3) antibody. C3 is a well-established apoptosis marker, which allows one to identify cells undergoing apoptosis, before they shrink or are washed off from the culture dish. C3 expression levels were measured in lower magnification images displaying multiple cells

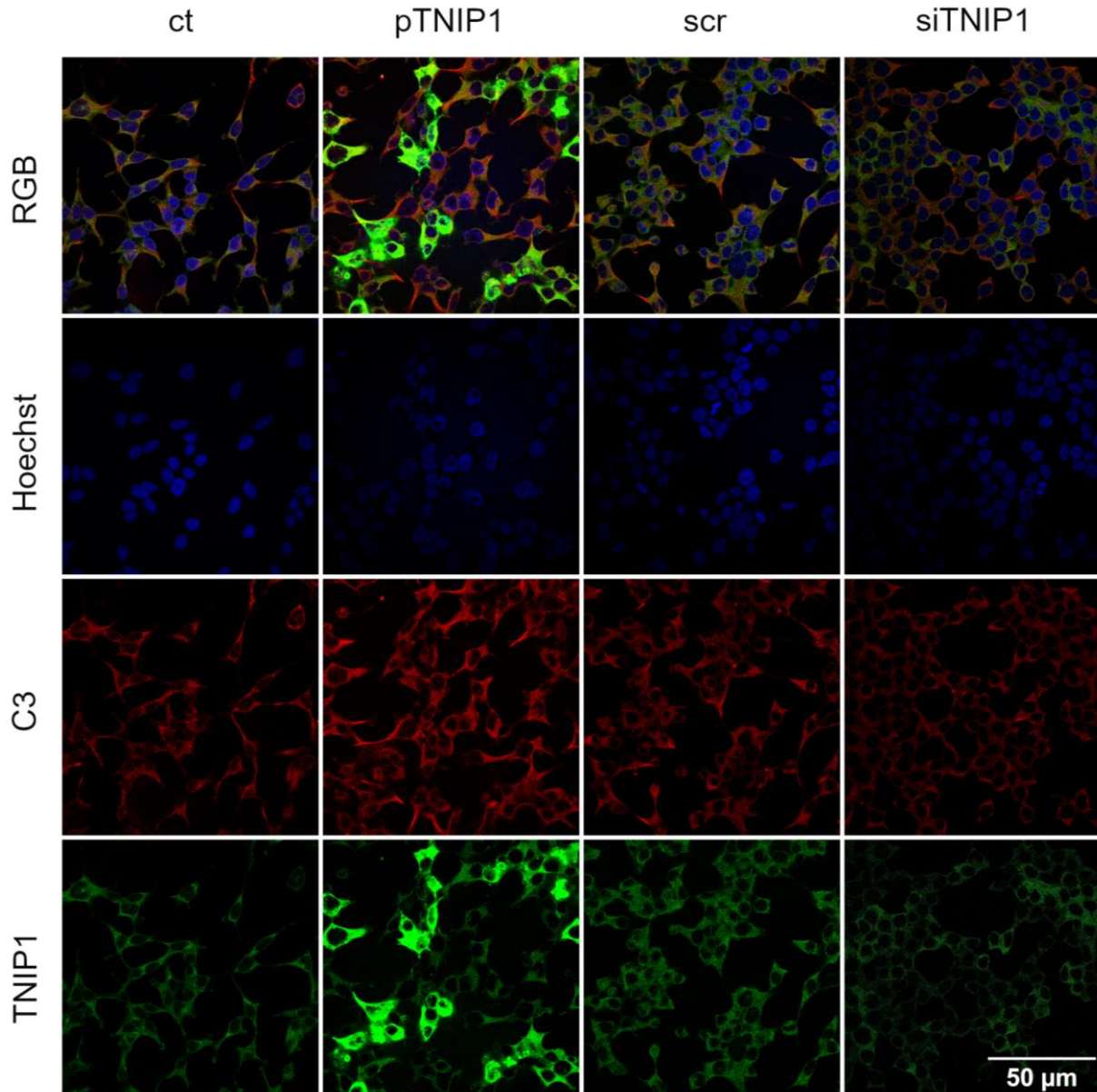


Figure 15: TNIP1 overexpression increased the number of Caspase-3 positive cells

HEK 293 cells were treated according to protocol. Immunocytochemical staining of Caspase-3 (C3, red), TNIP1 (green) and nuclear staining with Hoechst 33258 (blue) was performed after cells were fixed. A highly significant increase in C3 was detected in pTNIP1 cells (transfected with pcDNA3.1zeoTNIP1) vs. ct (mock transfected) cells (Two-Sided T-Test, $n = 3$, $p < 0.001^{***}$). No differences were observed between the scr (scramble)/ siTNIP1 (downregulating siRNA) groups (Two-Sided T-Test, $n = 3$, $p = 0.0749$).

and in higher magnification images of single cells. The intention was to get an insight into the overall expression pattern when looking at higher cell numbers and the C3 expression levels in individual cells. Additionally, the pTNIP1 group was inspected with greater detail to explore whether C3 expression levels differed between cells expressing endogenous levels of TNIP1 (pTNIP1(-)) and cells overexpressing TNIP1 (pTNIP1(+)) within the same culture dish.

At first, low magnification images of the different treatment groups in cell culture were inspected visually (Figure 15). In the pTNIP1 treatment group (transfected with the pcDNA3.1zeoTNIP1 vector) selected cells seem to exhibit higher levels of TNIP1. In parallel, higher amounts of C3 appeared to be present in this population. Contrastingly, the siTNIP1 group seemed to display lower levels of TNIP1 and C3. In order to quantify these impressions, I analyzed 9 different images from each treatment group.

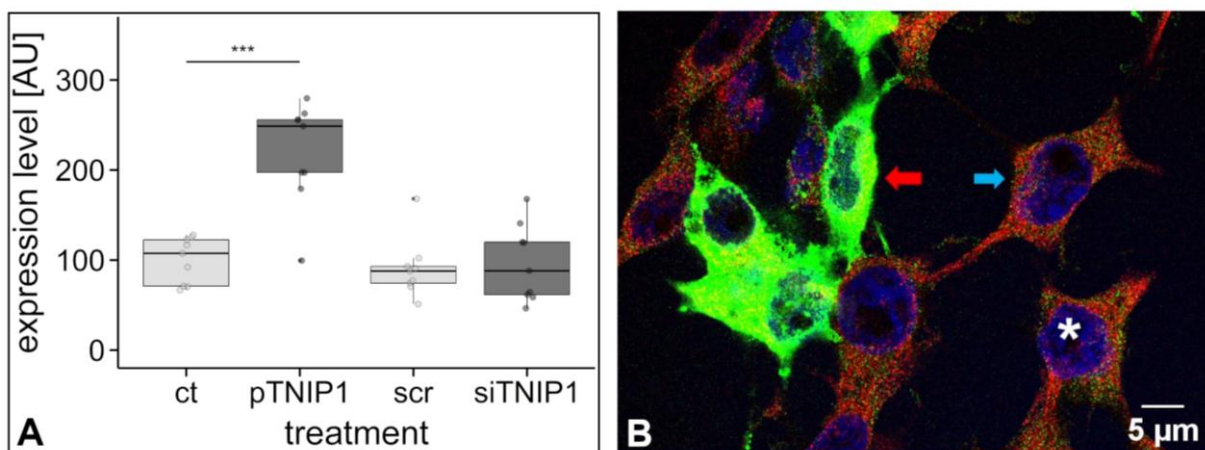


Figure 16 (A and B): TNIP1 upregulation resulted in higher Caspase-3 expression in HEK 293 cells

HEK 293 cells were treated according to protocol. Immunocytochemical staining of Caspase-3 (red), TNIP1 (green) and nuclear staining with Hoechst 33258 (blue) was performed after cells were fixed. A Two-Sided Two-Sample T-Test was performed and revealed a highly significant difference between groups ct/pTNIP1 ($n = 3$, $p < 0.001^{***}$). No significant difference was observed between scr and siTNIP1 ($n = 3$, $p = 0.749$).

A: Boxplot. Expression levels of C3 in AUs are shown on the y-axis, the x-axis displays the different treatment groups: ct (mock transfection, control for pTNIP1), pTNIP1 (transfected with pcDNA3.1zeoTNIP1, overexpression), scr (scramble, control for siTNIP1) and siTNIP1 (transfected with downregulating siRNA).

B: Immunocytochemically stained cells. This image was taken from the pTNIP1 group. Cells were immunocytochemically stained with C3 and nuclear Hoechst staining (white asterisk). pTNIP1(+) positive cells overexpressing TNIP1 (red arrow) are seen next to pTNIP1(-) cells only expressing endogenous TNIP1 levels (blue arrow).

To analyze these images, I used a Two-Sided T-Test to compare C3 expression levels between treatment groups, which showed a highly significant difference between groups ct/pTNIP1 ($n = 3$, $p < 0.001^{***}$) and no difference between scr/siTNIP1 ($n = 3$, $p = 0.749$), as can be seen in Figure 16. Thus, C3 is highly expressed in a pool of pTNIP1 expressing

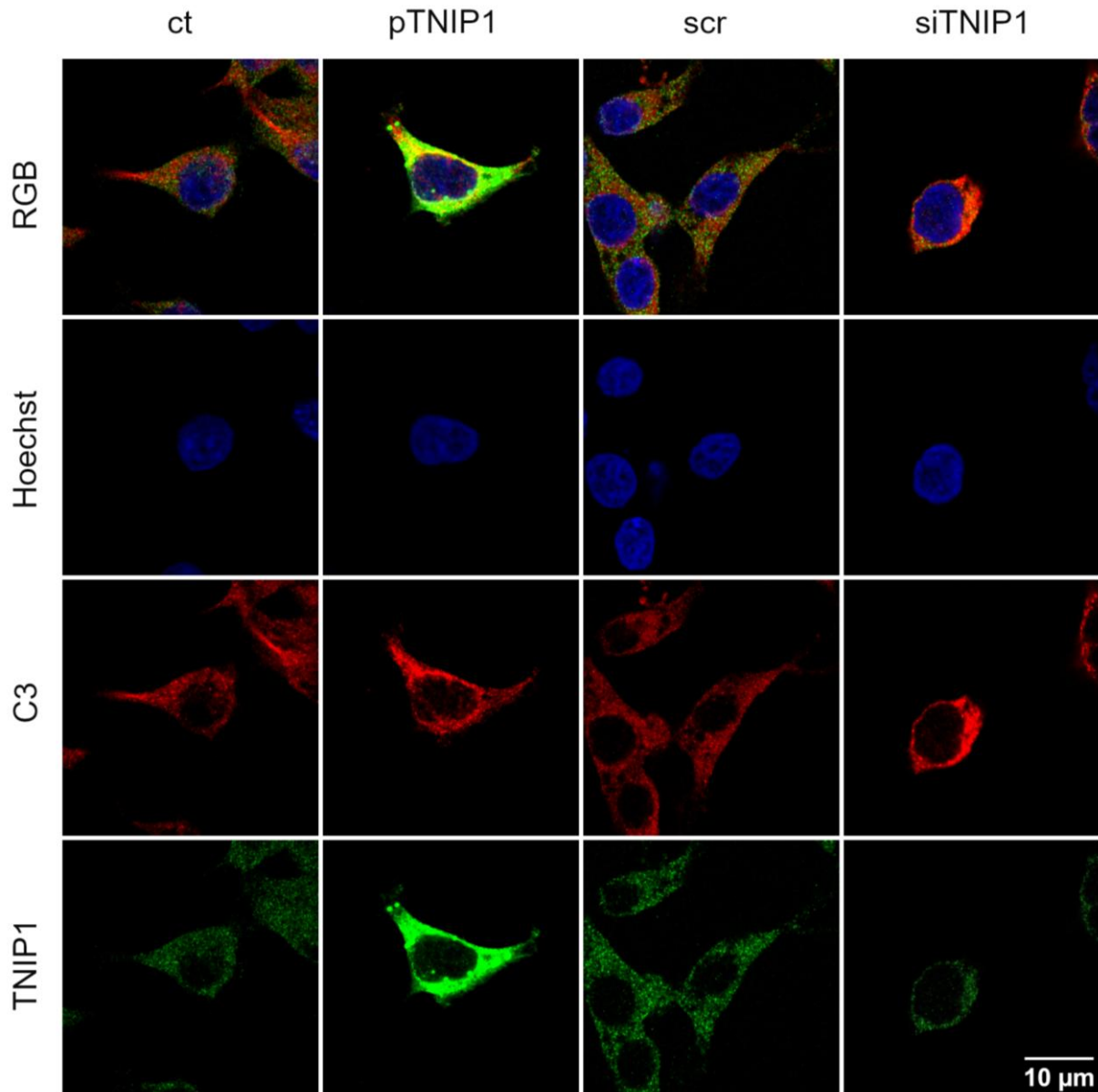


Figure 17: Cellular Caspase-3 expression levels were not affected by TNIP1 modulation

HEK 293 cells were treated according to protocol. Immunocytochemical staining of Caspase-3 (C3, red), TNIP1 (green) and nuclear staining with Hoechst 33258 (blue) was performed after cells were fixed. No significant differences in C3 expression levels were detected (Wilcoxon Rank Test, $n = 3$, $p = 0.901$ for ct/ pTNIP1, $p = 0.561$ for scr/ siTNIP1).

cells as compared to control cells, while C3 expression is not affected by siRNA treatments. Most likely, this increase in C3 expression is due to a higher number of cells expressing C3 in the pTNIP1 group. Theoretically, it might also be due to a difference in single cell C3 expression levels. I therefore analyzed levels of C3 expression in singular cells, using high magnification images (Figure 17).

The Wilcoxon Rank Test revealed there was no difference in between groups ($n = 3$, $p = 0.901$ for ct/ pTNIP1, $p = 0.561$ for scr/ siTNIP1). This suggests that the overexpression of TNIP1 increases the number of C3 positive cells, while C3 expression levels at the cellular basis remain unaffected (Figure 18A). In an effort to examine the pTNIP1 transfected group in more detail, I compared cells overexpressing TNIP1 (pTNIP1(+) cells) to cells expressing

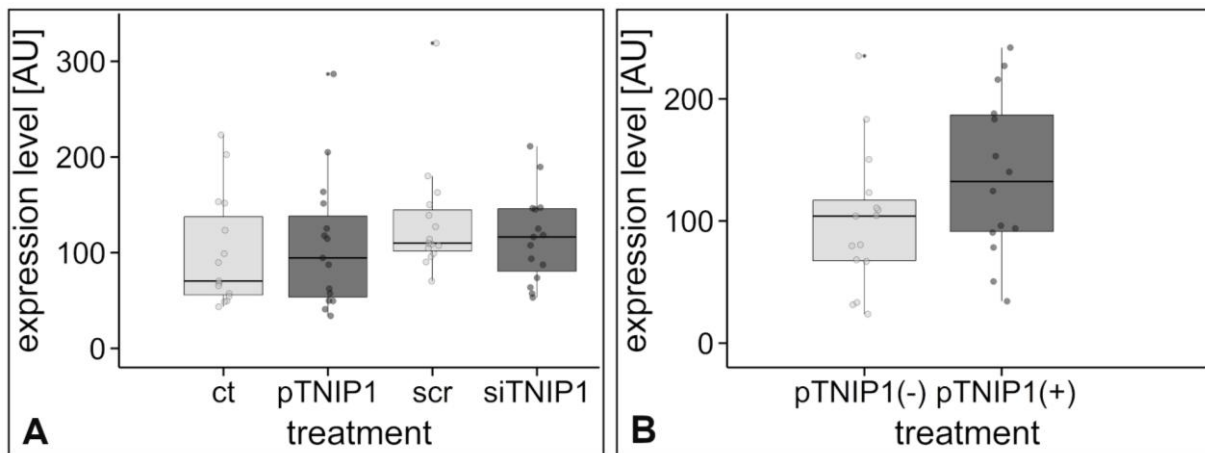


Figure 18 (A and B): Modulation of TNIP1 did not affect Caspase-3 expression on a cellular level

HEK 293 cells were treated according to protocol. Immunocytochemical staining of Caspase-3 (red), TNIP1 (green) and nuclear staining with Hoechst 33258 (blue) was performed after cells were fixed. Images were taken at a 4.0 zoom magnification factor. A: Boxplot. C3 expression levels are compared across all treatment groups. No significant differences in C3 expression were found (Wilcoxon Rank Test, $n = 3$, $p = 0.901$ for ct/ pTNIP1, $p = 0.561$ for scr/ siTNIP1). Expression levels of C3 in AUs are shown on the y-axis, the x-axis shows the different treatment groups: ct (mock transfection, control for pTNIP1), pTNIP1 (transfected with pcDNA3.1zeoTNIP1, upregulation), scr (scramble, control for siTNIP1) and siTNIP1 (downregulating siRNA).

B: Boxplot. C3 expression levels within the pTNIP1 group are compared. pTNIP1 overexpressing cells (pTNIP1(+)) were selected and compared to cells expressing normal levels of TNIP1 (pTNIP1(-)) within the group. No significant differences in C3 expression were found, although a slight bias towards pTNIP1(+) could be observed (Wilcoxon Rank Test, $n = 3$, $p = 0.132$). Expression levels of C3 are shown on the y-axis, the x-axis shows the different cell groups (pTNIP1(-) and pTNIP1(+)).

endogenous levels of TNIP1 (pTNIP1(-) cells) present in the same culture dish. The Wilcoxon Rank Test was then performed and revealed no significant difference in between groups ($n = 3$, $p = 0.132$), although there seems to be a slight tendency towards higher C3 expression in the pTNIP1(+) group (Figure 18B).

Based on the results depicted in Figures 15-18, I conclude that while TNIP1 modulation does not seem to affect C3 expression levels in individual cells, TNIP1 overexpression results in a slight increase in numbers of cells stained for C3.

3.4. Effect of TNIP1 on cell proliferation

Histon H3 is an integral structural protein of DNA chromatin, which is phosphorylated at the beginning of the prophase until early telophase (Sawicka and Seiser, 2012). Thus, phosphorylated Histon H3 (PHH3) serves as a very specific cell proliferation marker.

Although cultured cell lines have a high cell doubling rate, this is especially true for HEK 293 cells, PHH3 can only be found in a small number of cells, since PHH3 is only expressed during a very short time window during mitosis. This implies that analyzing a small number of cells would reveal very small numbers, rendering this approach less suitable for analysis (data not shown). Instead, I compared PHH3 expression in lower magnification images, showing a higher number of cells to increase data sample numbers.

HEK 293 cells were transfected with the pcDNA3.1zeoTNIP1 plasmid and the downregulating siRNA alongside the respective control groups (ct and scr). Images were then taken at a high resolution and evaluated using Image J, calculating the PHH3 ratio (the number of PHH3 positive cells divided by total cell number).

At first, images were visually inspected. In Figure 19 a discrete increase of TNIP1 immunofluorescence in pTNIP1 transfected cultures can be observed (green channel). At the same time the nuclear red fluorescent ring-like structures of the PHH3 staining can also be seen in the green channel as a result of sequential antibody staining. A sequential staining was performed since both the TNIP1 and PHH3 antibodies were raised in rabbits. Therefore, the PHH3 rabbit-polyclonal primary antibody (Invitrogen) was incubated first, followed by the secondary red fluorescent antibody (Goat-anti-Rabbit Alexa 546).

Afterwards, cells were thoroughly washed. Then, the TNIP1 rabbit polyclonal primary antibody (Proteintech) was incubated, followed by the secondary green fluorescent antibody (Goat-anti-Rabbit Alexa 488). Therefore PHH3-binding sites were stained twice,

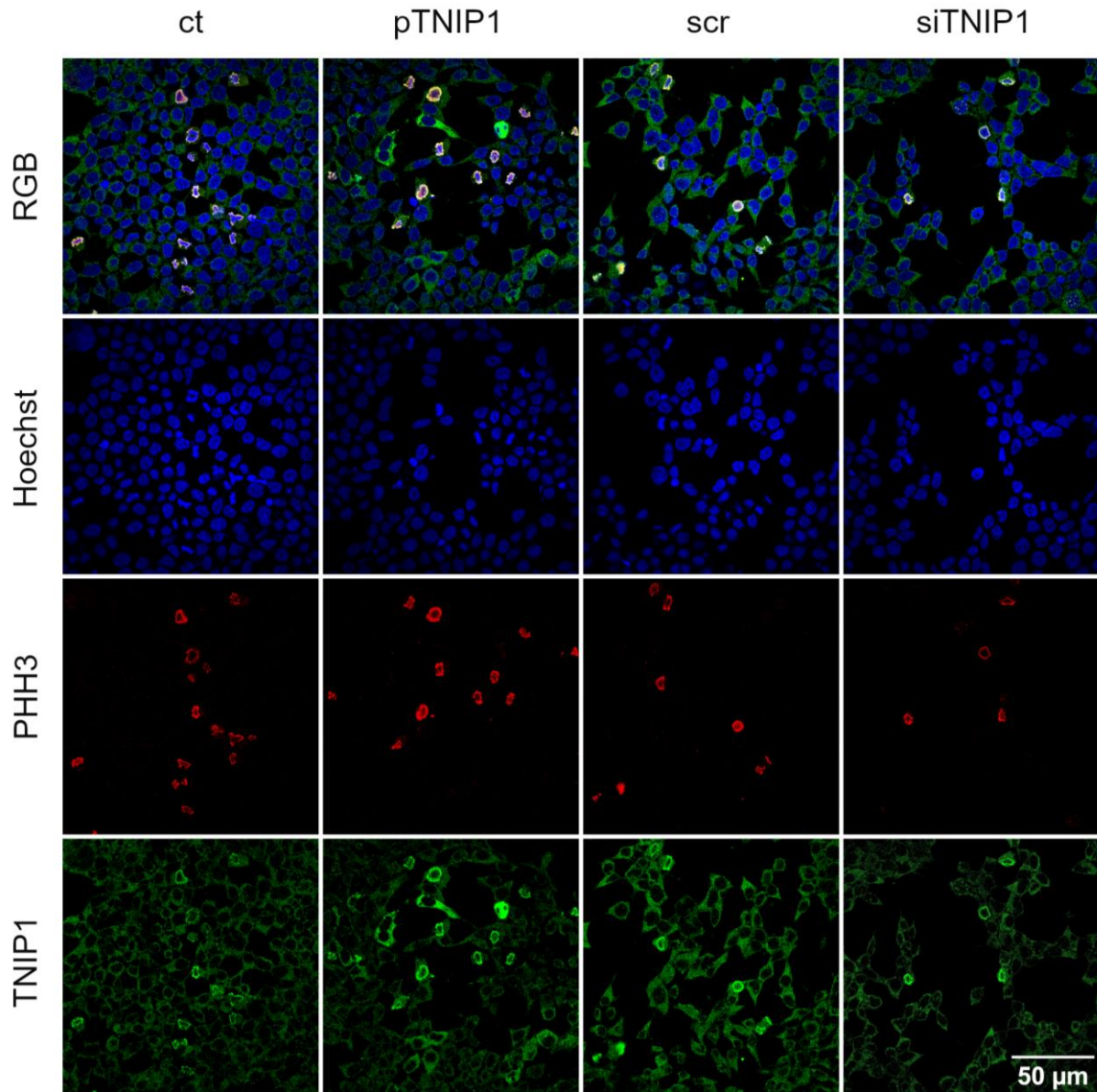


Figure 19: TNIP1 overexpression reduced PHH3 expression

HEK 293 cells were treated according to protocol. Immunocytochemical staining of PHH3 (red), TNIP1 (green) and nuclear staining with Hoechst 33258 (blue) was performed after cells were fixed. It should be mentioned that in the RGB image the PHH3 stained sections appear yellow due to overlay with the TNIP1 antibody, as both were Rabbit-derived antibodies. Please note, that in the TNIP1 (green) stained images, there is an overlay with the PHH3 staining (in red). Hence, not all green stained parts are TNIP1-binding sites, which can be easily verified by looking at the RGB image.

resulting in a yellow tone due to the overlap. By mere visual inspection it seems as though the ct cells exhibit the highest amount of PHH3 stained cells, whereas the TNIP1 diminished group (siTNIP1) presents the lowest number of these cells. Interestingly, there appears to be no concomitant overexpression of TNIP1 and PHH3 staining in the pTNIP1 group. To critically evaluate these visual impressions, quantitative analysis was performed. The Wilcoxon Rank Test showed a highly significant difference between mock transfected (ct) and pTNIP1 transfected cells ($n = 3$, $p = 0.002^{**}$), while the scr/siTNIP1 group showed no significant difference ($n = 3$, $p = 0.362$, Figure 20A). This is consistent with the observation that TNIP1 overexpressing cells (pTNIP1 group) express less PHH3.

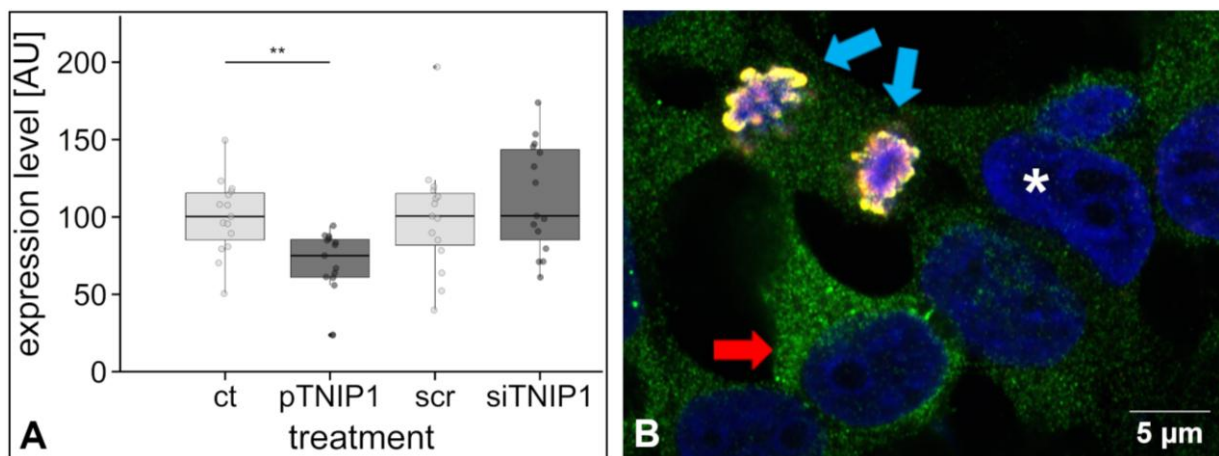


Figure 20 (A and B): Overexpression of TNIP1 resulted in decreased PHH3 expression

HEK 293 cells were transfected according to protocol. Immunocytochemical staining of PHH3 (red), TNIP1 (green) and nuclear staining with Hoechst 33258 (blue) was performed after cells were fixed.

A: Boxplot. Expression levels of PHH3 related to total cell number (PHH3 ratio in AUs) are shown on the y-axis, while the x-axis shows the different treatment groups: ct (mock transfection, control for pTNIP1), pTNIP1 (transfected with pcDNA3.1zeoTNIP1, upregulation), scr (scramble, control for siTNIP1) and siTNIP1 (downregulating siRNA). The pTNIP1 group revealed significantly lower amounts of PHH3 in comparison to the ct group (Wilcoxon Rank Test, $n = 3$, $p = 0.002^{**}$). No significant differences were detected in the scr/siTNIP1 group using the Wilcoxon Rank Test ($n = 3$, $p = 0.362$).

B: Image from the pTNIP1 group immunocytochemically stained with nuclear Hoechst staining (white asterisk), TNIP1 (green fluorescent) and PHH3 (red fluorescent, appearing yellow due to overlay). A pTNIP1(+) cell (cell overexpressing TNIP1) can be seen in the image (red arrow), as well as a cell in the anaphase of mitosis, stained with PHH3 (blue arrows).

Figure 20B displays two PHH3 marked cells (blue arrows) with yellow nuclei within the pTNIP1 treatment group. It appears that these PHH3 stained cells are in the anaphase of the mitotic cycle, since chromosomes seem to be oriented along the equatorial plane. The cell labeled by a red arrow depicts a pTNIP1(+) cell (hence TNIP1 overexpressing cell) not in mitotic division. The nucleus marked by an asterisk belongs to a pTNIP1(-) cell showing endogenous levels of TNIP1 expression.

The analysis shows that upregulation of TNIP1 expression significantly decreases PHH3 expression. Diminished TNIP1 expression did not affect the number of PHH3 stained cells.

Since the pTNIP1 group was found to exhibit reduced PHH3 expression rates, a more detailed analysis of this group ensued. Because the transfection rate of the pcDNA3.1zeoTNIP1 vector was only around 40 %, both pTNIP1(+) cells (overexpressing TNIP1) and pTNIP1(-) cells (expressing only endogenous levels of TNIP1) can be seen next to each other in the culture dish. The aim was thus to determine whether the expression of PHH3 was different in pTNIP1(+) cells, as compared to pTNIP1(-) cells. Because this comparison was made between cells cultured within the same dish, minimal technical variations were expected. A highly significant difference between groups was observed (Wilcoxon Rank Test, $n = 3$, $p < 0.001^{***}$), implying that pTNIP1(+) cells are less mitotically active than their pTNIP1(-) counterparts (Figure 21).

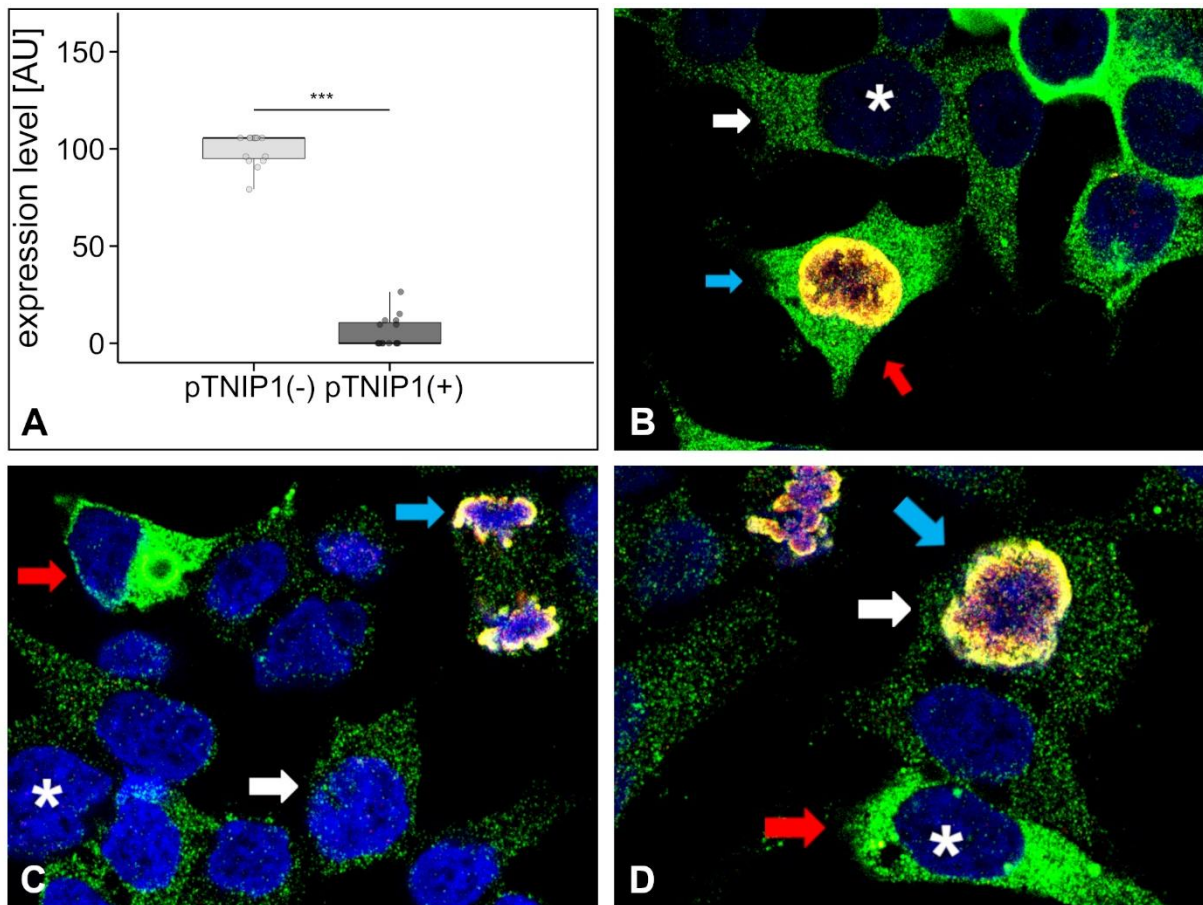


Figure 21 (A, B, C and D): TNIP1 overexpressing cells expressed less PHH3 than cells expressing endogenous TNIP1 levels

HEK 293 cells were transfected according to protocol and immunocytochemically stained with TNIP1 (green), nuclear Hoechst staining (blue) and PHH3 (red, however appearing yellow due to overlay). It should be mentioned that this overlay in staining resulted due to TNIP1 and PHH3 antibodies both being rabbit-derived antibodies. This assay was only done on cells from the pTNIP1 (pcDNA3.1zeoTNIP1 transfected) group to compare PHH3 expression rates in both pTNIP1(+) cells, cells overexpressing TNIP1, and pTNIP1(-) cells, which only expressed endogenous TNIP1 levels. A: Box plot. The y-axis shows the ratio of PHH3 expression in AUs, and the x-axis displays the different groups (pTNIP1(+)) and pTNIP1(-) cells). The Wilcoxon Rank Test revealed that pTNIP1(+) cells express significantly lower rates of PHH3 as compared to pTNIP1(-) cells ($n = 3$, $p < 0.001^{***}$), thus being less mitotically active.

B-D: All images were taken from the pTNIP1 group, stained with nuclear Hoechst staining (white asterisk), TNIP1 (green fluorescent) and PHH3 (red fluorescent, appearing yellow in RGB images). pTNIP1(+) cells (red arrows) stand next to pTNIP1(-) cells (white arrow), while some are stained overlappingly with PHH3 (blue arrow). In image B the cell stained with PHH3 (blue arrow) seems to be in the prophase of mitosis. In image C a cell (blue arrow) can be pictured in the late anaphase/ early telophase. In image D the cell (blue arrow) is likely between the prophase and metaphase of mitosis.

To further follow up on TNIP1's role in cell proliferation in HEK 293 cells, I performed flow cytometry, a standard procedure often used to measure cell proliferation (Shen et al., 2017). HEK 293 cells were transfected, split once to achieve a certain degree of cell synchronisation and then stained with propidium iodide (PI). Stained cells were then analyzed in a flow cytometer using appropriate fluorescent channels. The data was evaluated using Flowing Software 2. The ratio of cells in G1 versus G2 and S (mitotic index) was calculated. The Levene Test revealed no significant difference in variance in all groups ($p = 0.448$). The Shapiro-Wilk Test showed the control (ct) group was not normally distributed ($p = 0.019^*$). The Wilcoxon Rank test was thus used to compare overall PI distribution (in form of the mitotic index) in cell groups. The Wilcoxon Rank Test showed no difference between groups, neither for the overexpressing group ($n = 3$, $p = 1$

for ct/ pTNIP1), nor for the knockdown group ($n = 3$, $p = 0.383$ for scr/siTNIP1) (Figure 22). The mean value for the CV at the G1 peak was 12.867 %, which demonstrates a rather limited quality of the data.

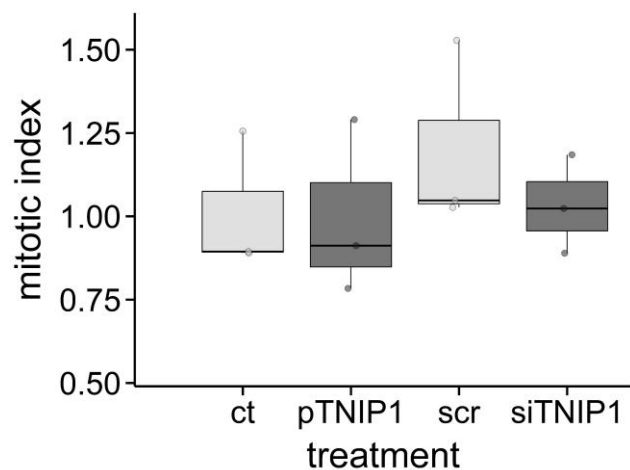


Figure 22: TNIP1 modulation did not affect the allocation of cells to distinct mitotic cycling phases

HEK 293 cells were transfected according to protocol. Cells were stained with nuclear staining propidium iodide solution. They were counted using a FACScan unit and analyzed with Flowing Software 2. The mitotic index (ratio of cells in G1 versus G2 or S) was calculated for each group and revealed no significant differences between treatment groups (Wilcoxon Rank Test, $n = 3$, $p = 1$ for ct/pTNIP1, $p = 0.383$ for scr/siTNIP1). The mean value for the CV at the G1 peak was at 12.867 %, which implies a restriction of S-phase estimation. The box plot shows the mitotic index on the y-axis, while the x-axis portrays the different treatment groups ct (mock transfection, control group for pTNIP1), pTNIP1 (transfected with upregulating pcDNA3.1zeoTNIP1), scr (control for siTNIP1) and siTNIP1 (downregulating siRNA).

3.5. Effect of TNIP1 on cell migration

The wound healing assay is a simple and effective method to investigate migration patterns in cell culture (Grada et al., 2017). Thus, it was used to explore whether the modulation of TNIP1 expression levels influenced cellular migration.

HEK 293 cells were transfected with upregulating pcDNA3.1zeoTNIP1 (pTNIP1) or downregulating siRNA (siTNIP1) and evaluated alongside their respective control groups (ct/ scr). The cells were grown to sub-confluency and a scratch was made through the middle of each well. The wells were then imaged every hour to document the closure of the scratches over time. In most cases, the scratch was not closed within the 20-hour period investigated (Figure 23).

To evaluate the images, the area covered by cells was related to the original scratch area at different times, i.e. 5, 10, 15 and 20 hours after transfection. The Levene Test revealed a difference in variance between compared groups. This is not astonishing, given that the two edges of the scratch are moving towards each other and will at some point stop moving to avoid overgrowth. Hence the Friedman Test was used, as it allows for analysis of non-parametric data using two factors (treatment and time). Afterwards, the Bonferonni post-hoc test was performed. No differences between ct (mock transfection) and pTNIP1 were found across all time values (Figure 24). Please note that the scratch was

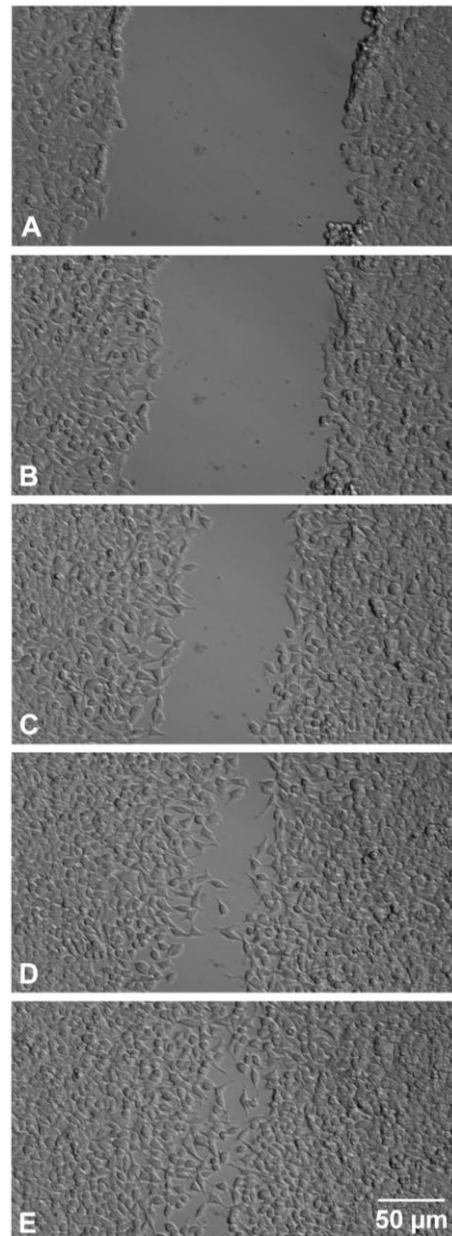


Figure 23: Wound healing assay

Images were taken from the scr group (siTNIP1 control group). A scratch was made, and images were taken every hour for 20 hours (A: start of imaging, B: after 5 hours, C: after 10 hours, D: after 15 hours, E: after 20 hours).

nearly closed in many assays after 10 hours, which might have had an impact on the interpretation of the results (see Discussion).

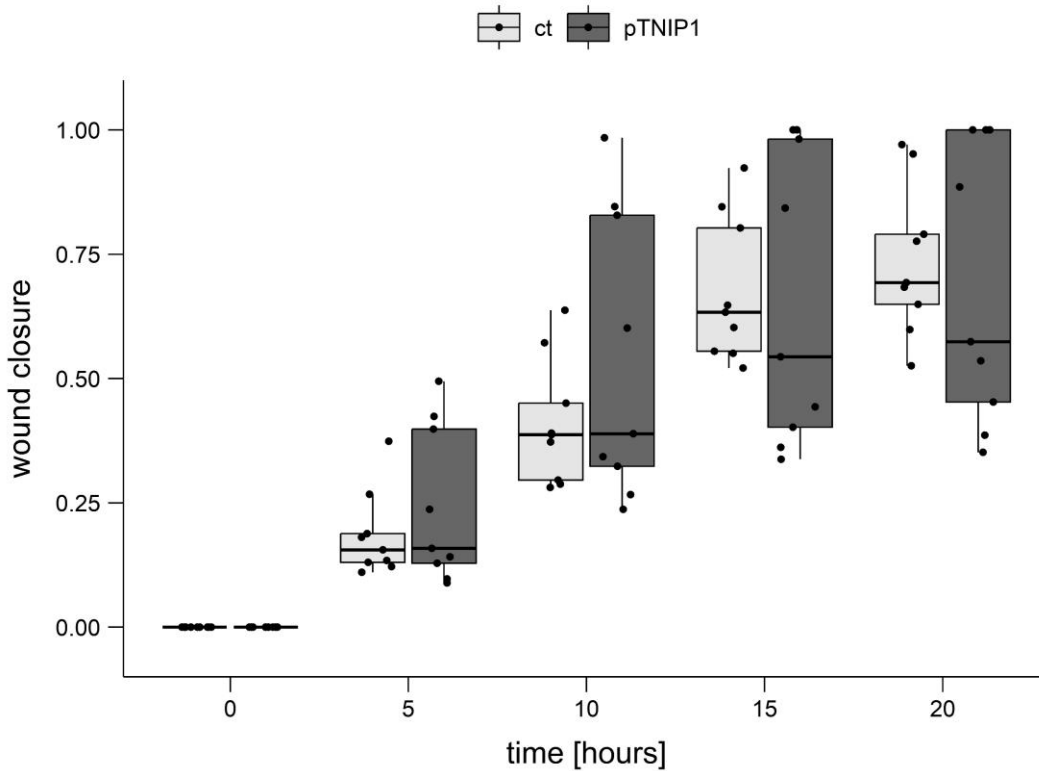


Figure 24: TNIP1 overexpression did not affect wound closure rate

Cells were transfected with pTNIP1 and compared to the respective control group (ct, mock transfection). Using a timelapse microscope, the scratched area was imaged every hour. The y-axis shows the wound closure (1 being fully closed and 0 fully open at the beginning). The x-axis shows the different time slots, at which the scratch area was measured. The Friedman Test revealed no significant differences at individual time slots (n=3, t=5 h: p= 1.0, t = 10 h: p = 1.0, t = 15 h: p = 0.51, t = 20 h: p = 1.0).

Contrastingly, visual inspection of the box plot in Figure 25 suggests there might be significant differences between scr and siTNIP1 treated cells. Indeed, the Friedman Test, followed by the Bonferroni post-hoc test, found significant differences at each individual time slot.

In this case, none of the siTNIP1 transfected cells could close the scratch at any point in time. Only one sample in the scr group presented with a closed scratch within the 20-hour time frame. The scratch closure appeared to take place in a linear manner.

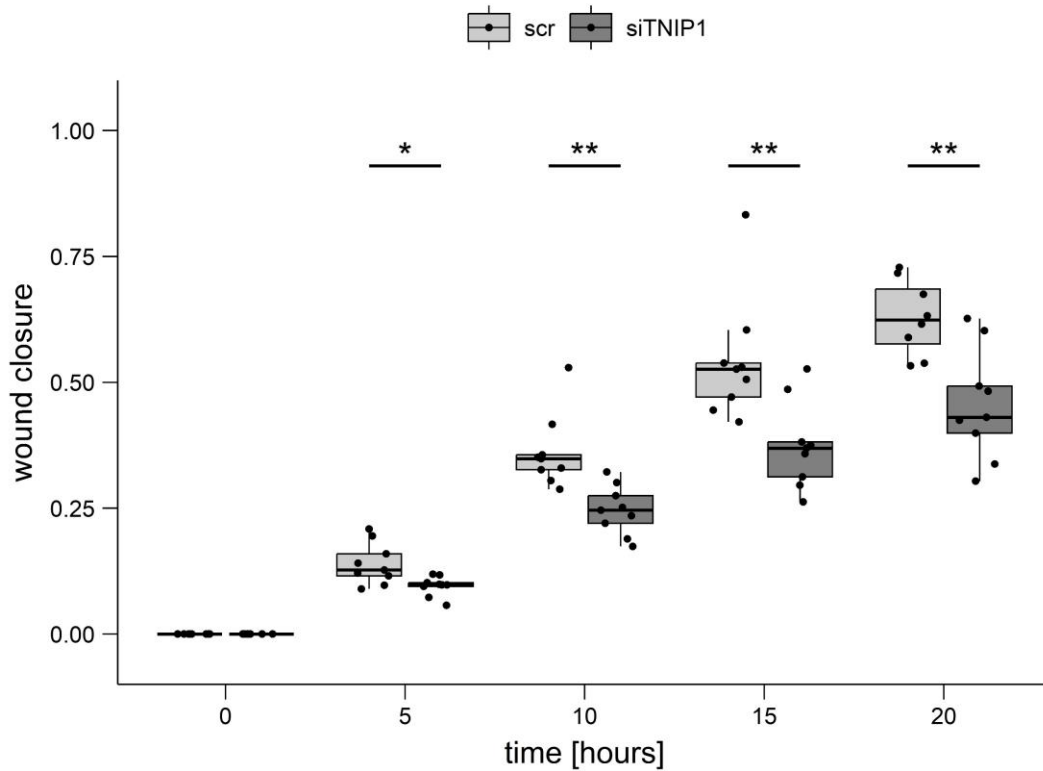


Figure 25: TNIP1 knockdown decreased wound closure rate

Cells were transfected with either scr or siTNIP1 (downregulating) siRNA. Timelapse images were captured every hour for 20 hours after the scratch was made. Then, the wound closure rate was calculated. The y-axis shows the wound closure (1 being fully closed and 0 fully open at the beginning). The x-axis shows the different time slots, at which the scratch area was measured. Using the Friedman Test, significant differences could be observed across all time slots: $t = 5 \text{ h: } p = 0.039^*$, $t = 10 \text{ h: } p = 0.004^{**}$, $t = 15 \text{ h: } p = 0.004^{**}$, $t = 20 \text{ h: } p = 0.004^{**}$ ($n = 3$).

In order to verify that measurements were not dependent on the observer, an inter-rater reliability assay was performed. Each of the three observers evaluated four probes, not knowing how the cells were treated. The inter-rater correlation coefficient was 1, demonstrating excellent reproducibility.

4. Discussion

Although TNIP1 associated molecular pathways are a matter of intense investigations, its function in a cellular context is less explored and rather controversially discussed. In this thesis, I established basic molecular tools to manipulate TNIP1 gene expression in cell culture. Using HEK 293 cells as a model system, I was able to show that TNIP1 overexpression increased cell apoptosis, decreased cell proliferation and affected cell migration. Even though these findings are focused on a simple cell line often used in basic research, the established tools are the basis for future research in more sophisticated cell cultures and further functional assays.

4.1. TNIP1 expression can be altered in HEK 293 cells

In order to manipulate TNIP1 levels in cells, an appropriate gene construct had to be established. Isoform 3 (transcript variant 5) of the human TNIP1 gene was chosen, as this transcript contains all currently known domains of the TNIP family and exhibits all known characteristics of this gene variant. It is often used in TNIP1 studies (Merline et al., 2023). Moreover, the sequence of this isoform was available from InvivoGen and could be used as a template for further cloning. During this process, I carefully examined the cloning product for correct orientation of the inserted coding sequence in relation to the promoter, scanned for potential frame shift mutations, and confirmed that the coding sequence itself was not changed during PCR amplifications. To prove this, the expression vector was sequenced using three different primers and compared to NCBI databases. The sequence obtained had no alterations in the nucleic acid sequence and thus enabled full length TNIP1 expression.

Having created an appropriate TNIP1 vector, it was imperative to select a suitable cell line for the purpose of this study. HEK 293 cells were chosen, as this cell line is easy to transfect, easy to culture and presents moderate TNIP1 expression levels, as revealed by *in silico* analysis. This moderate expression level was required, since the aim was to both up- and downregulate TNIP1 levels in cells.

The success of TNIP1 overexpression in HEK 293 cells revealed similar results, when analysed by immunocytochemistry and Western Blotting. The expression vector used in this study was based on a CMV (cytomegalovirus) promoter, which is active in most cell types, including HEK 293 cells, and is widely used in studies (Qin et al., 2010; Xia et al., 2006). Still, the regulation of this promoter is not yet completely understood. For instance, it is known that the expression level of the desired gene can be rather heterogeneous, especially after multiple passages of cultivated positively selected cells. Changing methylation patterns were identified as one possible explanation for this (Osterlehner et al., 2011). This impacts on the expression of TNIP1 and can cause downregulation of expression over time in culture. Although commonly used, results of CMV-promoter driven expression in stable HEK 293 cell lines must thus be critically evaluated. To avoid this problem, I only used constitutive expression of TNIP1 in HEK 293 cells. Experiments revealed that around 40 % of HEK 293 cells were overexpressing TNIP1 on average. Transiently transfected cells express TNIP1 temporarily, mostly between 24 and 72 hours after transfection. This is the time window during which all experiments were performed in this thesis.

Both the variable number of cells transfected with the pcDNA3.1zeoTNIP1 vector and the variability in TNIP1 expression intensity are possible reasons as to why changes in protein levels were not as significantly different in Western Blot analysis in comparison to the immunocytochemical assays. Yet, using a one-sided T-Test, significant upregulation in TNIP1 expression could be observed in the pTNIP1 group. To obtain further information about TNIP1 expression at the single cell level, immunocytochemical stains were performed. While these assays are often subject to variability in staining procedures, in this case, they might present as a reasonable approach. TNIP1 overexpressing cells and HEK 293 cells expressing only endogenous levels are present in the same culture dish and can even be visualized in the same image. Using densitometry in fluorescently labeled cells, I could show a highly significant difference in TNIP1 expression between control transfected and TNIP1 overexpressing cells. It must be mentioned that control cells had only undergone mock transfections, meaning all transfection reagents were applied, apart from a vector. Many off-target effects are produced by the transfection agent itself (Jacobsen et al., 2009) and this effect differs depending on the cell line and vector in question (Stepanenko and Heng, 2017). HEK 293 cells were found to be quite stable and

showed no difference in expression levels when comparing mock transfected (transfection reagent only) and vector transfected cells (Hagen et al., 2015). This was also experimentally confirmed by Holst (Dissertation, Bonn, 2007), the study from which the pcDNA3.1zeo vector has originally been derived.

A further important result of this study is the suitability of the TNIP1 antibody. The antibody allowed me to detect both TNIP1's native endogenous form and the engineered construct. This is significant, since TNIP1 immunocytochemical stains were used to differentiate between cells expressing only native TNIP1 and those overexpressing the pcDNA3.1zeoTNIP1 construct. The same stains were then used to investigate cellular functions like apoptosis and proliferation.

The suitability of the antibody was further verified by TNIP1 repression experiments using siRNA. I chose siPools (siTools Biotech), as they have been shown to limit siRNA off-target effects (Hannus et al., 2014). In addition, siPool RNAs only contain picomolar concentrations of each siRNA, which might reduce immune stimulatory effects in vivo (Robbins et al., 2008). This was not relevant to my study but might be of importance for further studies on this topic. Lastly, siTools Biotech provided a control group for the siRNA, containing a mixture of random siRNAs to control for off-target effects.

Concerned about the potential instability of siRNAs in a culture medium, the window of highest siRNA potency was tested. It was found to be at around 24 hours, in agreement with previous findings by Rao et al. (2009). Hence, all experiments were performed around this time window.

The downregulation of TNIP1 expression could not be verified by Western Blotting. The reason for this might be that siRNA mediated repression is a knock-down and not a knock-out procedure. Additionally, not all cells might have been properly addressed. To get a rough impression on siPool RNA transfection efficiency I used siGLO RNA, a chemically engineered red fluorescent RNA. Using siGLO, I could achieve a 100 % transfection rate. It is, however, not clear, whether this translates to siPool RNAs. The manufacturer assures a transfection efficiency of 70 %. When using TNIP1 immunocytochemical staining, a highly significant difference between control (scramble, scr) and siTNIP1 treated cultures could be observed. However, in contrast to the overexpression experiments,

downregulation of TNIP1 could not be identified at the single cell level, meaning a clear distinction between transfected and non-transfected cells in immunocytochemical stains was not possible. This prompted me to consider that the TNIP1 overexpression data might yield more reliable results.

4.2. TNIP1 promotes apoptosis

As outlined above, it is currently not known which function TNIP1 might have in a distinct cellular environment. While TNIP1's role in the complex TNF-alpha-induced NF-kappaB pathway has long been acknowledged (Van Quickenberghe et al., 2018) and TNIP1 is mainly thought of as an anti-apoptotic protein, literature is split and it remains unclear whether pro- or anti-apoptotic effects prevail. In this thesis, I used a cleaved Caspase-3 (C3) antibody to immunocytochemically identify apoptotic cells. C3 is a key player in apoptosis and is only activated by cleavage upon initiation of the programmed cell death cascade (Ponder and Boise, 2019; Porter and Jänicke, 1999). Though commonly used as an apoptosis marker (Asadi et al., 2022), it should not go unmentioned that C3 is also involved in pyroptosis (Wang et al., 2017), a cell death pathway TNIP1 has also been implicated in (Shamilov et al., 2020). As shown above, a significant rise in C3 positive cells among TNIP1 overexpressing cells could be observed. This difference in C3 expression was not due to the expression level at the single cell level, since C3 was expressed at comparable levels in mock-transfected and cells transfected with pcDNA3.1zeoTNIP1. Therefore, it is likely that the increase in C3 expression was due to an increased number of cells expressing activated C3. In my experiments, TNIP1 appeared to promote cell death, likely in the form of apoptosis. This observation seems to contradict the main view of TNIP1 function.

TNIP1 is involved in a TNF-alpha mediated pathway, it binds A20 to the NEMO/IKK and allows it to de-ubiquitinate the NEMO/IKK, hereby inhibiting the activation of NF-kappaB and its downstream effects (Mauro et al., 2006; Van Quickenberghe et al., 2018). This TNF-alpha mediated NF-kappaB pathway balances the opposing processes of cell survival and apoptosis (Van Antwerp et al., 1998). Depending on the cellular context, either pathway is chosen (Brenner et al., 2015; Flusberg and Sorger, 2015). The phase of

the cell cycle, epigenetic and genetic differences between cells are, among many others, key factors in cell fate decision. While TNF-alpha can initiate apoptosis by itself in NF-kappaB deficient cells, it seems to require additional inhibitors of protein synthesis or RNA for an effect in cells expressing normal levels of NF-kappaB. Interestingly, NF-kappaB requires protein synthesis to execute anti-apoptotic functions, as opposed to pro-apoptotic functions (Aggarwal, 2003). For anti-apoptotic effects a series of genes are induced, including genes encoding cellular inhibitors of apoptosis (Karin and Lin, 2002). I.e., IKK-driven NF-kappaB activation could lead to cell survival (Hoffmann and Baltimore, 2006; Israel, 2010), which would in turn imply, that TNIP1-led inhibition of the IKK-complex could result in a surplus of pro-apoptotic signals. Thus, similar signaling pathways can lead to either cell death or cell survival, a duality observed in many proteins, which were initially attributed to exhibit only pro- or only anti-apoptotic features (Flusberg and Sorger, 2015). TNIP1 also seems to exhibit this dichotomy in function. Studies by Oshima et al. (2009) discovered that TNIP1 had anti-apoptotic effects in the embryonic development of mice. In contrary, more recent studies revealed a pro-apoptotic effect in TNIP1 overexpressing renal clear cell carcinoma cells (Yang et al., 2019). In 2018, Dorn et al. uncovered that TNIP1 downregulation led to higher transcriptional activity in NF-kappaB in Luciferase assays. As intriguing as this link between TNIP1 downregulation and NF-kappaB expression may be, it does not allow for a prediction of the effects of TNIP1 downregulation on a cellular level. These effects must be studied in a cell culture model using multiple biological assays, which is why I chose to further investigate TNIP1's impact on apoptosis.

It has previously been shown that C3 is indispensable for DNA fragmentation, but is not necessarily involved in membrane blebbing or other cellular processes (Porter and Jänicke, 1999). This is consistent with the observations made here. There was no observation of cell shrinkage, rounding of cells or chromatin condensation, which is frequently seen after exposure of cells to peroxides (Bortner and Cidlowski, 2003; Grzanka et al., 2013; Son et al., 2009). In my HEK 293 cells, no differences in cellular volume or surface could be detected. However, a consistent observation, that the pTNIP1 group repeatedly had more dying cells in cell culture (data not shown), suggests an increased rate of cell death associated to TNIP1 overexpression.

It goes unspoken, that cell death in culture cannot be compared to a complex induction process which occurs in vivo. However, the advantage of this scenario is that cell culture conditions can be controlled very accurately. I.e., it was taken care to always plate the same number of cells for transfection in each group, since I had found that cell density can have an impact on TNIP1 expression. Given that higher rates of cell death may also result in lower cell numbers, one might question how this relates to TNIP1 expression levels. Seeing as experiments have shown that TNIP1 expression is decreased in lower density, subconfluent cell cultures, it is highly unlikely that TNIP1 overexpression per se reduces cell density. Cell death is thus rather a consequence of TNIP1 expression, than TNIP1 overexpression a consequence of low cell numbers.

There is, however, a further point to be considered. TNIP1 seems to be involved not only in apoptosis, but also in other non-apoptotic cell death pathways, namely necroptosis (Dziedzic et al., 2018; Li et al., 2022) and pyroptosis (Shamilov et al., 2020). These pathways are intrinsically connected and therefore difficult to untangle. While not involved in necroptosis, C3 is activated in both apoptosis and pyroptosis (Lu et al., 2022; Wang et al., 2017). Based on the current literature it is difficult to determine, which role of C3 prevails, biased by the fact, that apoptosis was long thought to be the only programmed cell death pathway. Considering that, apart from one study by Shamilov et al., 2020, literature on TNIP1 revolves mainly around apoptosis, I presume that these effects on cell death are likely of apoptotic nature.

4.3. TNIP1 attenuates cell proliferation

Cell proliferation and apoptosis are two opposing cellular pathways controlling cell numbers and connectivity. Consequently, their regulation is intrinsically linked (Guo and Hay, 1999). They are regulated by multiple pathways, like the MAPK/ERK pathway (Sun et al., 2015) and the PI3K/AKT/mTOR pathway (Yu and Cui, 2016). Chen et al. (2015) revealed that the downregulation of TNIP1 leads to increased cell proliferation in keratinocytes. Moreover, TNIP1 overexpression was not only shown to result in increased apoptosis, but also in decreased proliferation in different tumor cell types (Lei et al., 2020; Yang et al., 2019). This is consistent with the current observation that proliferation was

diminished in TNIP1 overexpressing HEK 293 cells. In this thesis, proliferation was measured by counting the number of cells expressing phosphorylated histone H3 (PHH3). This histone is specifically expressed during the G2-M phase transition (Sherman and Wang, 2020) and thus enables a more accurate identification of mitotically active cells than staining with e.g. Ki67. Ki67 is expressed over a long period of the mitotic cycle (Braun et al., 1988) and thus labels considerably more cells than PHH3. This is problematic since HEK 293 cells are highly mitotically active cells. Moreover, Ki67 stains cells very heterogeneously, hence making it more difficult to identify cells as clearly Ki67 positive or negative. Nevertheless, difficulties with the PHH3 staining must be acknowledged, namely, that the PHH3 staining was performed with a rabbit polyclonal antibody, which is the same species in which the TNIP1 antibody was raised. Thus, both stainings needed to be separated from each other. This was realized in two ways. Firstly, TNIP1 is primarily found in the cytoplasm, yet a possibility for nuclear shuttling has been described (Verstrepen et al., 2009). In my experiments I only observed minor nuclear association of TNIP1. Contrastingly, PHH3 can only be found within the nucleus, tightly associated with DNA (Goto et al., 1999; Hans and Dimitrov, 2001). To further increase the specificity of the staining, I did a sequential staining of the HEK 293 cells. First PHH3 antibodies were stained, then after thorough washing, TNIP1 antibodies followed. This way, the cytoplasmic stain of TNIP1 could not be altered by the PHH3 staining. However, it implied that PHH3 binding sites were “double” stained with a red fluorescent secondary antibody (for PHH3) and a green fluorescent secondary antibody (for TNIP1), rendering the PHH3 binding sites yellow in RGB images, red in the PHH3 channel and green in the TNIP1 channel. Therefore, the analysis of these images was not centered around the integrated density (ID) of each channel (as the TNIP1 channel portrayed both binding sites for TNIP1 and PHH3) but rather based on cell numbers. Figures 19-21 clearly show that mitotically active pTNIP1 positive cells (cells overexpressing the pcDNA3.1zeoTNIP1 vector) can easily be identified and distinguished from pTNIP1 negative cells (cells expressing only endogenous levels of TNIP1). Additionally, it was even possible to get an idea of the specific mitotic phase of said cells.

Using immunocytochemistry, I was able to show that proliferation was diminished in TNIP1 overexpressing cells. This observation could not be verified in flow cytometry. The mitotic index revealed no differences between treatment groups. However, the coefficient of

variance (CV) fraction of G1 was found to be roughly 13 %, which is outside the range considered to provide reliable results (Ormerod et al., 1998). This could be due to a lack of cell synchronization with an agent like nocodazole. At the time, this was discarded for fear of skewing the results, as nocodazole has shown to induce apoptosis by itself (Kook et al., 2000). The relatively high CV might also suggest that the staining of the cells was not uniform. I believe there are ways to optimize this assay, for instance by using a different cell synchronization agent like thymidine, which has been described to reduce unwanted side effects like apoptosis (Wang and Wang, 2022). Moreover, it could be interesting to stain cells with a fluorescent antibody for TNIP1, which does not interact with PI, to further correlate cellular TNIP1 expression levels and mitotic activity.

As outlined above, the flow cytometry analysis must be interpreted with care. Taken together, the PHH3 assay clearly showed that TNIP1 overexpression downregulates proliferation. Thus, while promoting apoptosis, TNIP1 rather attenuates cellular proliferation in HEK 293 cells. Taken together, the opposing nature of the proliferation and apoptosis pathways is reflected in the cellular effects of TNIP1.

4.4. TNIP1 deficiency decreases cell migration

Having shown that TNIP1 affects proliferation and apoptosis in opposing ways, I was also interested in looking at the effect of TNIP1 on cellular differentiation and migration. Although the HEK 293 cell line is primarily used to investigate signal transduction pathways, protein interactions and other molecular signaling events, it has been shown to differentiate into neuron like cell types (Lin et al., 2004). In this thesis I was able to show that decreased TNIP1 expression leads to slower scratch closure in the wound healing assay, proposing slower cell migration or a reduced rate of cell proliferation. Though initially established as an assay for migratory processes (Grada et al., 2017), it soon became obvious that scratch closure is also affected by proliferation. However, as previously shown in the PHH3 proliferation assay, TNIP1 repression did not modify proliferation patterns. It is therefore likely that the scratch closure was caused by migration of cells into the cell free space. Migration requires a complex interplay between cytoskeletal reorganization, membrane ruffling and organelle movements (Kroll and

Renkawitz, 2024). Previous studies by Shamilov et al. (2020) found TNIP1 to have a role in limiting inflammation during wound healing stages in keratinocytes, hereby promoting a successful healing process. In addition, oncogenic miR-210-3p manipulation caused TNIP1 dysregulation and was found to be related to prostate cancer metastasis (Ren et al., 2017). Currently, it is not yet known which molecular pathways are involved. First and earliest hints, however, suggest that TNIP1 is involved in cellular differentiation mediated by ERK2 signaling (Zhang et al., 2002).

As previously mentioned, I found that decreased TNIP1 expression led to a slower scratch closure, proposing that normal levels of TNIP1 might be integral for cell migration. In contrast, cells overexpressing TNIP1 did not show significant differences in scratch closure. Given the decrease in mitotic cycling in TNIP1 overexpressing cells, one could assume this would have resulted in a slower scratch closure. This was obviously not the case. This raises the question as to why TNIP1 overexpression did not show an effect. One possible explanation might be that overexpression of TNIP only occurs in a subpopulation of cells in a transient transfection approach. The numbers of transfected cells might not be sufficient to cause a significant limitation in scratch closure. Conversely, more cells seem to be targeted in TNIP1 repression with siRNA, as seen in the immunocytochemistry, even though the level of regulation might be lower. This intricate interplay between the number of cells affected by modulation and the degree of regulation occurring within these cells might cause different sensibilities in different cellular assays.

Demonstrating slower migration in TNIP1 knockdown cells partly contradicts previous observations made by Shamilov et al. (2020). In that study, at first TNIP1 deficient keratinocytes displayed enhanced wound healing. At the same time the group also showed increased priming of the inflammasome assembly, which later resulted in reduced re-epithelialization, most likely due to loss of cell viability. Consequently, they presumed that adequate levels of TNIP1 must be necessary for wound healing.

Taken together, I was able to show that diminished levels of TNIP1 expression impact cell migration, while higher levels of TNIP1 influence cell proliferation and apoptosis. It is important to keep in mind that it is currently not known whether up- and downregulation causes different effects or whether this is based on methodological obstacles, as mentioned above.

4.5. Influence of other TNIP family members

As previously described, TNIP1 shares some common characteristics with other TNIP family members, including the capability of binding both A20 and polyubiquitinated proteins (Heyninck et al., 2003). The NF-kappaB inhibitory effect seems to be redundant in the TNIP protein family (Van Huffel et al., 2001; Wullaert et al., 2007), which was postulated to be the reason why TNIP1 knockout mice only displayed minor NF-kappaB activation. Yet, there are still differences in structure and associated diseases. For one, unlike the other proteins, TNIP1 has a NEMO-binding domain, which allows it to interact directly with the regulating complex of NF-kappaB. TNIP1 also lies on another chromosome (5), as opposed to TNIP2 and TNIP3, which lie on chromosome 4. While TNIP2 has also been shown to be involved in NF-kappaB activation, it is missing the ABIN homologous domain 3 (AHD-3), which contains autophagy related motifs. When looking at disease association, unsurprisingly, all TNIP family members are connected to inflammatory disease, though TNIP1 consistently shows the strongest links.

Considering some of the redundant effects, the question to be asked is whether the effects presented in this thesis truly rely on TNIP1 repression and overexpression, or if other members of TNIP family might have influenced these results. While I can show that TNIP1 is overexpressed in cells transfected with pcDNA3.1zeoTNIP1, currently I cannot address the question of whether other TNIPs show compensatory effects. It might be, that the upregulation of TNIP1 expression results in downregulation of TNIP2 or TNIP3, which may potentially cause the observed cellular effects. However, even if some attenuating effects from counter-regulation of TNIP2 or TNIP3 expression levels were present, they were obviously not strong enough to prevent an effect from being witnessed. Nevertheless, this is an intriguing topic of inquiry and will be considered in future studies, where TNIP2 and TNIP3 levels could potentially be monitored alongside TNIP1, provided suitable antibodies are available.

4.6. Conclusion

Although first described in 1999 and linked to inflammatory processes and autophagy soon after, TNIP1's cellular function and complex biological integration is still poorly understood. In the current thesis, I was able to establish an expression system suitable for TNIP1 overexpression in mammalian cells and TNIP1 repression using siRNA technology. Furthermore, I identified a commercially available antibody which reliably recognizes both endogenous and exogenous TNIP1 in immunocytochemistry and Western Blotting. Using these tools, I could show that altering TNIP1 expression levels affects cell death, proliferation and migration in partly opposing, yet consistent directions. While TNIP1 was found to promote apoptosis, it also had moderating effects on cell proliferation and cellular migration. These cellular effects were investigated in easy-to-handle HEK 293 cells. Given that HEK 293 cells are often used as model system for other cell types, it is likely that the established tools are also functional in other cell lines. As TNIP1 has been implicated in neurodegenerative processes, in particular that of amyotrophic lateral sclerosis or Alzheimer's disease, it is of obvious interest to also manipulate neuronal or glial cell types. In addition, having shown that the antibody recognizes TNIP1, it can now be used in brain tissue sections to reveal its native expression pattern. This would be especially interesting when investigating TNIP1's role and expression in neurodevelopmental diseases such as autism spectrum disorder. And most importantly, having an antibody at hand enables the establishment and characterization of transgenic animal models.

5. Summary

TNIP1 is a protein associated with autophagy and inflammation, which is ubiquitously expressed in the brain. It mediates extracellular signals such as growth factor signaling, influences nuclear expression patterns driven by NF-kappaB transcriptional regulation and exhibits both pro- and anti-apoptotic properties. The involvement in these cellular pathways deems it an attractive candidate gene for neurodegenerative disease pathogenesis. In fact, gene variations of TNIP1 have recently been linked to both amyotrophic lateral sclerosis and Alzheimer's disease. Moreover, TNIP1 has been shown to interact with Engrailed-2, a transcription factor associated with autism spectrum disorder (ASD). While the linkage between ASD and TNIP1 is currently low, the fact that TNIP1 has long been considered a pleiotropic risk locus for autoimmune and chronic inflammatory disorders, is intriguing, considering these are common comorbidities of ASD.

Despite the plethora of links to cell death and inflammatory processes in the body, exact cellular and molecular pathways are not yet elucidated. In addition, proper animal models are not available thus far. Therefore, it was the aim of this thesis, to establish genetic tools to overexpress and repress TNIP1. Using these genetic tools, I was able to demonstrate that TNIP1 expression can be altered in the mammalian cell line HEK 293. I was able to identify an antibody suitable to track changes in TNIP1 expression and I demonstrated that the alteration of TNIP1 expression in HEK 293 cells enhanced apoptosis and diminished both proliferation and cellular migration.

Having these tools at hand now paves the way not only for the manipulation of neuronal cell cultures, but also for the investigation of TNIP1 expression patterns in brain tissue. It will also allow for the characterization of animal models, to hopefully provide further insights into TNIP1 mediated neurodegenerative processes.

6. List of Figures

Figure 1: Schematic drawing of domain structures of the TNIP family	10
Figure 2: TNIP1 expression in the brain	15
Figure 3: Characterization of pUNO-TNIP1	20
Figure 4: Characterization of pMini-TNIP1	23
Figure 5: Estimation of DNA quantity for ligation	24
Figure 6: Colony PCR of bacteria transformed with pcDNA3.1zeoTNIP1	47
Figure 7: Characterization of pcDNA3.1zeoTNIP1 using restriction analysis	48
Figure 8: Plasmid map of pcDNA3.1zeoTNIP1	49
Figure 9 (A and B): Cell density influenced TNIP1 expression in HEK 293 cells	50
Figure 10: HEK 293 cell transfection efficiency	51
Figure 11 (A and B): Overexpression and knockdown of TNIP1 in Western Blot	52
Figure 12: Modulation of TNIP1 expression in HEK 293 cells	53
Figure 13: HEK 293 cell size was not affected by TNIP1 modulation	54
Figure 14 (A and B): TNIP1 overexpression or knockdown did not affect HEK 293 cell size	55
Figure 15: TNIP1 overexpression increased the number of Caspase-3 positive cells ...	56
Figure 16 (A and B): TNIP1 upregulation resulted in higher Caspase-3 expression in HEK 293 cells	57
Figure 17: Cellular Caspase-3 expression levels were not affected by TNIP1 modulation .	58
Figure 18 (A and B): Modulation of TNIP1 did not affect Caspase-3 expression on a cellular level	59
Figure 19: TNIP1 overexpression reduced PHH3 expression	61
Figure 20 (A and B): Overexpression of TNIP1 resulted in decreased PHH3 expression..	62
Figure 21 (A, B, C and D): TNIP1 overexpressing cells expressed less PHH3 than cells expressing endogenous TNIP1 levels	64
Figure 22: TNIP1 modulation did not affect the allocation of cells to distinct mitotic cycling phases	65
Figure 23: Wound healing assay	66
Figure 24: TNIP1 overexpression did not affect wound closure rate	67
Figure 25: TNIP1 knockdown decreased wound closure rate	68

7. List of Tables

Table 1: Instruments	16
Table 2: Software	17
Table 3: Kits	17
Table 4: Chemicals	18
Table 5: Solutions	18
Table 6: Miscellaneous Materials for nucleic acid work.....	19
Table 7: Primers.....	19
Table 8: Miscellaneous materials for protein biochemical techniques.....	26
Table 9: Antibodies for Western Blot.....	27
Table 10: Miscellaneous materials for cell biological techniques	29
Table 11: Plasmids and siRNA.....	30
Table 12: Antibodies for Immunocytochemistry	30

8. References

- Adrianto I, Wang S, Wiley GB, ..., Gaffney PM. Association of two independent functional risk haplotypes in TNIP1 with systemic lupus erythematosus. *Arthritis Rheum.* 2012; 64: 3695–3705
- Aggarwal BB. Signalling pathways of the TNF superfamily: a double-edged sword. *Nat Rev Immunol.* 2003; 3: 745–756
- Akbar N, Nanda S, Belch J, Cohen P, Khan F. An important role for A20-binding inhibitor of nuclear factor- κ B-1 (ABIN1) in inflammation-mediated endothelial dysfunction: an in vivo study in ABIN1 (D485N) mice. *Arthritis Res Ther.* 2015; 17: 22
- Akiyama H. Inflammation and Alzheimer's disease. *Neurobiol Aging.* 2000; 21: 383–421
- Alarcón-Riquelme ME, Ziegler JT, Molineros J, ..., Jacob CO. Genome-Wide Association Study in an Amerindian Ancestry Population Reveals Novel Systemic Lupus Erythematosus Risk Loci and the Role of European Admixture. *Arthritis Rheumatol.* 2016; 68: 932–943
- Allanore Y, Saad M, Dieudé P, ..., Martinez M. Genome-Wide Scan Identifies TNIP1, PSORS1C1, and RHOB as Novel Risk Loci for Systemic Sclerosis. McCarthy MI, ed. *PLoS Genet.* 2011; 7: e1002091
- Allen Institute, 615 Westlake Ave North, Seattle, WA, 2024: Allen Brain Map. <https://portal.brain-map.org/> (Access Date: 11.02.2024)
- Asadi M, Taghizadeh S, Kaviani E, Vakili O, Taheri-Anganeh M, Tahamtan M, Savardashtaki A. Caspase-3: Structure, function, and biotechnological aspects. *Biotech and App Biochem.* 2022; 69: 1633–1645
- Ashwood P, Anthony A, Torrente F, Wakefield AJ. Spontaneous Mucosal Lymphocyte Cytokine Profiles in Children with Autism and Gastrointestinal Symptoms: Mucosal Immune Activation and Reduced Counter Regulatory Interleukin-10. *J Clin Immunol.* 2004; 24: 664–673

- Baurecht H, Hotze M, Brand S, ..., Brown SJ. Genome-wide Comparative Analysis of Atopic Dermatitis and Psoriasis Gives Insight into Opposing Genetic Mechanisms. *Am J Hum Genet.* 2015; 96: 104–120
- Bellenguez C, Küçükali F, Jansen IE, ..., Lambert JC. New insights into the genetic etiology of Alzheimer's disease and related dementias. *Nat Genet.* 2022; 54: 412–436
- Benayed R, Choi J, Matteson PG, Gharani N, Kamdar S, Brzustowicz LM, Millonig JH. Autism-Associated Haplotype Affects the Regulation of the Homeobox Gene, ENGRAILED 2. *Biol Psychiatry.* 2009; 66: 911–917
- Benyamin B, He J, Zhao Q, ..., Fan D. Cross-ethnic meta-analysis identifies association of the GPX3-TNIP1 locus with amyotrophic lateral sclerosis. *Nat Commun.* 2017; 8: 611
- Bertheloot D, Latz E, Franklin BS. Necroptosis, pyroptosis and apoptosis: an intricate game of cell death. *Cell Mol Immunol.* 2021; 18: 1106–1121
- Bortner CD, Cidlowski JA. Uncoupling Cell Shrinkage from Apoptosis Reveals That Na⁺ Influx Is Required for Volume Loss during Programmed Cell Death. *J Biol Chem.* 2003; 278: 39176–39184
- Brady MP, Korte EA, Caster DJ, Powell DW. TNIP1 /ABIN1 and lupus nephritis: review. *Lupus Sci Med.* 2020; 7: e000437
- Braun N, Papadopoulos T, Müller-Hermelink HK. Cell cycle dependent distribution of the proliferation-associated Ki-67 antigen in human embryonic lung cells. *Virchows Archiv B Cell Pathol.* 1988; 56: 25–33
- Brenner D, Blaser H, Mak TW. Regulation of tumour necrosis factor signalling: live or let die. *Nat Rev Immunol.* 2015; 15: 362–374
- Carrión-Barberà I, Salman-Monte TC, Vilchez-Oya F, Monfort J. Neuropsychiatric involvement in systemic lupus erythematosus: A review. *Autoimmun Rev.* 2021; 20: 102780
- CBDM group from JGU (Mainz), 2024: HIPPIE. <https://cbdm-01.zdv.uni-mainz.de/~mschaefer/hippie/> (Access Date: 28.01.2024)

Chen Y, Yan H, Song Z, ..., Hao F. Downregulation of TNIP1 Expression Leads to Increased Proliferation of Human Keratinocytes and Severer Psoriasis-Like Conditions in an Imiquimod-Induced Mouse Model of Dermatitis. Simon M, ed. PLoS ONE. 2015; 10: e0127957

Corporation for Digital Scholarship. 2024: Zotero. <https://www.zotero.org/> (Access date: 20.08.2024)

Cox JG, De Groot M, Cole JH, Williams SCR, Kempton MJ. A meta-analysis of structural MRI studies of the brain in systemic lupus erythematosus (SLE). Clin Rheumatol. 2023; 42: 319–326

Dalmasso MC, De Rojas I, Olivar N, ..., Ramírez A. The first genome-wide association study in the Argentinian and Chilean populations identifies shared genetics with Europeans in Alzheimer's disease. Alzheimers Dement. 2023: 1298–1308

Darzynkiewicz Z, Juan G. DNA Content Measurement for DNA Ploidy and Cell Cycle Analysis. CP Cytometry. 1997, 00: 7.5.1-7.5.24.

Deneubourg C, Ramm M, Smith LJ, ..., Jungbluth H. The spectrum of neurodevelopmental, neuromuscular and neurodegenerative disorders due to defective autophagy. Autophagy. 2022; 18: 496–517

Dorn S, Schoergenhofer C, Krainer M, Müller M, Jilma B. LUBAC and ABIN-1 Modulate TRAIL-Based NF- κ B Induction in Human Embryonic Kidney 293 Cells. Biores Open Access. 2018; 7: 81–89

Dziedzic SA, Su Z, Jean Barrett V, ..., Yuan J. ABIN-1 regulates RIPK1 activation by linking Met1 ubiquitylation with Lys63 deubiquitylation in TNF-RSC. Nat Cell Biol. 2018; 20: 58–68

Edgar R. Gene Expression Omnibus: NCBI gene expression and hybridization array data repository. Nucleic Acids Res. 2002; 30: 207–210

Eisinga R, Heskes T, Pelzer B, Te Grotenhuis M. Exact p-values for pairwise comparison of Friedman rank sums, with application to comparing classifiers. BMC Bioinformatics. 2017; 18: 68

El Bakkouri K, Wullaert A, Haegman M, Heyninck K, Beyaert R. Adenoviral Gene Transfer of the NF- κ B Inhibitory Protein ABIN-1 Decreases Allergic Airway Inflammation in a Murine Asthma Model. *J Biol Chem*. 2005; 280: 17938–17944

Elmaci İ, Altinoz MA, Sari R, Bolukbasi FH. Phosphorylated Histone H3 (PHH3) as a Novel Cell Proliferation Marker and Prognosticator for Meningeal Tumors: A Short Review. *Appl Immunohistochem Mol Morphol*. 2018; 26: 627–631

Enduru N, Fernandes BS, Bahrami S, Dai Y, Andreassen OA, Zhao Z. Genetic overlap between Alzheimer's disease and immune-mediated diseases: an atlas of shared genetic determinants and biological convergence. *Mol Psychiatry*. 2024; 29: 2447–2458

European Molecular Biology Laboratory. Hinxton, Cambridgeshire (United Kingdom). 2024: Decipher. <https://www.deciphergenomics.org/> (Access Date: 14.02.2024)

Eyre S, Bowes J, Diogo D, ..., Worthington J. High-density genetic mapping identifies new susceptibility loci for rheumatoid arthritis. *Nat Genet*. 2012; 44: 1336–1340

Fatemi SH, Halt AR. Altered levels of Bcl2 and p53 proteins in parietal cortex reflect de-regulated apoptotic regulation in autism. *Synapse*. 2001; 42: 281–284

Fatemi SH, Stary JM, Halt AR, Realmuto GR. Dysregulation of Reelin and Bcl-2 proteins in autistic cerebellum. *J Autism Dev Disord*. 2001; 31: 529–535

Fetit R, Hillary RF, Price DJ, Lawrie SM. The neuropathology of autism: A systematic review of post-mortem studies of autism and related disorders. *Neurosci Biobehav Rev*. 2021; 129: 35–62

Firth HV, Richards SM, Bevan AP, Clayton S, Corpas M, Rajan D, Vooren SV, Moreau Y, Pettett RM, Carter NP. DECIPHER: Database of Chromosomal Imbalance and Phenotype in Humans Using Ensembl Resources. *Am J Hum Genet*. 2009; 84: 524–533

Flores AM, Gurevich I, Zhang C, Ramirez VP, Devens TR, Aneskievich BJ. TNIP1 is a corepressor of agonist-bound PPARs. *Arch Biochem Biophys*. 2011; 516: 58–66

Flusberg DA, Sorger PK. Surviving apoptosis: life–death signaling in single cells. *Trends Cell Biol*. 2015; 25: 446–458

Fuchs O. Important Genes in the Pathogenesis of 5q- Syndrome and Their Connection with Ribosomal Stress and the Innate Immune System Pathway. *Leuk Res Treatment*. 2012; 2012: 179402

Fukushi M, Dixon J, Kimura T, Tsurutani N, Dixon MJ, Yamamoto N. Identification and cloning of a novel cellular protein Naf1, Nef-associated factor 1, that increases cell surface CD4 expression. *FEBS Lett*. 1999; 442: 83–88

Gharani N, Benayed R, Mancuso V, Brzustowicz LM, Millonig JH. Association of the homeobox transcription factor, ENGRAILED 2, 3, with autism spectrum disorder. *Mol Psychiatry*. 2004; 9: 474–484

Ghavami S, Shojaei S, Yeganeh B, ..., Łos MJ. Autophagy and apoptosis dysfunction in neurodegenerative disorders. *Prog Neurobiol*. 2014; 112: 24–49

Gong H, Gao S, Pu X, Kang X, Wu X. Association of rs610604 in TNFAIP3 and rs17728338 in TNIP1 gene polymorphisms with psoriasis susceptibility: a meta-analysis of case-control studies. *BMC Med Genet*. 2020; 21: 103

Goto H, Kosako H, Tomono Y, ..., Inagaki M. Identification of a Novel Phosphorylation Site on Histone H3 Coupled with Mitotic Chromosome Condensation. *J Biol Chem*. 1999; 274: 25543–25549

Grada A, Otero-Vinas M, Prieto-Castrillo F, Obagi Z, Falanga V. Research Techniques Made Simple: Analysis of Collective Cell Migration Using the Wound Healing Assay. *J Invest Dermatol*. 2017; 137: 11–16

Gregersen PK, Kosoy R, Lee AT, ..., Seldin MF. Risk for myasthenia gravis maps to a 151 Pro→Ala change in TNIP1 and to human leukocyte antigen-B*08. *Ann Neurol*. 2012; 72: 927–935

Grzanka D, Gagat M, Izdebska M. Actin is required for cellular death. *Acta Histochem*. 2013; 115: 775–782

- G'Sell RT, Gaffney PM, Powell DW. Review: A20-Binding Inhibitor of NF- κ B Activation 1 Is a Physiologic Inhibitor of NF- κ B: A Molecular Switch for Inflammation and Autoimmunity: ABIN-1 FUNCTION IN AUTOIMMUNE DISEASE. *Arthritis Rheumatol.* 2015; 67: 2292–2302
- Guo M, Hay B. Cell proliferation and apoptosis. *Curr Opin Cell Biol.* 1999; 11: 745–752
- Gurevich I, Zhang C, Francis N, Aneskievich BJ. TNIP1, a Retinoic Acid Receptor Corepressor and A20-binding Inhibitor of NF- κ B, Distributes to Both Nuclear and Cytoplasmic Locations. *J Histochem Cytochem.* 2011; 59: 1101–1112
- Hagen L, Sharma A, Aas PA, Slupphaug G. Off-target responses in the HeLa proteome subsequent to transient plasmid-mediated transfection. *Biochim Biophys Acta.* 2015; 1854: 84–90
- Hannus M, Beitzinger M, Engelmann JC, Weickert M-T, Spang R, Hannus S, Meister G. siPools: highly complex but accurately defined siRNA pools eliminate off-target effects. *Nucleic Acids Res.* 2014; 42: 8049–8061
- Hans F, Dimitrov S. Histone H3 phosphorylation and cell division. *Oncogene.* 2001; 20: 3021–3027
- Harrison PW, Amode MR, Austine-Orimoloye O, ..., Yates AD. Ensembl 2024. *Nucleic Acids Res.* 2024; 52: 891–899
- He Y, Chen X, Liu M, ..., Hao G. The potential DNA methylation markers of cardiovascular disease in patients with type 2 diabetes. *BMC Med Genomics.* 2023; 16: 242
- Heyninck K, Kreike MM, Beyaert R. Structure-function analysis of the A20-binding inhibitor of NF- κ B activation, ABIN-1. *FEBS Lett.* 2003; 536: 135–140
- Heyninck K, Van Huffel S, Kreike M, Beyaert R. Yeast Two-Hybrid Screening for Proteins Interacting With the Anti-Apoptotic Protein A20. in: Humana Press, ed. *Apoptosis Methods and Protocols.* New Jersey, 2004: 223–242
- Hinchcliff M, Garcia-Milian R, Di Donato S, Dill K, Bundschuh E, Galdo FD. Cellular and Molecular Diversity in Scleroderma. *Seminars in Immunology.* 2021; 58: 101648

- Ho G, Lam L, Tran T, Wei J, Hashimoto M. Innate neuroimmunity across aging and neurodegeneration: a perspective from amyloidogenic evolvability. *Front. Cell Dev. Biol.* 2024; 12: 1430593
- Hoffmann A, Baltimore D. Circuitry of nuclear factor κ B signaling. *Immunol Rev.* 2006; 210: 171–186
- Holst MI, 2007: Identifikation und Charakterisierung differenziell exprimierter Gene in einer Mausmutanten mit prolongierter Engrailed-2 Expression mithilfe der Array-Technologie. <https://nbn-resolving.org/urn:nbn:de:hbz:5N-10978> (Access Date: 20/07/2024)
- Huang L, Verstrepen L, Heyninck K, Wullaert A, Revets H, De Baetselier P, Beyaert R. ABINs inhibit EGF receptor-mediated NF- κ B activation and growth of EGF receptor-over-expressing tumour cells. *Oncogene.* 2008; 27: 6131–6140
- Hughes HK, R.J.Moreno, Ashwood P. Innate immune dysfunction and neuroinflammation in autism spectrum disorder (ASD). *Brain Behav Immun.* 2023; 108: 245–254
- Hutsler JJ, Zhang H. Increased dendritic spine densities on cortical projection neurons in autism spectrum disorders. *Brain Res.* 2010; 1309: 83–94
- Igarashi H, Yahagi A, Saika T, Hashimoto J, Tomita T, Yoshikawa H, Ishihara K. A pro-inflammatory role for A20 and ABIN family proteins in human fibroblast-like synoviocytes in rheumatoid arthritis. *Immunol Lett.* 2012; 141: 246–253
- Ippagunta SK, Gangwar R, Finkelstein D, Vogel P, Pelletier S, Gingras S, Redecke V, Häcker H. Keratinocytes contribute intrinsically to psoriasis upon loss of Tnip1 function. *Proc. Natl. Acad. Sci. U.S.A.* 2016; 113: 6162 - 6171
- Ishigaki K, Sakaue S, Terao C, ..., Raychaudhuri S. Multi-ancestry genome-wide association analyses identify novel genetic mechanisms in rheumatoid arthritis. *Nat Genet.* 2022; 54: 1640–1651
- Israel A. The IKK Complex, a Central Regulator of NF- κ B Activation. *Cold Spring Harb Perspect Biol.* 2010; 2: a000158

- Ito Y, Ofengeim D, Najafov A, ..., Yuan J. RIPK1 mediates axonal degeneration by promoting inflammation and necroptosis in ALS. *Science*. 2016; 353: 603–608
- Jacobsen LB, Calvin SA, Lobenhofer EK. Transcriptional effects of transfection: the potential for misinterpretation of gene expression data generated from transiently transfected cells. *BioTechniques*. 2009; 47: 617–624
- Jiang NM, Cowan M, Moonah SN, Petri WA. The Impact of Systemic Inflammation on Neurodevelopment. *Trends Mol Med*. 2018; 24: 794–804
- Jonkman JEN, Cathcart JA, Xu F, Bartolini ME, Amon JE, Stevens KM, Colarusso P. An introduction to the wound healing assay using live-cell microscopy. *Cell Adh Migr*. 2014; 8: 440–451
- Karin M, Lin A. NF- κ B at the crossroads of life and death. *Nat Immunol*. 2002; 3: 221–227
- Khunsriraksakul C, Li Q, Markus H, ..., Liu DJ. Multi-ancestry and multi-trait genome-wide association meta-analyses inform clinical risk prediction for systemic lupus erythematosus. *Nat Commun*. 2023; 14: 668
- Koo TK, Li MY. A Guideline of Selecting and Reporting Intraclass Correlation Coefficients for Reliability Research. *J Chiropr Med*. 2016; 15: 155–163
- Kook S, Shim SR, Kim JI, Ahnn JH, Jung YK, Paik SG, Song WK. Degradation of focal adhesion proteins during nocodazole-induced apoptosis in rat-1 cells. *Cell Biochem. Funct*. 2000; 18: 1–7
- Korte EA, Caster DJ, Barati MT, ..., Powell DW. ABIN1 Determines Severity of Glomerulonephritis via Activation of Intrinsic Glomerular Inflammation. *Am J Pathol*. 2017; 187: 2799–2810
- Kroll J, Renkawitz J. Principles of organelle positioning in motile and non-motile cells. *EMBO Rep*. 2024; 25: 2172–2187
- Le Guerroué F, Bunker EN, Rosencrans WM, Nguyen JT, Basar MA, Werner A, Chou T-F, Wang C, Youle RJ. TNIP1 inhibits selective autophagy via bipartite interaction with LC3/GABARAP and TAX1BP1. *Mol Cell*. 2023; 83: 927-941

- Lei Q, Gu H, Li L, Wu T, Xie W, Li M, Zhao N. TNIP1-mediated TNF- α /NF- κ B signalling cascade sustains glioma cell proliferation. *J Cellular Molecular Medi.* 2020; 24: 530–538
- Lessard CJ, Li H, Adrianto I, ..., Sivils KL. Variants at multiple loci implicated in both innate and adaptive immune responses are associated with Sjögren's syndrome. *Nat Genet.* 2013; 45: 1284–1292
- Li M, Liu Y, Xu C, ..., Zhang H. Ubiquitin-binding domain in ABIN1 is critical for regulating cell death and inflammation during development. *Cell Death Differ.* 2022; 29: 2034-2045
- Li X, Chauhan A, Sheikh AM, Patil S, Chauhan V, Li XM, Ji L, Brown T, Malik M. Elevated immune response in the brain of autistic patients. *J Neuroimmunol.* 2009; 207: 111–116
- Lin HJ, Shaffer KM, Sun Z, Jay G, He W, Ma W. AF1q, a differentially expressed gene during neuronal differentiation, transforms HEK cells into neuron-like cells. *Brain Res Mol Brain Res.* 2004; 131: 126–130
- Litwiniuk A, Juszczak GR, Stankiewicz AM, Urbańska K. The role of glial autophagy in Alzheimer's disease. *Mol Psychiatry.* 2023; 28: 4528–4539
- Liu S, Liu Y, Hao W, ..., Fassbender K. TLR2 Is a Primary Receptor for Alzheimer's Amyloid β Peptide To Trigger Neuroinflammatory Activation. *J Immunol.* 2012; 188: 1098–1107
- Liu WK, Yen PF, Chien CY, Fann MJ, Su JY, Chou CK. The inhibitor ABIN-2 disrupts the interaction of receptor-interacting protein with the kinase subunit IKK γ to block activation of the transcription factor NF- κ B and potentiate apoptosis. *Biochem J.* 2004; 378: 867–876
- Lobo V, Shcherbinina E, Westholm JO, Nowak I, Huang HC, Angeletti D, Anastasakis DG, Sarshad AA. Integrative transcriptomic and proteomic profiling of the effects of cell confluency on gene expression. *Sci Data.* 2024; 11: 617
- Lobry C, Lopez T, Israël A, Weil R. Negative feedback loop in T cell activation through I κ B kinase-induced phosphorylation and degradation of Bcl10. *Proc. Natl. Acad. Sci. U.S.A.* 2007; 104: 908–913

Lu L, Zhang Y, Tan X, ..., Chen Y. Emerging mechanisms of pyroptosis and its therapeutic strategy in cancer. *Cell Death Discov.* 2022; 8: 338

Majerczyk D, Ayad EG, Brewton KL, Saing P, Hart PC. Systemic maternal inflammation promotes ASD via IL-6 and IFN- γ . *Biosci Rep.* 2022; 42: BSR20220713

Márquez A, Kerick M, Zhernakova A, ..., Martín J. Meta-analysis of ImmunoChip data of four autoimmune diseases reveals novel single-disease and cross-phenotype associations. *Genome Med.* 2018; 10: 97

Martin LJ, Liu Z. Opportunities for neuroprotection in ALS using cell death mechanism rationales. *Drug Discov Today Dis Models.* 2004; 1: 135–143

Matta SM, Hill-Yardin EL, Crack PJ. The influence of neuroinflammation in Autism Spectrum Disorder. *Brain Behav Immun.* 2019; 79: 75–90

Mauro C, Pacifico F, Lavorgna A, Mellone S, Iannetti A, Acquaviva R, Formisano S, Vito P, Leonardi A. ABIN-1 Binds to NEMO/IKK γ and Co-operates with A20 in Inhibiting NF- κ B. *J Biol Chem.* 2006; 281: 18482–18488

Mejlvang J, Olsvik H, Svenning S, ..., Johansen T. Starvation induces rapid degradation of selective autophagy receptors by endosomal microautophagy. *J Cell Biol.* 2018; 217: 3640–3655

Meltzer A, Van de Water J. The Role of the Immune System in Autism Spectrum Disorder. *Neuropsychopharmacol.* 2017; 42: 284–298

Merline R, Rödiger H, Zeng-Brouwers J, ..., Schaefer L. A20 binding and inhibitor of nuclear factor kappa B (NF- κ B)-1 (ABIN-1): a novel modulator of mitochondrial autophagy. *Am J Physiol Cell Physiol.* 2023; 324: 339–352

Meyer T. Amyotrophe Lateralsklerose (ALS) – Diagnose, Verlauf und neue Behandlungsoptionen. *Dtsch Med Wochenschr.* 2021; 146: 1613–1618

Meyer-Puttlitz B, Hayashi Y, Waha A, Rollbrocker B, Boström J, Wiestler OD, Louis DN, Reifenberger G, von Deimling A. Molecular genetic analysis of giant cell glioblastomas. *Am J Pathol.* 1997; 151: 853–857

- Mizushima N, Komatsu M. Autophagy: Renovation of Cells and Tissues. *Cell*. 2011; 147: 728–741
- Modabbernia A, Velthorst E, Reichenberg A. Environmental risk factors for autism: an evidence-based review of systematic reviews and meta-analyses. *Mol Autism*. 2017; 8: 13
- Moreno P, Fexova S, George N, ..., Papatheodorou I. Expression Atlas update: gene and protein expression in multiple species. *Nucleic Acids Res*. 2022; 50: 129–140
- Morris DL, Sheng Y, Zhang Y, ..., Vyse TJ. Genome-wide association meta-analysis in Chinese and European individuals identifies ten new loci associated with systemic lupus erythematosus. *Nat Genet*. 2016; 48: 940–946
- Nagabhushana A, Bansal M, Swarup G. Optineurin Is Required for CYLD-Dependent Inhibition of TNF α -Induced NF- κ B Activation. *Vij N, ed. PLoS ONE*. 2011; 6: e17477
- National Center for Biotechnology Information (NCBI). Bethesda (MD): National Library of Medicine (US), National Center for Biotechnology Information. 1988: <https://www.ncbi.nlm.nih.gov/> (Access Date: 14.02.2024)
- Newton K, Strasser A, Kayagaki N, Dixit VM. Cell death. *Cell*. 2024; 187: 235–256
- Nordmark G, Wang C, Vasaitis L, ..., Syvänen AC. Association of Genes in the NF- κ B Pathway with Antibody-Positive Primary Sjögren's Syndrome. *Scand J Immunol*. 2013; 78: 447–454
- Ohja K, Gozal E, Fahnestock M, Cai L, Cai J, Freedman JH, Switala A, El-Baz A, Barnes GN. Neuroimmunologic and Neurotrophic Interactions in Autism Spectrum Disorders: Relationship to Neuroinflammation. *Neuromol Med*. 2018; 20: 161–173
- Ormerod MG, Tribukait B, Giaretti W. Consensus Report of the Task Force on Standardisation of DNA Flow Cytometry in Clinical Pathology. *Anal Cell Pathol*. 1998; 17: 103–110
- Oshima S, Turer EE, Callahan JA, ..., Ma A. ABIN-1 is a ubiquitin sensor that restricts cell death and sustains embryonic development. *Nature*. 2009; 457: 906–909

Osterlehner A, Simmeth S, Göpfert U. Promoter methylation and transgene copy numbers predict unstable protein production in recombinant chinese hamster ovary cell lines. *Bio-technol Bioeng.* 2011; 108: 2670–2681

Ponder KG, Boise LH. The prodomain of caspase-3 regulates its own removal and caspase activation. *Cell Death Discov.* 2019; 5: 56

Porter AG, Jänicke RU. Emerging roles of caspase-3 in apoptosis. *Cell Death Differ.* 1999; 6: 99–104

Qin JY, Zhang L, Clift KL, Hular I, Xiang AP, Ren B-Z, Lahn BT. Systematic Comparison of Constitutive Promoters and the Doxycycline-Inducible Promoter. Hansen IA, ed. *PLoS ONE.* 2010; 5: e10611

Qiu Z, Zhang H, Xia M, Gu J, Guo K, Wang H, Miao C. Programmed Death of Microglia in Alzheimer's Disease: Autophagy, Ferroptosis, and Pyroptosis. *J Prev Alz Dis.* 2023; 10: 95-103

Rajesh Y, Kanneganti TD. Innate Immune Cell Death in Neuroinflammation and Alzheimer's Disease. *Cells.* 2022; 11: 1885

Ramirez VP, Gurevich I, Aneskievich BJ. Emerging roles for TNIP1 in regulating post-receptor signaling. *Cytokine Growth Factor Rev.* 2012; 23: 109–118

Rao DD, Vorhies JS, Senzer N, Nemunaitis J. siRNA vs. shRNA: Similarities and differences. *Adv Drug Deliv Rev.* 2009; 61: 746–759

Rasmussen NL, Zhou J, Olsvik H, Kaeser-Pebernard S, Lamark T, Dengjel J, Johansen T. The inflammation repressor TNIP1/ABIN-1 is degraded by autophagy following TBK1 phosphorylation of its LIR. *Autophagy.* 2023; 19: 2819–2820

R Core Team. R: A Language and Environment for Statistical Computing. R Foundation for Statistical Computing, Vienna, Austria. 2023: <https://www.R-project.org>. (Access Date: 22.04.2023)

Ren D, Yang Q, Dai Y, Guo W, Du H, Song L, Peng X. Oncogenic miR-210-3p promotes prostate cancer cell EMT and bone metastasis via NF- κ B signaling pathway. *Mol Cancer*. 2017; 16: 117

Restuadi R, Steyn FJ, Kabashi E, ..., Garton FC. Functional characterisation of the amyotrophic lateral sclerosis risk locus GPX3/TNIP1. *Genome Med*. 2022; 14: 7

Revelle W. 2024: psych: Procedures for Psychological, Psychometric, and Personality Research. Northwestern University, Evanston, Illinois, R package version 2.4.1., <https://CRAN.R-project.org/package=psych> (Access Date: 14.04.2024)

Robbins M, Judge A, Ambegia E, Choi C, Yaworski E, Palmer L, McClintock K, MacLachlan I. Misinterpreting the Therapeutic Effects of Small Interfering RNA Caused by Immune Stimulation. *Hum Gene Ther*. 2008; 19: 991–999

Robinson-Agramonte MDLA, Noris García E, Fraga Guerra J, Vega Hurtado Y, Antonucci N, Semprún-Hernández N, Schultz S, Siniscalco D. Immune Dysregulation in Autism Spectrum Disorder: What Do We Know about It? *IJMS*. 2022; 23: 3033

Rubenstein JLR. Annual Research Review: Development of the cerebral cortex: implications for neurodevelopmental disorders. *J Child Psychol Psychiatry*. 2011; 52: 339–355

Russell WC, Graham FL, Smiley J, Nairn R. Characteristics of a Human Cell Line Transformed by DNA from Human Adenovirus Type 5. *J Gen Virol*. 1977; 36: 59–72

Sathasivam S, Ince PG, Shaw PJ. Apoptosis in amyotrophic lateral sclerosis: a review of the evidence. *Neuropathology Appl Neurobio*. 2001; 27: 257–274

Sawicka A, Seiser C. Histone H3 phosphorylation – A versatile chromatin modification for different occasions. *Biochimie*. 2012; 94: 2193–2201

Schindelin J, Arganda-Carreras I, Frise E, ..., Cardona A. Fiji: an open-source platform for biological-image analysis. *Nat Methods*. 2012; 9: 676–682

Shamilov R, Ackley TW, Aneskievich BJ. Enhanced Wound Healing- and Inflammasome-Associated Gene Expression in TNFAIP3-Interacting Protein 1- (TNIP1-) Deficient HaCaT Keratinocytes Parallels Reduced Reepithelialization. *Mediators Inflamm.* 2020; 2020: 1–14

Shamilov R, Aneskievich BJ. TNIP1 in Autoimmune Diseases: Regulation of Toll-like Receptor Signaling. *J Immunol Res.* 2018; 2018: 1–13

Sheikh AM, Li X, Wen G, Tauqeer Z, Brown WT, Malik M. Cathepsin D and apoptosis related proteins are elevated in the brain of autistic subjects. *Neuroscience.* 2010a; 165: 363–370

Sheikh AM, Malik M, Wen G, Chauhan A, Chauhan V, Gong C, Liu F, Brown WT, Li X. BDNF-Akt-Bcl2 antiapoptotic signaling pathway is compromised in the brain of autistic subjects. *J of Neuroscience Research.* 2010b; 88: 2641–2647

Shen Y, Vignali P, Wang R. Rapid Profiling Cell Cycle by Flow Cytometry Using Concurrent Staining of DNA and Mitotic Markers. *Bio Protoc.* 2017; 7: e2517

Sherman J, Wang R. Rapid profiling of G2 phase to mitosis progression by flow cytometry in asynchronous cells. *Cell Cycle.* 2020; 19: 2897–2905

Shinkawa Y, Imami K, Fuseya Y, Sasaki K, Ohmura K, Ishihama Y, Morinobu A, Iwai K. ABIN1 is a signal-induced autophagy receptor that attenuates NF- κ B activation by recognizing linear ubiquitin chains. *FEBS Lett.* 2022; 596: 1147–1164

Shuid AN, Jayusman PA, Shuid N, Ismail J, Kamal Nor N, Mohamed IN. Association between Viral Infections and Risk of Autistic Disorder: An Overview. *IJERPH.* 2021; 18: 2817

Signorell A. 2024: DescTools: Tools for Descriptive Statistics. R package version 0.99.56. <https://github.com/AndriSignorell/DescTools/> (Access Date: 14.04.2024)

Skefos J, Cummings C, Enzer K, Holiday J, Weed K, Levy E, Yuce T, Kemper T, Bauman M. Regional Alterations in Purkinje Cell Density in Patients with Autism. *PLoS ONE.* 2014; 9: e81255

Son Y-O, Jang Y-S, Heo J-S, Chung W-T, Choi K-C, Lee J-C. Apoptosis-inducing factor plays a critical role in caspase-independent, pyknotic cell death in hydrogen peroxide-exposed cells. *Apoptosis*. 2009; 14: 796–808

Song Y, Yan M, Li J, Li J, Jin T, Chen C. Association between TNIP1, MPHOSPH6 and ZNF208 genetic polymorphisms and the coronary artery disease risk in Chinese Han population. *Oncotarget*. 2017; 8: 77233–77240

Soria Lopez JA, González HM, Léger GC. Chapter 13: Alzheimer's disease. in: Elsevier, ed. *Handbook of Clinical Neurology Volume 167*. Elsevier, 2019: 231–255

Stelzer G, Rosen N, Plaschkes I, ..., Lancet D. The GeneCards Suite: From Gene Data Mining to Disease Genome Sequence Analyses. *Curr Protoc Bioinformatics*. 2016; 54: 1.30.1-1.30.33

Stepanenko AA, Dmitrenko VV. HEK293 in cell biology and cancer research: phenotype, karyotype, tumorigenicity, and stress-induced genome-phenotype evolution. *Gene*. 2015; 569: 182–190

Stepanenko AA, Heng HH. Transient and stable vector transfection: Pitfalls, off-target effects, artifacts. *Mutat Res Rev Mutat Res*. 2017; 773: 91–103

Sun Y, Liu W-Z, Liu T, Feng X, Yang N, Zhou H-F. Signaling pathway of MAPK/ERK in cell proliferation, differentiation, migration, senescence and apoptosis. *J Recept Signal Transduct Res*. 2015; 35: 600–604

Tang G, Gudsnuk K, Kuo SH, ..., Sulzer D. Loss of mTOR-Dependent Macroautophagy Causes Autistic-like Synaptic Pruning Deficits. *Neuron*. 2014; 83: 1131–1143

Thal DR, Walter J, Saido TC, Fändrich M. Neuropathology and biochemistry of A β and its aggregates in Alzheimer's disease. *Acta Neuropathol*. 2015; 129: 167–182

The GIMP Development Team. 2019: GIMP. <https://www.gimp.org> (Access Date: 11.04.2022)

Theoharides TC, Tsilioni I, Patel AB, Doyle R. Atopic diseases and inflammation of the brain in the pathogenesis of autism spectrum disorders. *Transl Psychiatry*. 2016; 6: e844

Van Antwerp DJ, Martin SJ, Verma IM, Green DR. Inhibition of TNF-induced apoptosis by NF- κ B. *Trends Cell Biol.* 1998; 8: 107–111

Van Huffel S, Delaei F, Heyninck K, De Valck D, Beyaert R. Identification of a Novel A20-binding Inhibitor of Nuclear Factor- κ B Activation Termed ABIN-2. *J Biol Chem.* 2001; 276: 30216–30223

Van Quickenberghe E, De Sutter D, van Loo G, Eyckerman S, Gevaert K. A protein-protein interaction map of the TNF-induced NF- κ B signal transduction pathway. *Sci Data.* 2018; 5: 180289

Van Rheenen W, Van Der Spek RAA, Bakker MK, ..., Veldink JH. Common and rare variant association analyses in amyotrophic lateral sclerosis identify 15 risk loci with distinct genetic architectures and neuron-specific biology. *Nat Genet.* 2021; 53: 1636–1648

Varghese M, Keshav N, Jacot-Descombes S, ..., Hof PR. Autism spectrum disorder: neuropathology and animal models. *Acta Neuropathol.* 2017; 134: 537–566

Verstrepen L, Carpentier I, Beyaert R. The Biology of A20-Binding Inhibitors of NF- κ B Activation (ABINS). In: Ferran C, ed. *The Multiple Therapeutic Targets of A20*. New York, NY: Springer New York, 2014: 13–31

Verstrepen L, Carpentier I, Verhelst K, Beyaert R. ABINs: A20 binding inhibitors of NF- κ B and apoptosis signaling. *Biochem Pharmacol.* 2009; 78: 105–114

Wang L, Wang B, Wu C, Wang J, Sun M. Autism Spectrum Disorder: Neurodevelopmental Risk Factors, Biological Mechanism, and Precision Therapy. *IJMS.* 2023; 24: 1819

Wang RC, Wang Z. Synchronization of Cultured Cells to G1, S, G2, and M Phases by Double Thymidine Block. In: Wang Z, ed. *Cell-Cycle Synchronization*. New York, NY: Springer US, 2022: 61–71

Wang Y, Gao W, Shi X, Ding J, Liu W, He H, Wang K, Shao F. Chemotherapy drugs induce pyroptosis through caspase-3 cleavage of a gasdermin. *Nature.* 2017; 547: 99–103

Webb LV, Ventura S, Ley SC. ABIN-2, of the TPL-2 Signaling Complex, Modulates Mammalian Inflammation. *Trends Immunol.* 2019; 40: 799–808

Wegiel J, Flory M, Kuchna I, ..., Brown WT. Stereological study of the neuronal number and volume of 38 brain subdivisions of subjects diagnosed with autism reveals significant alterations restricted to the striatum, amygdala and cerebellum. *acta neuropathol commun.* 2014; 2: 141

Wickham H. *Ggplot2*. New York, NY: Springer International Publishing, 2016

Wightman DP, Jansen IE, Savage JE, ..., Posthuma D. A genome-wide association study with 1,126,563 individuals identifies new risk loci for Alzheimer's disease. *Nat Genet.* 2021; 53: 1276–1282

Wolff JJ, Jacob S, Elison JT. The journey to autism: Insights from neuroimaging studies of infants and toddlers. *Dev Psychopathol.* 2018; 30: 479–495

Wullaert A, Verstrepen L, Van Huffel S, ..., Beyaert R. LIND/ABIN-3 Is a Novel Lipopolysaccharide-inducible Inhibitor of NF- κ B Activation. *J Biol Chem.* 2007; 282: 81–90

Xia W, Bringmann P, McClary J, ..., Cobb RR. High levels of protein expression using different mammalian CMV promoters in several cell lines. *Protein Expr Purif.* 2006; 45: 115–124

Yang Y, Fan J, Han S, Li E. TNIP1 Inhibits Proliferation And Promotes Apoptosis In Clear Cell Renal Carcinoma Through Targeting C/Ebp β . *OTT.* 2019; 12: 9861–9871

Yin X, Low HQ, Wang L, ..., Liu J. Genome-wide meta-analysis identifies multiple novel associations and ethnic heterogeneity of psoriasis susceptibility. *Nat Commun.* 2015; 6: 6916

Yu JSL, Cui W. Proliferation, survival and metabolism: the role of PI3K/AKT/mTOR signalling in pluripotency and cell fate determination. *Development.* 2016; 143: 3050–3060

Zhang S, Fukushi M, Hashimoto S, ..., Tsuchida N. A new ERK2 binding protein, Naf1, attenuates the EGF/ERK2 nuclear signaling. *Biochem Biophys Res Commun.* 2002; 297: 17–23

Zhang Z, Yang X, Song Y-Q, Tu J. Autophagy in Alzheimer's disease pathogenesis: Therapeutic potential and future perspectives. *Ageing Res Rev.* 2021; 72: 101464

Zhou J, Wu R, High AA, Slaughter CA, Finkelstein D, Rehg JE, Redecke V, Häcker H. A20-binding inhibitor of NF- κ B (ABIN1) controls Toll-like receptor-mediated CCAAT/enhancer-binding protein β activation and protects from inflammatory disease. *Proc. Natl. Acad. Sci. U.S.A.* 2011; 108: 998-1006

9. Acknowledgments

First and foremost, I would like to thank Prof. Dr. Stephan Baader for the opportunity to conduct my thesis research at the Institute of Anatomy and Cell Biology. Further, I would like to thank him for supervising my work, critically interpreting my data and the invaluable support I received during each and every step of this process.

Furthermore, I would like to express my gratitude to all the other members of the Institute. Many thanks to Prof. Dr. Karl Schilling, as well as Dr. Sebastian Franken for generously providing their knowledge and scientific expertise. I would also like to thank Dr. Sebastian Röser for his supervision and support during his time at the Institute. A special thanks goes out to Sabine, Steffi and Andrea, who were always there to provide a helping hand and words of advice.

Lastly, this endeavor would not have been possible without my family and friends. I am deeply grateful for their moral support, kind feedback and endless patience. I would like to extend a special thanks to my father Fernando, my mother Katja, my sister Raquel, my brother Mário and my partner Dennis. Their belief in me has kept my motivation and spirits high during this process. I am very thankful for their love and support.